universität wien

MASTERARBEIT / MASTER'S THESIS

Titel der Masterarbeit / Title of the Master's Thesis

„ The role of the zinc finger motif in topoisomerase 3 in *Caenorhabditis elegans* meiosis “

verfasst von / submitted by

Nina Vojtassáková B.Sc.

angestrebter akademischer Grad / in partial fulfilment of the requirements for the degree of

Master of Science (MSc)

Wien, 2020 / Vienna, 2020

Studienkennzahl lt. Studienblatt / degree programme code as it appears on the student record sheet:	A 066 877
Studienrichtung lt. Studienblatt / degree programme as it appears on the student record sheet:	Masterstudium Genetik und Entwicklungsbiologie
Betreut von / Supervisor:	Univ.-Prof. Mag. Dr. Verena Jantsch-Plunger

Acknowledgements

I wish to show my sincere gratitude to Verena Jantsch for giving me the opportunity to work on this interesting project at the Department of Chromosome Biology in Max F. Perutz Laboratories, University Vienna. Her professional and emotional guidance encouraged me throughout the entire time of my master research.

This project would have been impossible without the support of Maria Rosaria Dello Stritto. I would like to thank for her help, enthusiasm and knowledge that motivated and inspired me during the work in the lab as well as writing. I could not have imagined having a better mentor for my master thesis.

I am also very grateful for friendly and cheerful atmosphere created by my co-workers: Antoine Baudrimont, Angela Graf, Dimitra Paouneskou, Jana Link, Maria Velkova and Nicola Silva, who shared with me their constructive advices and supported me emotionally. I enjoyed the time we spent together.

I would like to recognize the valuable training provided by the master programme Genetics and Developmental Biology and the Faculty of Life Sciences that prepared me for my scientific career.

Last but not least, I want to extend my deepest gratitude to my dearest parents Ingrid and Daniel and my beloved boyfriend Marian, who believed in my abilities, comforted me and encouraged me to be brave while confronting the scientific tasks.

Contents

1. Abstract English

Meiosis halves the diploid set of chromosomes in gametes, a necessity to compensate the doubling of chromosome numbers after fertilization during sexual reproduction of eukaryotes.

Crossovers that occur during meiotic repair of DNA double strand-breaks (DSBs) are not only important for exchange of genetic material, but also establish chiasmata between homologous chromosomes that generate essential tension for the correct chromosome segregation. As the number of DSBs exceeds the number of crossovers, a variety of enzymes is required to repair most recombination intermediates to noncrossovers in order to restore genome integrity. Several studies shed new light on such enzymes by introducing the BTR complex as "chaperone" that resolves joint molecules at multiple recombination steps to prevent the occurrence of extra crossovers and heterologous recombination intermediates. The mammalian complex is composed of type IA topoisomerase (TOP-3 in worms), Bloom helicase (HIM-6) and RMI1/2 scaffolding proteins (RMH-1 and RMH-2). Depletion of the complex has been shown to cause lethal hyperrecombination and chromosomal missegregation. Absence of BLM leads to Bloom Syndrome, a cancer prone condition defined by genome instability. Understanding this complex and its activities would therefore help to elucidate the recombination process and it might be important for future development of diagnostic and therapeutic methods.

Studies in my hosting lab displayed an involvement of *rmh-1* in distinct complexes that promote both crossover and noncrossover recombination during *C. elegans* meiosis and *C. elegans* is the model organism, where the less well understood pro crossover function becomes best apparent. During my master thesis I have investigated the function of the TOP-3 zinc finger motif (ZnF) in meiotic prophase I of *C. elegans*. TOP-3 harbors a catalytic domain and a carboxyterminal ZnF domain of the GRF type (characterized through three conserved amino acids Gly Arg Phe in the center) that shares more than 50% of its sequence with zinc fingers found in *Hs* TOPIIIα. By generating the truncated version of TOP-3 which lacks the ZnF motif, I was able to analyze the role of the motif during multiple steps of meiotic recombination. I found that its removal did not affect the worms with regard to viability and fertility at all, which contrasts the phenotype of the *top-3 delta* deletion mutant that produces only dead eggs. Nevertheless, I detected rare aberrant diakinesis chromosomes with circle shaped bodies and rare chromosome bridges between bivalents, but those did not affect the hatch rate of the offspring. In the ZnF deletion mutant, I saw increased amounts of RAD-51 marked recombination foci, indicating the relevance of the motif for early steps of recombination, however the disappearance of the RAD-51 would suggest that an alternative route of processing removes the intermediates. I also showed that *top-3* ZnF deleted mutants and *mus-81* mutants displayed synthetic defects, which indicates that *mus-81* is needed to resolve aberrant joint molecules that are being produced in the absence of the ZnF motif in *top-3*. I was able to determine that the ZnF is not necessary for the localization of the complex to the recombination intermediates during pachynema,

where all the BTR proteins concentrate into prominent recombination foci. However, I could detect a delay in the kinetics of loading, implicating the involvement of the ZnF motif in early recombination. Likewise, the loading of the crossover factor MSH-5 into recombination foci was delayed and reduced. Nevertheless, I found that the TOP-3 ZnF cooperates with RMH-2 for proper and timely loading of the complex and the double mutants displayed severe synthetic phenotypes despite the health of the single mutants. Detailed phenotypic characterization of the *top-3_ZnF* single mutant suggests that most defects are subtle: a slight increase of extra crossovers, a slight increase in heterologous recombination. Overall, the results of my master thesis suggest redundant functions of RMH-2 and the TOP-3 ZnF motif in complex assembly at recombination sites.

2. Zusammenfassung

Meiose halbiert den diploiden Chromosomensatz in eukaryotischen Gameten, um die Verdoppelung der Chromosomen, die nach Befruchtung während sexueller Reproduktion erfolgt, zu kompensieren. Crossovers, die während der meiotischen Reparatur von DNA- Doppelstrangbrüchen entstehen, sind nicht nur wichtig für den Austausch von genetischem Material, sondern reifen zu Chiasmen. Diese zeichnen sich durch physische Verbindungen zwischen homologen Chromosomen aus, die eine wesentliche Spannung für korrekte Chromosomensegregation erzeugen. Da die Anzahl der Doppelstrangbrüche die Menge der Crossovers überschreitet, stellt eine Vielfalt von Enzymen die Genomintegrität wieder her, indem sie die meisten Rekombinationsintermediate zu Noncrossovers reparieren. Mehrere Studien werfen ein neues Licht auf solche Enzyme, indem sie den BTR Komplex als „Chaperon“ einführen, das Rekombinationsintermediate auflöst, um zusätzliche Crossovers und heterologe Rekombination zu verhindern. Der Säuger BTR Komplex besteht aus Topoisomerase Typ IA (TOP-3 in Würmer), BLM Helikase (HIM-6) und den Gerüstproteinen RMI1/2 (RMH-1 und RMH-2). Depletion von Komplexmitgliedern verursacht letale Hyperrekombination und chromosomale Missegregation. Abwesenheit von BLM führt zum Bloom-Syndrom, einer krebsanfälligen Erkrankung, die durch Genominstabilität definiert wird. Das Verständnis dieses Komplexes und seiner Aktivitäten würde daher zur Aufklärung des Rekombinationsprozesses beitragen und könnte für die zukünftige Entwicklung diagnostischer und therapeutischer Methoden wichtig sein.

Studien in meinem Hosting-Labor haben eine Beteiligung von *rmh-1* an verschiedenen Komplexen gezeigt, die sowohl homologe Crossover- als auch Noncrossover Rekombination während der Meiose in *C. elegans* fördern. Im Rahmen meines Masterprojektes habe ich die Funktion von TOP-3 Zinkfinger (ZnF) Motiv in der meiotischen Prophase I in *C. elegans* untersucht. TOP-3 trägt eine katalytische Domäne und einen carboxyterminalen ZnF Motiv vom GRF-Typ (charakterisiert durch drei zentrale konservierte Aminosäuren Gly Arg Phe), das mehr als 50% ihrer Sequenz mit Zinkfingern von *Hs* TOPIIIα teilt. Durch die Erzeugung einer verkürzten Version von TOP-3, dem das ZnF Motiv fehlt, konnte ich die Rolle des Motivs während mehrerer Schritte der meiotischen Rekombination analysieren. Ich fand heraus, dass ZnF Deletion in TOP-3 die Würmer in Bezug auf ihre Lebensfähigkeit und Fruchtbarkeit überhaupt nicht beeinflusste, was dem Phänotyp der *top-3* Deletionsmutante gegenübersteht, die nur tote Eier produziert. Trotzdem entdeckte ich seltene aberrante Diakinese Chromosomen mit kreisförmigen Körpern und seltene Chromosomenbrücken zwischen zwei Bivalenten. Diese hatten jedoch keinen Einfluss auf die Schlupfrate der Nachkommen, weil Würmer ohne ZnF Motiv genauso lebensfähig wie der Wildtyp waren. In der Deletionsmutante sah ich erhöhte Mengen von RAD-51 markierten Rekombinationsintermediaten, was auf die Relevanz des Motivs für frühe Rekombinationsschritte indiziert. Das Verschwinden des RAD-51 würde jedoch darauf hindeuten, dass ein alternativer Verarbeitungsweg die Zwischenprodukte entfernt. Ich zeigte

auch, dass *top-3_ZnF* und *mus-81* Mutanten synthetische Defekte aufweisen, was bedeutet, dass MUS-81 Rekombinationsintermediate auflöst, die in der Abwesenheit des ZnF Motivs in *top-3* produziert werden. Ich stellte fest, dass das ZnF Motiv für die Lokalisierung des BTR Komplexes auf den Rekombinationsintermediaten in Pachynema nicht notwendig ist. Ich konnte eine Verzögerung in der Kinetik der Komplex Beladung beobachten, was eine Beteiligung von TOP-3 ZnF an der frühen Rekombination impliziert. Ebenso wurde die Beladung des Crossover Faktors MSH-5 verzögert und reduziert. Weiterhin fand ich heraus, dass TOP-3 ZnF mit RMH-2 zusammenarbeitet, um den Komplex richtig und rechtzeitig auf Rekombinationsintermediate zu beladen, und dass die Doppelmutanten trotz der Gesundheit der Einzelmutanten defekte Phänotypen zeigten. Dennoch schlägt eine detaillierte phänotypische Charakterisierung von *top-3_ZnF* Mutante vor, dass die meisten Defekte subtil sind: eine leichte Zunahme zusätzlicher Crossovers und eine leichte Zunahme der heterologen Rekombination. Insgesamt deuten die Ergebnisse meiner Masterarbeit darauf hin, dass TOP-3 ZnF Motiv und RMH-2 redundante Funktionen haben, die bei der Komplex Beladung und Assemblierung auf den Rekombinationsintermediate wichtig sind.

3. List of abbreviations

BLM	Bloom Syndrome
BTR	BLM helicase, Topoisomerase IIIα, RMI1 and RMI2 complex in mammals
CO	Crossover
CRISPR	Clustered Regularly Interspaced Short Palindromic Repeats
D loop	Displacement loop
DAPI	4',6-diamidino-2-phenylindole
dHJ	double Holliday Junction
DSB	double strand break
dsDNA	double stranded DNA
DTC	Distal Tip Cell
DG	distal tip of gonad
GFP protein	Green Fluorescent Protein
HA tag	Human influenza hemagglutinin tag
HR	homologous recombination
NCO	Noncrossover
NGM	Nematode Growth Medium
PC	Pairing Centre
PCD	programmed cell death
PCR	Polymerase Chain Reaction
PG	proximal tip of gonad
RTR	RecQ helicase, Type IA topoisomerase, RMI1 complex in metazoans
SC	Synaptonemal Complex
SDSA	Synthesis-Dependent Strand Annealing
Sp	spermatheca
ssDNA	single stranded DNA
STR	Sgs1 helicase, Top-3, Rmi1 complex in yeast

4. Introduction

4.1 Meiosis

Sexual reproduction gives rise to genetically distinct individuals generating the biodiversity of eukaryotes and diploid organisms. Their reproductive organs contain gamete precursors whose diploid set of chromosomes is subjected to meiosis. They undergo this specialized cell division in order to become haploid gametes with only one copy for each chromosome (Cooper 2000). This is accomplished by two rounds of chromosome segregation that follow one round of DNA replication (Kleckner 1996). In the first meiotic division homologous chromosomes are segregated and in the second meiotic division sister chromatids are partitioned into the daughter cells. Meiosis and fertilization are two events of sexual reproduction whose main functions are to ensure that each offspring carries a unique set of genetic material from its ancestors and that the doubling of the chromosome content through fertilization is compensated (Ohkura 2015).

Meiosis consists of many steps completion of which is essential for haploidy generation (figure 1). After the DNA is replicated during the interphase, meiocytes enter prophase I (top in figure 1), a stage that can be divided in the following substages (Alberts et al. 2002). In leptonema, each replicated chromosome consists of two chromatids associated via cohesion complexes and chromosomes start to condense. In zygonema, chromosomes search for their homologous partners. Once they find each other, a specific protein structure called the synaptonemal complex (SC) is assembled between homologous chromosomes to stabilize their pairwise alignment. At the same time DNA double strand breaks are introduced by the highly conserved enzyme Spo11 (Keeney 2001). The pachytene stage is characterized by fully paired chromosomes. During pachynema, in the context of fully synapsed chromosomes, recombination progresses (for detailed steps of recombination, see chapter 4.3.3). The homologs exchange genetic material in a process called crossing-over. After crossovers are formed, chromosomes enter the diplotene stage during which they undergo restructuring to a condensed form. Thanks to this condensation, during the next stage, diakinesis, homologous chromosomes (also known as bivalents) are held together by the chiasmata, the cytological manifestation of the previous recombination events that led to crossovers. The diakinesis transitions to metaphase I that takes place when tetrads migrate and align to the metaphase plate and associate to the meiotic spindle. Aligned bivalents are defined as metaphase I (top in figure 1). Combination of inter-homolog chiasmata and inter-sister cohesion generates tension that secures accurate segregation of homologous chromosomes to opposite poles during the next stage called anaphase I (Wood et al. 2010). Segregation is followed by telophase and cytokinesis I during which two daughter cells are formed (bottom in figure 1). Each daughter cell contains only cohesion-joined sister chromatids. These become aligned again (metaphase II) and separated during anaphase II. The last two stages, telophase and cytokinesis II, lead in case of

spermatogenesis to formation of four haploid gametes-sperms (bottom in figure 1). During oogenesis, however, the meiotic divisions generate only one haploid ovum and three polar bodies that do not possess the ability to be fertilized.

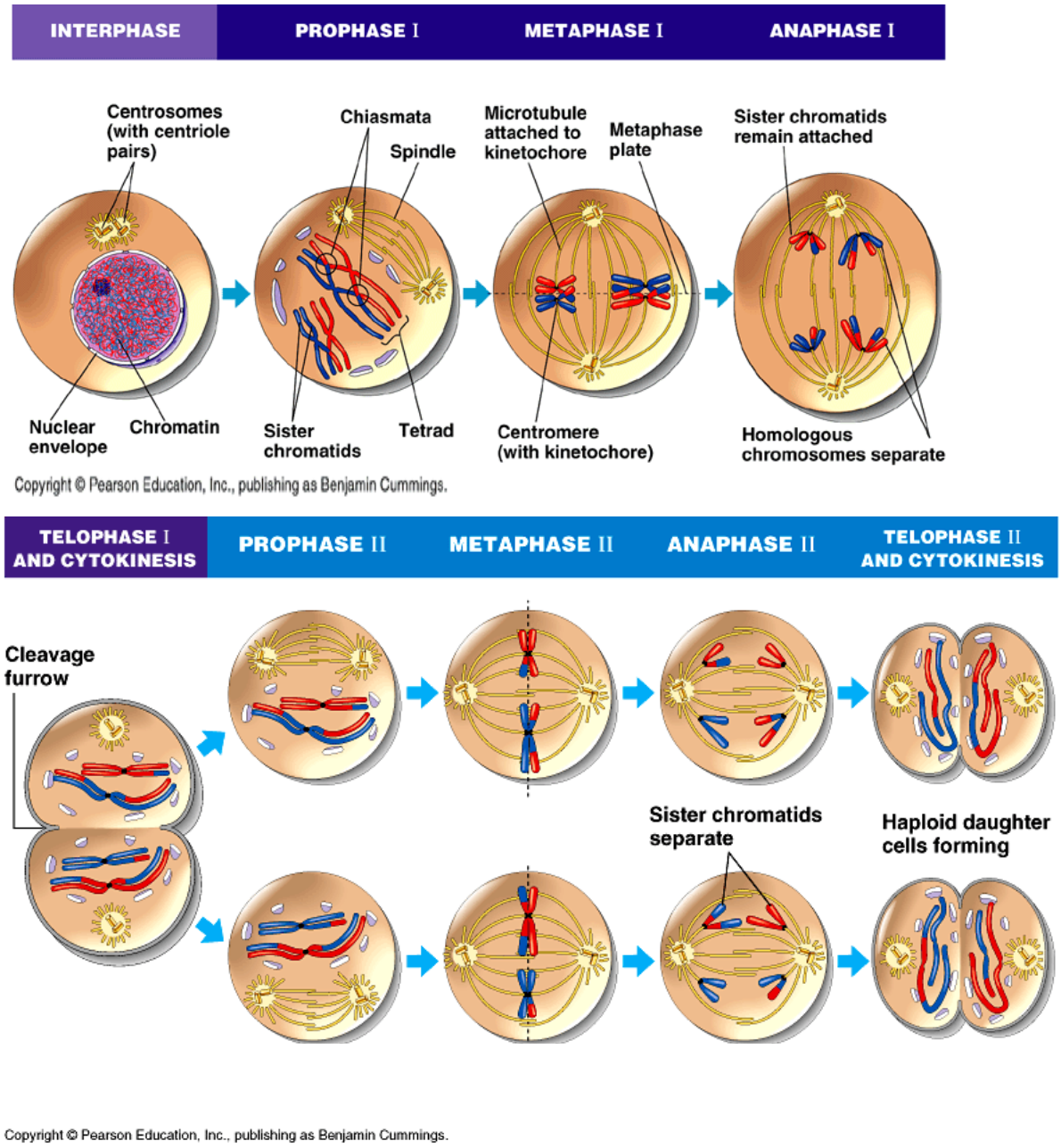

Figure 1: Schematic representation of meiotic stages. *Paternal and maternal chromosomes are visualized by blue and red, respectively. On the top, there is the interphase and first three stages of meiosis I. On the bottom, there are the last two stages of meiotic division I and the entire meiosis II. (Taken from © Pearson Education Inc. published by Benjamin Cummings).*

If the segregation process fails, chromosomes (or chromatids) are not correctly separated to opposite poles. This nondisjunction results in aneuploid gametes. The term aneuploidy defines any chromosome set differing from wild type in the number of chromosomes (Griffiths et al. 2000). Most reported aneuploidies are trisomies, with three chromosome copies, or monosomies, with only one. They are known to be the most common causes of miscarriages and genetic diseases in humans, often incompatible with life (Hassold and Hunt 2001; Nagaoka et al. 2012). Despite many approaches, basic mechanisms of meiosis are not known in all details. Researchers investigate this process utilizing *C. elegans* and other model organisms in hope to better understand the risk factor for chromosomal segregation.

4.2 *Caenorhabditis elegans*, the model organism used in this thesis

Introduction of *C. elegans* happened in the early 1960s, when Sidney Brenner studied the development of nervous system on this worm (Brenner 1988). Few years later, it became the first metazoan with an entirely described cell lineage (Sulston and Horvitz 1977; Kimble and Hirsh 1979) and completely sequenced genome (*C. elegans* Genome Consortium, 1998). Since then, researches work with *C. elegans* in a variety of studies to elucidate basic mechanisms functioning in many different pathways to use it as model system to understand human diseases and basic mechanisms in biology.

C. elegans is a nematode (round worm) belonging to the clade Ecdysozoa characterizing animals that molt their cuticle (Bourlat et al. 2008). It can be found in organic-rich soils, where it feeds of microorganisms. In laboratory conditions, it is cultivated on agar plates seeded with the *E. coli* strain OP50, which the worm indigests. This strain cannot synthetize uracil and is therefore restricted to form a small bacterial lawn generating good conditions for worm cultivation, observation and mating (Brenner 1974; Corsi et al. 2015). Adult worms reach the length of 1 mm (figure 2). They live mostly as self-fertilizing hermaphrodites carrying 5 autosomes and two X-chromosomes (XX). Males are born with a frequency of 0,002% as a result of X-chromosome nondisjunction with only one X-chromosome (XO) (Hodgkin and Brenner 1977). Worm sexes can be distinguished best by body morphology differences either in the L4 larval stages or adult worms (figure 2): L4 hermaphrodites have a developing vulva appearing as transparent half-circle in the central region of their bodies. The only characteristics of L4 males is their wider tail. However, when males reach adulthood, their tails become fan-shaped and can be clearly distinguished form the tapered tail of adult hermaphrodites (Corsi et al. 2015). The life cycle of *C. elegans* is very fast, even though larvae have to mature through four larval stages in order to become adults (figure 2). Hermaphrodites lay approximately 200-300 eggs that need about 3.5 days at 20°C to become egg-laying adults. If the environmental conditions are not favorable for further growth, like in absence of nutrients, worms may enter an arrested state called the dauer larvae, at the end of the L2 larvae, in which their development is arrested for many months.

The dauer state ends when the animal experiences favorable conditions, like upon contact with bacteria. The animal exits the dauer stage, starts to feed, and after about 10 hours it molts to the L4 stage (Hu 2007). Moreover, *C. elegans* life cycle can be slowed or accelerated by growth on temperatures ranging from 14 to 25°C. All this makes the worm easy to maintain and manipulate.

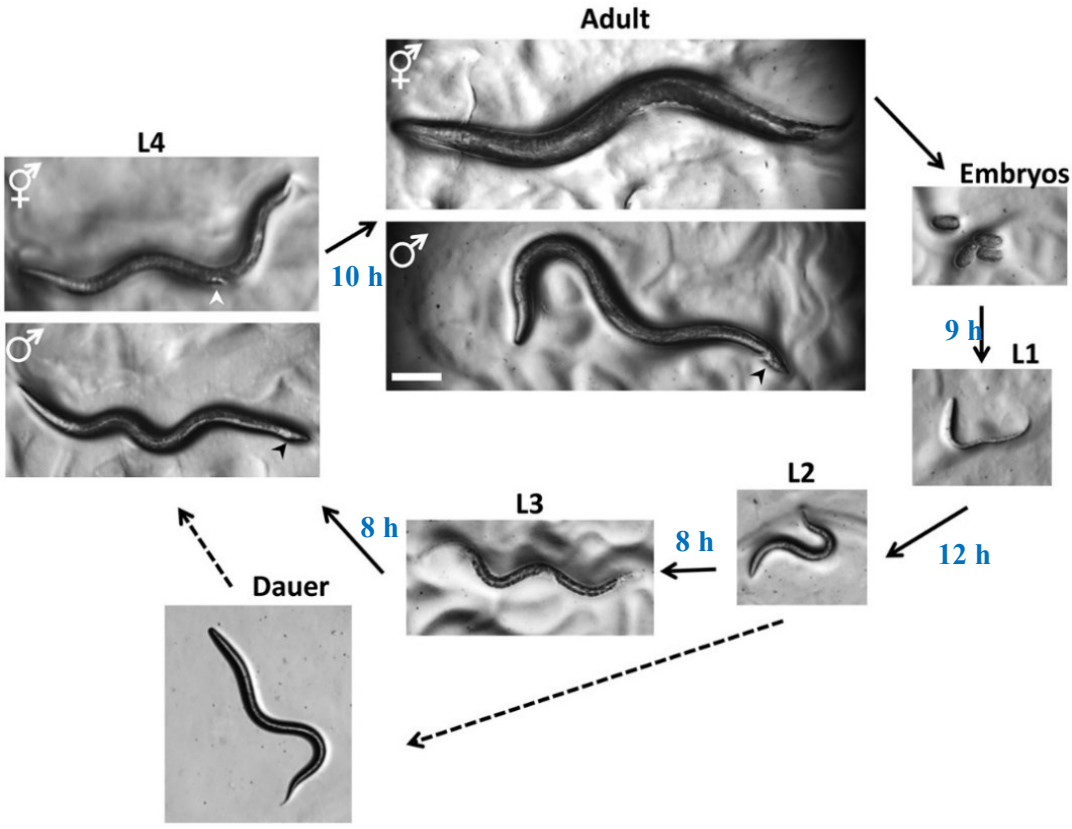

Figure 2: Life cycle and larval development of C. elegans. *Pictures illustrate the body morphology of all developmental stages. Black arrowheads depict the characteristic feature of males, the fan-shaped tails, while white arrowhead shows the transparent developing vulva of L4 hermaphrodites. C. elegans life cycle comprises the ex utero development of embryos and four larval stages. Dauer is arrested development of L2 larvae that occurs only in absence of favorable growth conditions. (Taken from © 2015 Ann K. Corsi, Bruce Wightman, and Martin Chalfie, WormBook).*

Despite the rapid life cycle, large brood size and easy cultivation, there are many other features that make *C. elegans* suitable for basic or advanced studies of meiosis. Homozygous mutations (if not lethal) can be easily obtained and maintained through self-fertilization of hermaphrodites (Brenner 1988). Mutations causing sterility or lethality are balanced with specific chromosomal balancers that keep the mutation of interest in heterozygosity by preventing the recombination and being lethal if homozygous. In addition, balancers carry markers or mutations enabling easy visual selection of mutant and wild-type phenotypes (Edgley et al. 2006). Due to the short life cycle and the hermaphrodite genetics, *C. elegans* is a great model organism for forward and reverse genetic

approaches. Advanced genetic techniques such as gene-editing, RNA interference or CRISPR facilitate rapid generation of targeted mutants. All data are easily accessible in various databases such as WormBase (https://wormbase.org/), WormBook (http://www.wormbook.org/) or WormMethods (http://www.wormbook.org/toc_wormmethods.html) (Corsi et al. 2015). Moreover, its gonad, where nuclei of meiotic prophase I are arranged in spatiotemporal manner (Hillers et al. 2017), is suitable for high resolution cytological analysis of chromosomes and nuclear organization, and the readily accessible meiotic time course allows the identification of primary defects in mutants. Overall, *C. elegans* is a model organism amenable to a wide range of genetic, molecular, cytological and biochemical approaches to study meiosis. The transparency of the animal throughout the life cycle makes it possible to not only image development, but also processes taking place in the gonad, such as chromosome dynamics, oocyte formation and many more.

4.3 Meiosis in *C. elegans* hermaphrodites

4.3.1 Reproductive system

Adult hermaphrodites have two gonads that open into one common uterus and vulva (figure 3). Both arms display distal-proximal polarity. Mitotically proliferating cells are located at the distal tip of the gonad (DG), while the spermatheca opens into the uterus at the proximal end (PG). Meiotic cells move proximally as they progress through meiotic stages. Since the spermatheca (Sp) stores sperm produced during the L4 stage, oocytes are the only germ cells generated during adulthood (Hubbard and Greenstein 2000).

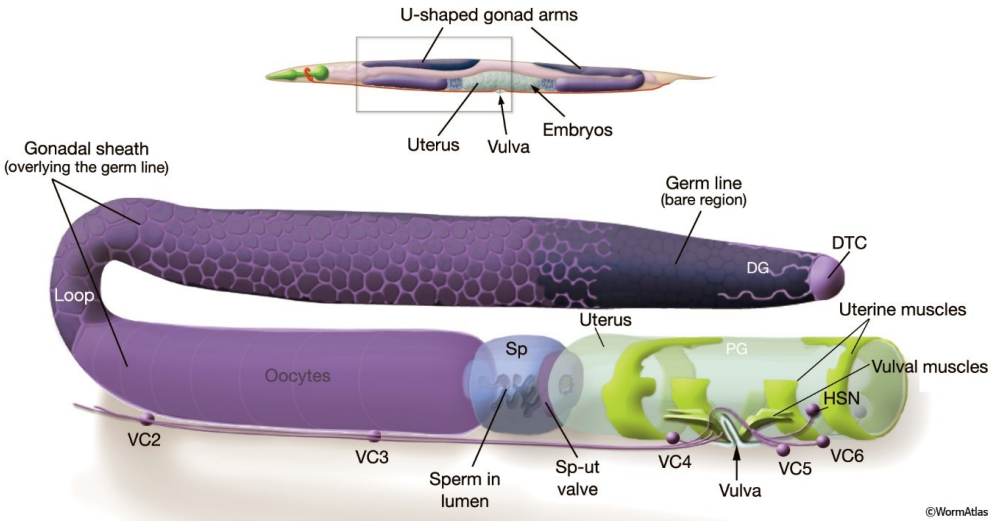

Figure 3: Schematics of reproductive system in adult hermaphrodite. *Top: two gonads build the reproductive organ. Bottom: enlargement of one gonad with distal (DG) and proximal gonad parts (PG). Distal tip cell (DTC) is the distalmost gonad part. The most proximal is the uterus. It is connected with the Spermatheca (Sp) via the spermathecal-uterine valve (Sp-ut). Motor neurons VC1-6 and HSNL/R promote laying of eggs through the vulva (Taken from © 2009 Lints and Hall, Reproductive system, overview. In* WormAtlas*).*

4.3.2 Meiotic prophase I

Accurate development and function of adult germline is ensured by a single somatic cell, called Distal Tip Cell (DTC in figure 4) that is located at the distalmost part of the gonad (Hall et al. 1999). DTC cytonemes reach adjacent cells to maintain their self-renewal abilities (Crittenden et al. 2003). Stem-cells proliferate mitotically creating a niche called the mitotic zone. As cells move towards the proximal end of the mitotic zone, they start to undergo premeiotic DNA replication and soon thereafter they enter meiosis and start to express meiosis specific proteins (Hillers et al. 2017).

The first two meiotic stages, leptonema and zygonema, are commonly referred to as the transition zone, where the chromatin adopts a specific crescent shape. In the transition zone, replicated chromosomes move actively within nuclei in order to achieve side-by-side alignment without entanglements, which gets fixed by the establishment of the synaptonemal complex (SC), an intricate structure made up of many proteins (Hillers et al. 2017). Chromosome movement is facilitated by specific *cis*-acting regions, represented by repetitive DNA sequences called homology recognition regions (HRRs) or pairing centers (PCs), that are located near chromosome ends (Villeneuve 1994; McKim et al. 1988; Sanford and Perry 2001). PC sequences are bound by the HIM/ZIM proteins to form nucleoprotein complexes (Phillips and Dernburg 2006). They trigger the PCs to locate next to the nuclear envelope and as a consequence the SUN-1 and ZYG-12 proteins comprising proteins that locate in the inner and outer nuclear envelope, couple to the site of PCs (Sato et al. 2009). They form SUN/KASH bridges that span the nuclear envelope. The SUN/KASH couples to the PC nucleoprotein complexes in order to connect the chromosome ends to the nuclear periphery. The SUN/KASH bridge connects the chromosomes via their PCs to the cytoskeleton and motor proteins to facilitate the movement of chromosomes within nuclei (Penkner et al. 2009; Sato et al. 2009). Tracking of PC nucleoprotein complexes demonstrated their short as well as long range movements, either in groups, pairs or solo (Baudrimont et al. 2010; Wynne et al. 2012). Despite bringing homologs in close juxtaposition, this dynamic behavior prevents pairing between non-homologous chromosomes by enabling their dissociation and facilitates the assembly of the SC between homologous chromosomes.

Paired chromosomes become stabilized by the SC (Sato et al. 2009; MacQueen et al. 2002), leading to disappearance of the half-moon shaped appearance of the chromatin. The SC is a specific protein structure between the aligned homologs. It is composed of central region that contains transverse filaments necessary to bridge the axial elements between the paired homologs. The central region is composed of six SYP proteins that are interdependent for their loading on the chromosomes. SYP proteins interact with axis components of homologs (MacQueen et al. 2002; Colaiácovo et al. 2003). The assembly of the axis requires HORMA-domain proteins HIM-3, HTP-1/2 and HTP-3 that each have either specific or redundant function (Zetka et al. 1999; Couteau and Zetka 2005; Martinez-Perez

et al. 2005; Kim et al. 2014). Once that the SC is fully established, it can be visualized by the spaghetti-like alignment typical for pachynema (figure 4 and figure 5). The SC is believed to promote recombination that results in formation of crossovers between homologs and to regulate crossover interference (MacQueen et al. 2002). Successfully designated crossovers trigger the disassembly of the SC and progression of nuclei to diplonema (Nabeshima et al. 2005), which is located at the loop of the gonad (figure 4). During the diplotene stage, paired chromosomes undergo remodeling in order to be condensed to 6 bivalents (Hiller et al. 2017) that are characteristic for diakinesis oocytes (figure 5). Diplonema condensation redistributes axial and SC proteins generating a specific bivalent organization. Since chromosomes are holocentric, crossover position regulates this organization in functionally distinct domains (de Carvahlo et al. 2008). Each bivalent has short and long arms (Albertson et al. 1997). As a result of mentioned reorganization, HTP-1/2 and LAB-1 become localized at long arms and SYP proteins at short arms, whereas HTP-3 is concentrated at both arm types (Martin-Perez et al. 2008). The function of this redistribution is not fully understood. However, it is believed to support the correct chromosome segregation. Moreover, the characteristic marks of short and long arms can be used to visualize bivalent organization, since bivalents serve as first readout of recombination defects. Diakinesis oocytes fill the entire space of gonads and mature as they progress towards the spermatheca. The most mature oocyte is the one that is in immediate vicinity to the spermatheca (figure 5). Meiotic prophase I ends, when oocytes leave the stage of diakinesis and in worms, they undergo an arrest at metaphase I. Fertilization triggers the meiotic divisions.

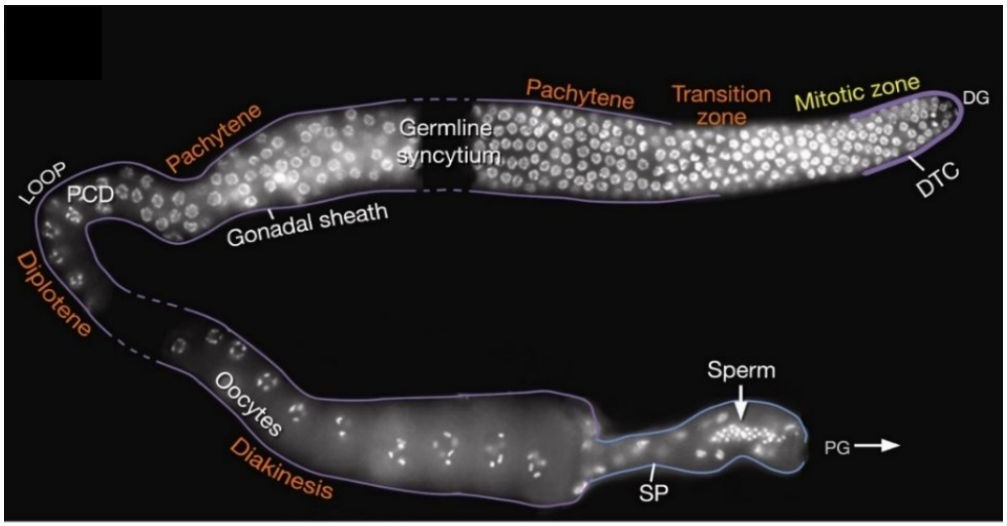

Figure 4: DAPI-stained gonad of adult hermaphrodite. *Distal Tip Cell (DTC) creates together with mitotic cells the niche called Mitotic zone at the distal tip of the gonad (DG)* ***Zones of meiotic prophase I:*** *Transition zone, pachytene zone, the progression between pachytene and diplotene stages is situated in the loop of the gonad, PCD are cells undergoing programmed cell death, diplotene zone and diakinesis show oocytes, that fill the entire space of the gonad and mature as they move proximally towards the spermatheca (SP). Sp opens to the uterus (not shown) at the proximal end of the gonad (PG) (Taken from: J. Maciejowski and E.J. Hubbard. © 2009 Lints and Hall, Reproductive system, germ line. In* WormAtlas*).*

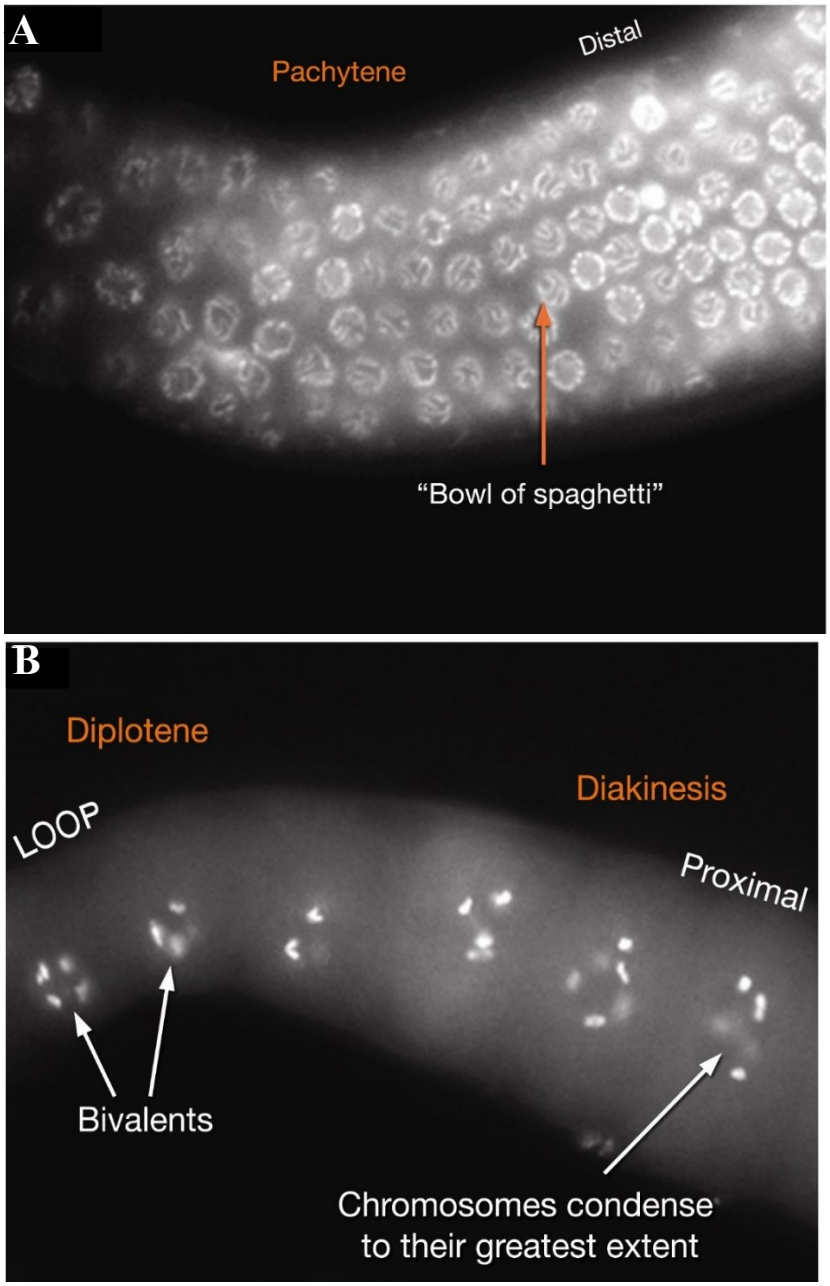

Figure 5: Parts of DAPI-stained gonads of adult hermaphrodites (A) *Pachytene stage with nuclei showing the spaghetti-like shape of chromosomes.* ***(B)*** *Diplotene zone with oocytes progressing proximally towards the diakinesis that contains chromosomes with the greatest degree of condensation. (Taken from: J. Maciejowski and E.J. Hubbard. © 2009 Lints and Hall, Reproductive system, germ line. In* WormAtlas*).*

4.3.3 Recombination

Key events taking place during meiotic prophase I serve the purpose of recombination. Its main role is the formation of crossovers between homologous chromosomes that in cooperation with cohesion secure the accurate segregation of homologous chromosomes during the first meiotic division. The second essential aspect of crossovers is the inter-homolog exchange of genetic material that lays the basis for new combination of alleles (Alberts et al. 2002).

Recombination is initiated, when the topoisomerase SPO-11 induces double strand breaks (DSBs) along replicated chromosomes (Dernburg et al. 1998; Keeney 2001). In absence of DSBs induction, like in the *spo-11* mutant, crossovers cannot be formed, therefore in *spo-11* diakinesis, nuclei display 12 achiasmatic chromosomes, also known as univalents (Hiller et al. 2017). Even if the breaks are programmed, they may cause harmful genome rearrangements. Therefore, distinct repair pathways to restore the integrity of genome are in place (figure 6). The break can be repaired either by non-homologous end joining (NHEJ) or homology directed repair (HDR). In contrast to the HDR, the NHEJ doesn't require homologous template. In my thesis, I focused more on the HDR, as it is the predominant repair pathway used in the *C. elegans* germline. Repair of DSBs starts with a process called resection, during which exonucleases cleave broken strands that end with 5'-termini in order to reveal 3'-single stranded overhangs (Sun et al. 1991). MRE-11 has been shown to cooperate with RAD-50 and NBS-1 as part of the MRN complex soon after the DSBs induction by removing SPO-11, which is covalently linked to generated breaks, and by resecting the breaks together with COM-1 (Girard et al. 2018). EXO-1 is another exonuclease which contributes to the resection in absence of COM-1 or when MRE-11 is compromised (Yin and Smolikove 2013). Resected ssDNA is immediately stabilized by the nucleoprotein RPA-1 that is then substituted, thanks to BRC-2, with RAD-51 generating a RAD-51 nucleoprotein filament (Alpi et al. 2003; Martin et al. 2005). The function of RAD-51 is to search the region of homology in the entire genome and to mediate strand invasion (Lui and Colaiácovo 2013), during which ssDNA invades dsDNA by displacing its one strand. This generates metastable single-end invasion or nascent D-loop (Hunter and Kleckner 2001). RAD-51 is then removed and followed by second end capturing. Extended D-loop can be then resolved to noncrossovers via ejection of the invading strand during the synthesis dependent strand annealing SDSA (described below) or transformed to a more complex intermediate with two branched homologous duplexes known as the double Holliday junction (Holliday 1964; Schwacha and Kleckner 1994). This intermediate requires specific factors promoting its resolution either to crossover or noncrossover (Hiller et al. 2017).

In *C. elegans*, every homologous pair receives mostly one obligate crossover (Hiller and Villeneuve 2003). Factors, that promote crossover maturation, are MSH-4/5 which are the homologs of the yeast

ZMM proteins Msh4 and Msh5, respectively; and SC-associated protein ZHP-3 (Winand et al. 1998; Zalevsky et al. 1999; Jantsch et al. 2004). Those proteins are also known as pro-crossover factors. Their localization into recombination foci exceeds the final number of crossovers in the early pachytene region. In late pachynema they are restricted to the only obligate crossover per homologous chromosome pair (Yokoo et al. 2012), indicating that their presence helps the maturation of recombination intermediates to crossovers. MSH-4 and MSH-5 have been shown to localize as foci on chromosomes, where they bind dHJ intermediates in order to stabilize and protect them against anti-crossover activities. ZHP-3 is initially present along the entire SC in mid pachynema and then gradually becomes restricted to crossover sites in late pachynema as one focus per chromosome pair, likely labeling late crossover sites (Bhalla et al. 2008). Another factor mediating a positive crossover outcome, is the cyclin-related protein COSA-1. It is considered to reinforce the crossover formation and mark the late crossover sites as well (Yokoo et al. 2012). However, genetic evidence suggests that it already acts at a much earlier time to drive the crossover designation. Mutants lacking MSH-4/5 or ZHP-3 display 12 univalents at diakinesis in *C. elegans* (Zalevsky et al. 1999; Jantsch et al. 2004; Hiller et al. 2017), supporting their important role as crossover promoting factors. An important step for eventual chromosome segregation after the crossover recombination is the cleavage of DNA strands to open the joint molecules for segregation by endonucleases. Depending on the placement of the cut, crossover and noncrossover products will ensue. *C. elegans* has a redundant system of such resolvases. SLX-1 cooperates with MUS-81 in a pathway that is considered to be parallel to the resolution activity of XPF-1 and HIM-6 (Agostinho et al. 2013; Saito et al. 2013). The activities of both pathways are supported by scaffold proteins SLX-4/HIM-18 (Saito et al. 2009; Gaur et al. 2015). Mutants lacking these resolvases display chromatin bridges (Agostinho et al. 2013; Saito et al. 2013). However, these become dissolved by the late function of LEM-3/Ankle1 nuclease before second meiotic division (Hong et al. 2018). Surprisingly, mutants lacking the crossover resolving nucleases generate only 30-50% less crossovers, implying the existence of an extra resolution pathway (Bellendir und Sekelsky 2013).

The above described pro-crossover factors are considered to promote a pathway that generates crossovers also referred to as class I. These are regulated by crossover assurance and interference (Hunter 2015; Hiller et al. 2017). Crossover assurance secures the formation of an obligate crossover that fulfills the condition for correct homologous segregation (Rosu et al. 2011). Crossover interference regulates distribution of multiple crossovers spacing them evenly and widely from each other throughout the chromosome (Hunter et al. 2015). In *C. elegans*, crossover interference appears to prevent the formation of additional crossovers along the entire chromosome, even though autosomes receive occasionally a second crossover (Deshong et al. 2014). This additional exchange seems to differ from obligate class I pathway (Hiller et al. 2017), since it is impossible to detect them by cytology using MSH-5, COSA-1 or ZHP-3 as markers (Youds et al. 2010; Yokoo et al. 2012). They

might be generated by other crossover pathway known as class II. Crossovers of class II have been shown to be resolved by structure-specific nucleases Mus-81-Mms4 in *S. cerevisiae* (de los Santos et al. 2003; Kohl and Sekelsky 2013). In *C.elegans*, there isn't currently any visual marker for class II crossovers. Nevertheless, they seem to occur as shown in mutants lacking MUS-81 or RTEL-1 nucleases that increased the numbers of crossovers (Youds et al. 2010).

Since the quantity of DNA breaks greatly exceeds the number of crossovers, alternative pathways restore genome integrity by producing noncrossovers. The anti-recombinase RTEL-1, that works in the SDSA pathway, has been shown to dismantle inter-homolog invasions at the level of nascent or extended D-loop. Dissociated ssDNA then pairs complementary to the opposite end of the break which is then repaired by extending its ends to generate a noncrossover (Barber et al. 2008; Youds et al. 2010). Despite the RTEL-1 mediated resolution, noncrossovers are produced by process called dHJ dissolution. It is performed by specific STR dissolvasome complex in *S. cerevisiae* or BTR/RTR complex in humans/metazoans (Bizard and Hickson 2014). Functions of this complex are object of studies in many organisms including *C. elegans.*

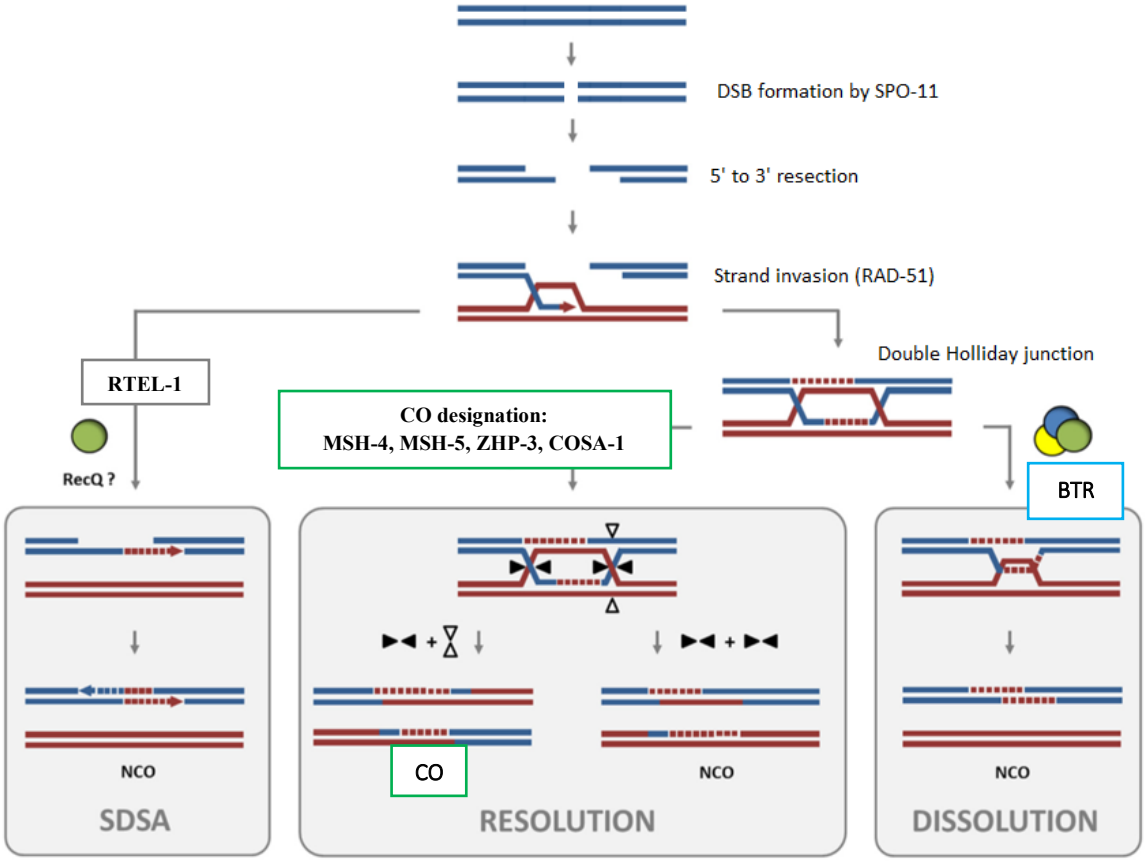

Figure 6: Simplified schematics representing the three different pathways of DSBs repair during meiotic recombination*. Parallel lines of the same color illustrate the sister chromatids. Homologous chromosomes are represented by blue and red. (Taken from Knoll et al. 2014).*

4.4 The dissolvasome complex as recombination chaperone

The process of dHJ dissolution exposed its relevance in mutant situations by preventing toxic genome rearrangements, that may result from excess or defects of homologous recombination (Wu and Hickson 2003; Krejci et al. 2012). The dissolvasome complex is highly conserved in all eukaryotes and certain components were also observed in prokaryotes. It is composed of RecQ helicases, topoisomerase Iα and scaffolding proteins. The scaffolding proteins were observed to vary from organism to organism (Bizard and Hickson 2014). The RecQ helicase was first identified in *E. coli* (Nakayma 2005). Its eukaryotic homologs, that participate on dissolution are known as *Sc* Sgs1 and *Ce* HIM-6 (Cejka and Kowalczykowski 2010; Wicky et al. 2004). In *A. thaliana*, there are two RecQ helicases considered to act redundantly (Séguéla-Arnaud et al. 2016). Humans have five different RecQs, but only BLM is the ortholog of yeast Sgs1 (Kusano et al. 1999). Mutations in BLM are causative of Bloom Syndrome in humans, a cancer prone condition characterized by premature aging, genome instability and developmental defects. Patients' cells show chromosomal aberrations and elevated frequency of sister chromatid exchange (German et al. 1993; Ellis et al. 1995). A similar phenotype of increased occurrence of crossovers was detected in *sgs1* mutants (Ira et al. 2003), revealing the anti-crossover activity of the helicase and likely of the complex. RecQ helicases have conserved core domains giving them their unwinding activity in 3' to 5' direction (Lu et al. 1996). In addition, *Hs* BLM and *Sc* Sgs1 share similar sequences considered to be important for interaction with the other complex members or other proteins. RecQ helicases perform the first step of dHJ dissolution, when they migrate branches of dHJ or more complex intermediates (Karrow et al. 2000; Cejka and Kowalczykowski 2010) towards one another producing an hemicatenated intermediate.

The hemicatenate is subsequently dissolved by the subclass of type IA topoisomerases to yield noncrossovers (Wu and Hickson 2002). Higher eukaryotes contain two topoisomerases of type IA: TOPIIIα and TOPIIIβ, but only TOPIIIα is considered to be functionally homologous to *Ce* TOP-3 (Kim et al. 2000). Topoisomerases of type IA disassemble the hemicatenated intermediate by introducing a break into one strand through which the second uncut strand moves and afterwards, the cut ends are reconnected (Champoux 2001; Bocquet, et al. 2014). Deletion of TopIIIα and its homologs generates various phenotypes. In *S. cerevisiae,* mutants showed chromosomal missegregation and hyperrecombination (Wallis et al. 1989), whereas lethality and developmental defects were observed in mammals, *S. pombe* or *D. melanogaster* (Li and Wang 1998; Godwin et al. 1999; Plank et al. 2005). The activity of strand cleavage and passage is facilitated by the catalytic core region that is conserved among all type IA topoisomerases. In some species they have C-terminal extension carrying a domain with various numbers of zinc fingers (ZnF) motifs. Humans and plants have more than one ZnF, on the contrary, yeast does not have any at all (Bizard and Hickson, 2014). The ZnF motifs are suggested to mediate protein-DNA or protein-protein interactions, but their exact

function is unknown (Berg and Shi, 1996). However, recent studies in *A. thaliana* have shown that zinc fingers harboring domain of *At*TOP3α suppresses together with *At*RMI1 the generation of class II crossovers (Séguéla-Arnaud et al. 2016), and that the ZnF called T1, which is conserved in all homologs of *Hs* TOP-IIIα, plays an important role by targeting the topoisomerase to specific DNA structures that arise during the repair of DNA replication intermediates like the dHJ (Dorn et al. 2018).

Other important components of the complex are the scaffolding proteins RMI1 and RMI2 (in some higher eukaryotes). Similar to TOPIIIα, RMI1 homologs are important in *S. pombe*, *A. thaliana*, *C. elegans* and mammals (Mullen et al. 2005; Hartung et al. 2008; Guiraldelli et al. 2013; Jagut et al. 2016). *Drosophila melanogaster* is an exception in that its genome does not encode any RMI1 homolog (Chen et al. 2012). The OB1 domain has been shown to be conserved among RMI1 proteins. Its function is to interact with helicase and topoisomerase. Human RMI1 has an additional OB2 domain for interacting with RMI2 (Bizard and Hickson 2014). An essential role of RMI1 scaffold protein is to increase the dissolution efficiency (Raynard et al. 2006; Cejka et al. 2010). It doesn't have any catalytic function, but it affects the dynamics of decatenation by stabilizing the open form of topoisomerase type Iα (Cejka et al. 2012; Bocquet et al. 2014). In addition, it has been found to form stable heterodimer only with Top3, generating a subcomplex (TR) which can work without the helicase (Chen and Brill 2007).

Many studies indicated, that dHJ dissolution is not the only function of the complex. In fact, it may act as a recombination chaperone. Figure 7 is depicting a model for the activities of STR (Sgs1-Top3-Rmi1) or TR (Top3-Rmi1) complexes proposed by two independent studies in yeast (Kaur et al. 2015; Tang et al. 2015). An early role is to prevent the stabilization of aberrant single-end invasions that are known to give rise to inter-sister or multichromatid connections in the absence of STR (Oh et al. 2007). Sgs1 has been suggested to avoid their accumulation (Oh et al 2007; Zakharyevich et al. 2012), but in vitro studies indicate, that Sgs1 may not work alone, since it can only dismantle Rad51-free D-loops (Fasching et al. 2015). On the contrary, Top3 cuts Rad51 coated ssDNA and increases Sgs1 affinity for branched DNA in vitro (Cejka et al. 2010; Fasching et al. 2015). In consequence of these findings, the complex members are proposed to work together on early intermediates. Sgs1 unwinds aberrant D-loops and prepares the substrate for Top3-Rmi1 decatenation. This activity makes the complex act as a chaperone that channels disassembled invasions towards different fates. They can be repaired as noncrossovers by SDSA or returned back to the state of a free singled stranded Rad51 covered intermediate, which can start the invasion again and eventually become stabilized by ZMMs as potential crossovers (Kaur et al. 2015; Tang et al. 2015). This indirect role in crossover regulation has been already proposed for BLM homologs in *D. melanogaster* or *S. pombe*, when their depletions showed reduced levels of crossovers (McVey et al.,2007; Cromie et al. 2008) or in *C. elegans*, when

him-6 generated a subset of achiasmate diakinesis and accumulated RAD-51 indicating disrupted processing of early intermediates (Wicky et al. 2004; O'Neil et al. 2013).

By resolving ectopic early intermediates, STR complex prevents the accumulation of aberrant off-pathway molecules. Some off-pathway molecules have a topology that specifically requires the action of TR as suggested by the model in yeast, else they can also be eliminated by the Mus81 endonuclease. The cleavage products are a mixture of crossovers and noncrossovers. Since absence of the TR complex led to formation of intermediates causing chromosomal missegregation, TR has been suggested to remove a fraction of aberrant molecules in an Sgs1-independent way (Kaur et al. 2015; Tang et al. 2015). Additionally, in *A. thaliana*, TOP3α-RMI1 were shown to suppress additional crossovers resulting from unregulated class II crossover pathway intermediates (Séguéla-Arnaud et al. 2016). This coincides with the model in yeast, where TR prevents the formation of intermediates, whose structure requires Mus-81 Mms4 mediated resolution. Such structures differ from regulated dHJ and could arise through ectopic invasions indicating that the complex acts as surveillance on early and late intermediates to ensure the accurate noncrossover as well as crossover resolution (Kaur et al. 2015; Tang et al. 2015).

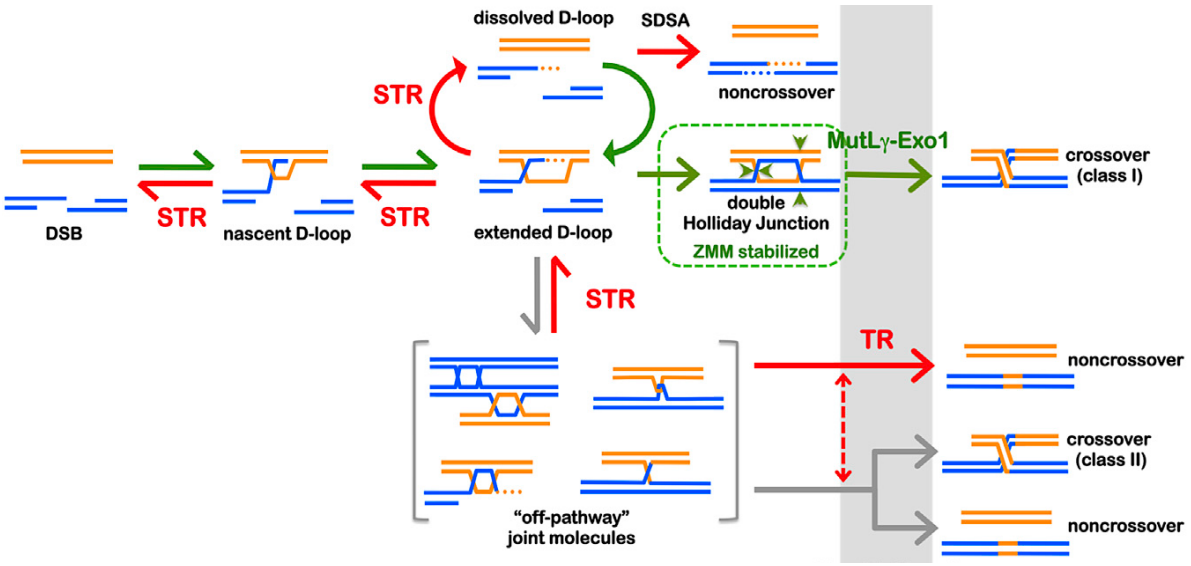

Figure 7: Model depicting different types of intermediates that are resolved/dissolved by STR and TR complex during prophase I of S. cerevisiae meiosis. *It illustrates the indirect role of STR activity which channels resolved intermediates either back to earlier steps of recombination or towards distinct pathways leading to noncrossover or crossover resolution. Off-pathway joint molecules have aberrant topology that requires dissolution activity of the complex. Indicated late function of TR complex that dissolves aberrant off-pathway molecules indirectly promotes their late resolution to noncrossovers. Some joint molecules have been suggested to require cooperation between TR and nucleases (characterized by dashed red line) which may resolve aberrant JMs to noncrossovers or crossovers of class II (Taken from Tang et al., 2015).*

4.5 The activities of the dissolvasome complex in *C. elegans*

Over the past years, many studies revealed the importance of the dissolvasome complex for accurate regulation of recombination (Wicky et al. 2004; O'Neil et al. 2013; Schvarzstein et al. 2014; Jagut et al. 2016). The aforementioned model in yeast explains in detail that despite the dHJ dissolution, the STR and TR complexes can act as a recombination chaperone. They remove aberrant joint molecules and with this contribute to recombination at different levels (depicted above in chapter 4.4). Since yeasts are unicellular, researchers analyze different model organisms in the hope to understand the activities of the complex in metazoans. Development of tools and *in situ* markers that can be applied in *C. elegans* cytology and genetics enabled the progress of such studies by visualizing different recombination steps upon which the dissolvasome may act.

HIM-6 is considered to facilitate the generation of noncrossovers as well as class I crossovers (Schvarzstein et al. 2014; Hatkevich and Sekelsky 2017). As already mentioned, mutants lacking the helicase fail to display RAD-51 turnover in recombination foci in a wild-type manner (Wicky et al. 2004; O'Neil et al. 2013). This suggests an early role that may be analogous to the yeast, where the helicase (eventually together with TR) is involved in D-loop disassembly. These single-end intermediates can be channeled back to the invasion process or repaired by SDSA to mature into noncrossovers. In addition, *him-6* mutants showed an increased frequency of inter-homolog connections that persisted in diakinesis and were independent of pro-crossover factors. This implies the role of HIM-6 in disassembling the intermediates which were not determined to become crossovers (Schvarzstein et al. 2014). Another function of the helicase was exposed, when a subset of intermediates didn't mature to crossovers, even though *him-6* mutants loaded pro-crossover factors in wild-type manner (Schvarzstein et al. 2014). This coincides with findings that HIM-6 may act in combination with XPF-1 in the crossover resolution pathway parallel to SLX-1-MUS-81 resolution (Agostinho et al. 2013). HIM-6 is proposed to unwind dHJ producing an intermediate that can be resolved by XPF-1 to mature crossover. However, it is unclear, whether HIM-6 and XPF-1 interact physically and how they cooperate by coordinated resolution of duplex branches (Hatkevich and Sekelsky 2017).

C. elegans has two RMI1 homologs RMH-1 and RMH-2. A study performed by Jagut et al. focused on RMH-1, since the *rmh-2* mutant didn't display any major meiotic defects. The double mutant *rmh-1(jf54); rmh-2(jf94)* was inviable, suggesting a redundant function of the two genes during development (Jagut et al. 2016). RMH-1 was shown to promote the crossover outcome, since the mutant displayed the presence of univalents at diakinesis stages. A functional RMH-1::GFP transgenic line showed distinct localization into repair foci. They appeared on chromosomes in early pachynema, and gradually increased to about 25 foci in mid pachynema. In late pachynema RMH-1 was found in

the six crossover precursor sites, where it co-localized with ZHP-3 or COSA-1 which are validated as crossover markers. By high resolution microscopy it has been shown that RMH-1 colocalized with HIM-6 in form of doublets or as one lengthened focus on the intermediates that are designated to become crossovers (Jagut et al. 2016; Woglar and Villeneuve 2018). RMH-1 is required to stabilize and enrich HIM-6 in foci, in fact, HIM-6 foci were completely absent or smaller and fainter. HIM-6 is required for RMH-1 localization in mid pachynema but not in late pachynema, because in *him-6* mutants, RMH-1 still localized in late pachynema, even though with reduced numbers compared to wild type. In addition, localization of RMH-1 is independent of ZMMs during early and mid pachynema, and at this stage a mixture of foci co-localizing with MSH-5 and foci free of MSH-5 signal can be found. This might imply that RMH-1 foci free of MSH-5 are those recombination intermediates undergoing dissolution together with TOP-3. The presence of RMH-1 foci at later pachytene stages strongly depends on pro-crossover factors, such as ZHP-3. In the end, Jagut et al. showed that RMH-1 suppresses excessive non-homologous recombination in parallel to SMC-5. Additionally, it is involved in positioning the crossovers near chromosome arms, known to be important for correct differentiation of bivalents and with this it suppresses the accumulation of crossovers in the chromosome center (Jagut et al. 2016).

C. elegans TOP-3 (homolog of *Hs* TOPIIIα and *Sc* Top3) was shown to relax negatively supercoiled DNA in vitro (Kim et al. 2000). Hermaphrodites with depleted TOP-3 by RNAi exhibited partial loss of function phenotype displaying either full sterility or wild-type fertility. Sterile individuals contained abnormal gonads with several defects: longer transition zone, short late pachynema and aberrant bivalents in diakinesis (Kim et al. 2000). Moreover, depletion of TOP-3 by RNAi led to increased levels of RAD-51, suggesting defects in early steps of recombination (Wicky et al. 2004). Beside the catalytic domain, the C-terminus of TOP-3 carries the GRF domain containing one C4 ZnF motif. The GRF domain is defined by three conserved amino acids Gly Arg and Phe in the centre. The function of the ZnF as well as the role of TOP-3 in general in meiosis remain to be elucidated and are subjected to ongoing studies in my hosting lab. The activity of the ZnF motif was investigated in the course of this master thesis.

4.6 Aim of the study

Homologs of *Hs* TOPIIIα contain up to five ZnF motifs that share more than 50% of amino acids with ZnF motifs of other model organisms, indicating their conserved role among eukaryotes (alignment displayed in figure 8 taken from Séguéla-Arnaud et al. 2016). Zinc fingers are considered to mediate interactions between proteins or DNA by utilizing Zinc as chelator (Berg and Shi, 1996). However, which activities these interactions mediate or how important the topoisomerase III ZnF motifs are in recombination, remains to be understood. The C-terminus of Top3α in *D. melanogaster*, that harbors

the ZnF has been shown to interact with DNA and Blm, which were postulated to have important functions for the dissolution reaction *in vivo* (Plank et al. 2004; Hartman Chen et al. 2012). A recent study in *A. thaliana* proposed, that four ZnF motifs of *At*TOP3α cooperate with the OB2 domain of *At*RMI1 in the suppression of additional crossovers (Séguéla-Arnaud et al. 2016) and that the ZnF T1 is particularly important for targeting the topoisomerase to specific recombination intermediates (Dorn et al. 2018).

The aim of this master project was to investigate the function of the ZnF motif in TOP-3 during meiotic prophase I in *Caenorhabditis elegans*. Applying reverse genetics (CRISPR/Cas9 mediated genome modifications), I deleted the motif and generated a truncated version of TOP-3 lacking only the ZnF. This allowed me to examine its phenotype in the *C. elegans* germline in combination with various factors, that are known to be essential in meiotic recombination. Moreover, I added a tag to the truncated version in order to be able to detect the truncated protein. This enabled me to perform the cytological analysis of its localization as well as potential effect of the ZnF deletion on other complex members. Using different types of assays, I set out to analyze the role of the ZnF that may affect different recombination intermediate in comparison with the topoisomerase domain mutation, which is an actual subject of studies in my hosting lab. The long-range goal of this project was: 1) to gain deeper insight into the multiple functions of the dissolvasome complex during meiosis 2) and to differentiate whether the ZnF motif is only needed for a subset of those activities or whether it is necessary for all activities.

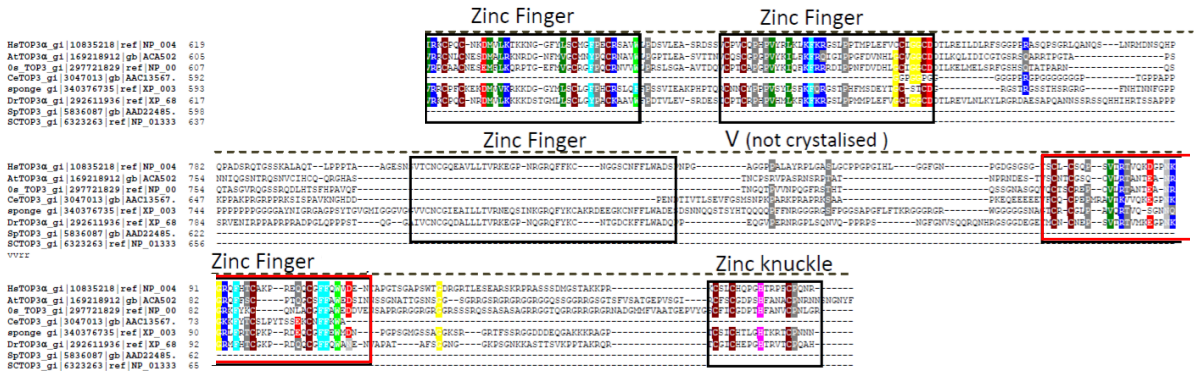

Figure 8: Aligned protein sequences of TOP-3 zinc-finger motifs show colorized amino acids that are conserved in more than 50% of depicted species: *Hs: Homo Sapiens, At: Arabidopsis Thaliana, Os: Oriza Sativa, Ce: Caenorhabditis elegans; Aq: Amphimedon queenslandica, Dr: Danio rerio, Sp: Schizosaccharomyces pombe, Sc: Saccharomyces cerevisiae. Zinc-finger of C. elegans is marked with the red square (Taken from Séguéla-Arnaud et al. 2016).*

5. Materials and Methods

5.1 Worm strains

Worms were fed with *E.coli* strain OP50 and maintained on nematode growth medium plates at 20°C/16°C or when sealed, at 14°C.

Materials used:

Nematode Growth Medium (NGM):

- 3 g/l NaCl
- 3.5 g/l peptone
- 17 g/l agar
- add double distilled water to reach final volume of 1l

autoclave and add:

- 1 ml cholesterol (5 mg/ml)
- 1 ml 1 M $CaCl_2$
- 1 ml 1M $MgSO_4$
- 25 ml 1 M KH_2PO_4 (pH 6)
- 50 mg/l streptomycin
- 50 mg/l nystatin

Strains listed in table 1 were generated using two distinct techniques:

5.1.1 Generation of strains by crossing

Crosses were performed on mating plates (plate with small drop of bacteria) by combining L4/young adult hermaphrodites and males in a ratio 1:3. Worms were allowed to mate for two days at 16°C. After that, hermaphrodites were singled on new small plates and kept at 16°C or 20°C. Successful mating resulted in 50% male offspring.

5.1.2 Generation of strains by homology-directed genome editing

Genes of interest were edited by CRISPR-Cas9 system. Specific mutations were introduced using designed repair templates (table 2). To start the procedure 40 to 50 L4 hermaphrodites were incubated for 24h at 16°C. On the next day, injection mix was prepared and injected into one gonad of prepared worms. After that worms were singled on small plates and stored for 24h at 20°C, moved on fresh plates and stored again for 24h at 20°C. Their progeny was screened for rollers, an injected co-event,

as a possible carrier of mutations of interest. We increased the likelihood of HDR by using the method of co-injection with second marker (Paix et al. 2015). We co-injected CRISPR for *dpy-10* locus that in case of successful insertion generates dominant roller phenotype. This facilitates easier detection of desired edit (Paix et al. 2015; Arribere et al. 2014).

Materials used:

One locus editing injection mix using home-made Cas9:

- 6 µl of Cas9 prep (10 µg/ µl)
- 5 µl of tracrRNA (4 µg/ µl)
- 0.4 µl of dpy-10 crRNA (8 µg/ µl)
- 0.55 µl of dpy-10 ssODN (500 ng/ µl)
- 1 µl of crRNA of targeted gene 8 µg/µl
- 2.2 µl of ssODN of targeted gene 1µg/µl
- 0.5 µl of KCl (1M)
- 0.75 µl of Hepes pH 7.4 (200mM)
- add water to reach final volume of 20 µl

Multi-loci editing injection mix using home-made Cas9:

- 5 µl of Cas9 prep (10 µg/ µl)
- 6.7 µl of tracrRNA (4 µg/ µl)
- 0.4 µl of dpy-10 crRNA (8 µg/ µl)
- 0.55 µl of dpy-10 ssODN (500 ng/ µl)
- 0.75 µl of crRNA1 of targeted gene 8 µg/µl
- 0.75 µl of crRNA2 of targeted gene 8 µg/µl
- 2.2 µl of ssODN of targeted gene concentration
- 0.5 µl of KCl (1M)
- 0.75 µl of Hepes pH 7.4 (200mM)
- add water to reach final volume of 20 µl

Table 1: *List of strains and genotypes.*

strain	genotype
1	*N2 (Bristol wild type)*
121	*spo-11(ok79) //nT1[qIs51] (IV;V)*
1163	*mus-81(tm1937)I*
1269	*him-6(jf93[him-6::ha]) IV; jfsi38 [gfp::rmh-1, cb-unc-119(+)] II*
1417	*oxTi539[eft-3p::TdTomato::H2B::unc-54 3UTR + Cbr-unc-119(+)] III*
1457	*T07C12.12(jf94[T07C12.12::unc-119(+)]) V./nT1 [qIs51] (IV;V)*
1481	*CB4856 (Hawaii wild type)*
1601	*mus-81(tm1937); lem-3(mn155)/hT2*
1702	*lem-3(mn155)*
1960	*cosa-1::ollas III; msh-5::gfp IV*
2075	*top-3_ZnF(jf153)*
2089	*him-6(jf93[him-6::ha]) IV; jfsi38 [gfp::rmh-1, cb-unc-119(+)] II, top3_ZnF(jf153)*
2097	*top-3_ZnF(jf153) in CB4856 (Hawaii wild type)*
2098	*top-3_ZnF(jf153) / hT2*
2108	*lem-3(mn155); top-3_ZnF(jf153)*
2109	*spo-11(ok79)/nT1IV/V; top-3_ZnF(jf153)*
2132	*mIn1[mIs14 (gfp)rol-1(e91)]/dpy-25(e817) II.*
2134	*mus-81(tm1937); top-3_ZnF(jf153)*
2136	*cosa-1::ollas top-3_ZnF(jf153) III; msh-5::gfp IV*
2143	*mus-81(tm1937); lem-3(mn155)/hT2; top-3_Znf(jf153)/hT2*
2144	*cosa-1::ollas III; msh-5::gfp,T07C12.12(jf94[T07C12.12::unc-119(+)])V./nT1[qIs51]*
2163	*top3::ha(jf158)*
2164	*top3_ZnF::ha(jf159)*
2152	*mIn1[mIs14 (gfp)rol-1(e91)]/dpy-25(e817) II; top-3-ZnF(jf153)*
2200	*rmh-2(jf168)*
2201	*rmh-2 (jf168) in CB4856 (Hawaii wild type)*
2204	*jfsi38 [gfp::rmh-1, cb-unc-119(+)] II,top-3::ha(jf158)*
2205	*jfsi38 [gfp::rmh-1, cb-unc-119(+)] II, top-3_ZnF::ha(jf159)*
2219	*rmh-2 V / nT1 [qIs51] (IV;V); top-3::ha(jf158) III*
2220	*rmh-2 V /nT1 [qIs51] (IV;V); top-3_ZnF::ha(jf159) III*

Table 2: *Repair templates used for generation of new strains by genome editing.*

genotype	repair template
top-3_ZnF	AGAAAACCACGTGCTCCACGAAAAAGTGCTGCTCCAAAAGAACAGGAAG AGGAAGAAGAAGTGTAATGCCAGTGCCCAGAGCCGATGAGAGCCGTCAC GAAAGTGGTGCAGAAG
rmh-2	CTAATTCTCGAACATGTAACAGAAAAAACATGAAAAATTATTCAATAGAC ATCGATTAGCTCTGATATTGTTTAAATTCATCTTAGGACGCGGCGGTTGCA GTGTGGGTTTACGGAGCTCCACCTACTTTATTGGACGCAGTTTCAAATTTA TTTTTTTCTCATAAAA TTCAATTCTTGC
top-3::HA	GGTGGAGGCCCACCAAGAGGACCTGGAGGTGGTGGTTACCCATACGATG TTCCAGATTACGCTGGGGGAGGCCCTACAGGCCCGCCGGCTCCTCCAAA

5.2 Verification of genotypes

Strains' genotypes were verified in the following manner:

5.2.1 Worm lysis

Single worms were placed in 10 µl of lysis buffer containing protease K and frozen for 10 min at -80°C. Samples were incubated for 1h at 60°C in order to extract the DNA. After that, protease K was inactivated for 15 min at 95°C.

Materials used:

Lysis buffer

- 50 mM KCl
- 10 mM Tris pH 8.2
- 2.5 mM MgCl2
- 0.45% NP-40
- 0.45% Tween
- 3 µl=ml protease K (20 mg=ml) per 1ml

5.2.2 TAQ-Polymerase chain reaction

Worm lysates were added to the PCR reaction mixture (1 µl of lysate per sample) to provide DNA template. Samples were incubated according to a PCR program (table 3) with specific conditions for each gene of interest (table 4)**.**

Materials used:

Reaction mixture for one sample

- 2.5 µl 10x TAQ Buffer
- 0.5 µl of dNTPS (10mM each)
- 0.5 µl of primer1 (10mM)
- 0.5 µl of primer2 (10mM)
- 0.5 µl of primer3 (10mM) if necessary
- 0.2 µl DreamTAQ
- 1 µl lysate
- add water to reach final volume of 25 µl

Table 3: *PCR program was adapted for each genotype. Annealing temperature depends on primers and extension time was adjusted according to the length of the amplicon.*

cycle step	temperature	time	cycles
initial denaturation	95°C	3’	1
denaturation	95°C	30’’	34
annealing	X °C	30’’	
extension	72°C	1’ per kb	
final extension	72°C	5’	1
cooling	4°C	-	

Table 4: *Primers used to verify genotypes including their melting temperature T_m , annealing temperature T_a. Extension time was adjusted according to the length of amplicon.*

internal number	primer sequence	T_m	T_a	extension time	amplicon
VJ2708	gaggtgttcggcagtatg	56	55	1’	***top-3_ZnF***
VJ2709	tgtatacggtaacgagcatgt	60	55	1’	
VJ2450	gagtctgaacgcaaaattgg	58	60	30’’	**HA insertion:** 1.2 kb
VJ2451	tcttcactgctgggcttatc	60	60	30’’	

VJ2444	cgtggaaacattgcttgaaa	56	56	2’	***spo-11:*** 500 bp
VJ2445	ggactgatggaaccgagaa	58	56	2’	*wt:*1.8 kb
VJ1797	tttttcgcttgtcactcacg	58	53	1’	***lem-3(mn155)***
VJ1798	ctgctggagagattccgaac	62	53	1’	*mn155* point mutation
VJ2697	aaggccccgggtgctataagcgaatacttttgagtttc	60	57	2’	***mus-81***
VJ2698	ggccttcatatgaatggaaattctttaaattcg	62	57	2’	
VJ2554	gtttttcagcaacctttctt	56	57	1’	**MSH-5::GFP:** 1 kb shift
VJ2555	attatcatcacggggtaagg	58	57	1’	
VJ2574	actttgtattggtctcgcac	58	57	1’	**OLLAS::COSA-1**
VJ2575	aacctgattcgctgctgata	58	57	1’	
VJ1447	acttggaggaggaggaggat	62	58	30’’	**HIM-6::HA**
VJ1448	tgacacacgattcatttggca	60	58	30’’	
VJ882	caattcatcccggtttctgt	58	60	30’’	**GFP::RMH-1** 500 bp insertion
VJ1427	cgttcatacggccgaaattt	58	60	30’’	
VJ1428	caagacacccgggtttgtct	62	60	30’’	
VJ2827	catcgaattggtgagcacat	58	55	1’	***rmh-2:*** 684 bp
VJ2828	cgcaacggtctcttcaattc	60	55	1’	
VJ2829	agcttctcgtttcgcagcta	60	55	1’	

5.2.3 Restriction

Restriction enzymes listed in table 5 were applied to cut the amplified DNA in case of several genotypes.

Table 5: *Restriction enzymes including activation and inactivation conditions.*

enzyme	buffer	activation conditions	inactivation	genotype and products
HpaII	CutSmart	37 °C for 1h	80°C	***top-3_ZnF:*** 88bp, 113 bp *wt*: 201 bp
BamHI	CutSmart	37°C for 2h	80°C	**HIM-6::HA:** 230bp,160bp *wt:* 400bp

5.2.4 Gel electrophoresis

Products of above described PCR (often combined with restriction) were analyzed utilizing agarose gels. The amount of agarose added to the 1X TAE buffer varied from 1% to 3% in dependence on the amplicon sizes to be separated. Once the gel was polymerized, DNA samples were loaded into its wells and separated by size with help of electric current. Ethidium bromide as DNA intercalator (2.5 µl per 100 ml agarose gel) was applied to visualize the separated DNA bands.

Materials used:

50×TAE buffer:

- 2 M Tris
- 1 M CH3COONa
- 50 mM EDTA
- use acetic acid to adjust pH to 7.4

5.2.5 Sample preparation for sequencing

Alternately to gel electrophoresis, genotypes were verified by sequencing. After PCR amplification, samples were purified using a column, as follows:

1. Add equal volume of Membrane Binding Solution to the PCR product.
2. Insert SV Minicolumn into Collection Tube.
3. Transfer PCR product to the Minicolumn assembly. Incubate at room temperature for 1 min.
4. Centrifuge at 16000xg for 1 min. Transfer the flowthrough back to the Minicolumn and repeat the centrifugation. Discard the flowthrough and reinsert the Minicolumn into collection tube.
5. Add 700 µl Membrane Washing Solution (with added ethanol). Centrifuge at 16000xg for 5 min. Discard the flowthrough.
6. Add 500 µl Membrane Washing Solution (with added ethanol). Centrifuge at 16000xg for 1 min. Discard the flowthrough.
7. Re-centrifuge Minicolumn for 4 min to allow evaporation of residual ethanol.
8. Transfer Minicolumn to 1.5 ml tube and add 30 µl of warm distilled water. Incubate at room temperature for 1 min.
9. Discard the Minicolumn. DNA product is prepared for sequencing.

5.3 Viability Test

All generated strains were tested for their hatch rate. 8 - 10 L4 hermaphrodites were singled on small NGM plates and allowed to lay eggs for 24h at 20°C. Every 24h worms were moved to fresh plates and after 72h they were removed. Upon every transfer hatched and unhatched eggs were recorded to calculate the final rate corresponding to strain viability. Additionally, occurrence of males and larval arrest were defined when the progeny reached adulthood.

5.4 Immunostaining

Following protocols were applied to prepare worms for immunostaining:

5.4.1 Dissection and fixation of worm gonads

Day 1

1. Coat SuperFrost glass slides with 11 µl of poly-L-lysine solution (0.1% P8920 Sigma-Aldrich) and incubate over night at 65°C.
2. Select 40-50 L4 hermaphrodites and incubate them at 20°C for 24h.

Day 2

1. Prepare Cut mix and Fix mix.
2. Place 15 µl of Cut mix on coated slides.
3. Transfer 6-10 worms to the Cut mix drop.
4. Dissect worms with a syringe needle to release their gonads.
5. Add 15 µl of Fix mix, mix gently by pipetting and remove 15 µl of liquid.
6. Put cover slips on slides and incubate them for 5 min at room temperature.
7. Freeze slides in liquid nitrogen.
8. Store at -80°C or continue with immunostaining procedure.

Materials used:

10x PBS:

- 1.37 M NaCl
- 27 mM KCl

- 43 mM Na2HPO4
- 14 mM KH2PO4

Cut mix:

- 1 x PBS (10x PBS)
- 10 µl of levamisole

Fix mix:

- 1 x PBS (10x PBS)
- 2% PFA (16% PFA)

5.4.2 Staining

Day 1

1. Remove the coverslips and incubate slides in methanol for 5 min at -20°C.
2. Wash slides in 1x PBST for 10 min at room temperature. Wash 3 times, use fresh 1x PBST.
3. Place 50 µl of blocking buffer on plastic film coverslips and cover the slides. Incubate them for 30 to 60 min at room temperature in dark humid chamber.
4. Place 50 µl of primary antibody on fresh plastic film coverslips and cover the slides. Incubate over night at 4°C in dark humid chamber.

Day 2

1. Wash slides in 1x PBST for 10-15 min at room temperature. Wash 3 times.
2. Apply 50 µl of secondary antibody conjugated with a fluorophore on fresh plastic film coverslips and cover the slides. Incubate for 1-2h at room temperature in dark humid chamber.
3. Wash slides in 1x PBST for 10-15 min at room temperature. Wash 3 times.
4. Add 50 µl of DAPI (4',6'-diamidino-2-phenylindole; diluted 1:1000 in water) on each slide. Incubate for 1 min at room temperature. Wash in 1x PBST for 20 min at room temperature.
5. Mount slides with 11 µl of Vectashield. Seal the coverslips with nail polish.
6. Store at 4°C.

Materials used:

Washing solution PBST:

- 1x PBS (10x PBST)
- 1% Tween (Tween-20)

Blocking Buffer:

- 1x PBS (10x PBST)
- 1% BSA

Antibodies (table 6 and 7):

- diluted in 1%PBS-T

Table 6: *List of primary antibodies with dilution factors used for immunostaining.*

internal number	primary antibody	provider	dilution
1481	rabbit anti RAD-51	ZETKA	1:1000
1488	rabbit anti HA	SIGMA	1:100
1497	guinea pig anti HTP-3	YUMI KIM	1:500
1443	rabbit anti HTP-1	FADRI	1:400
1369	mouse anti pH3	Cell Signaling Technology	1:1000
1485	rabbit anti OLLAS	Genscript	1:1500

Table 7*: List of secondary antibodies including conjugates and dilution factors used for immunostaining.*

internal number	secondary antibody	conjugate	provider	dilution
1333	goat anti rabbit	Alexa Fluor 488	Invitrogen	1:500
1184	goat anti rabbit	Alexa Fluor 568	Invitrogen	1:500
1364	goat anti guinea pig	Alexa Fluor 647	Life Technologies	1:200
1422	goat anti mouse	Cy3	Jackson	1:600

5.4.3 Antibody preabsorption (Fadri)

The preabsorption procedure (as described below) was applied to increase the sensitivity of 1488 antibody against HA tag.

1. Wash 200 adult worms 2 times with 500 µl M9 buffer and collect the worms in a 1.5ml tube.
2. Centrifuge the tube at 3000xg for 30 sec. Remove the supernatant and add 250 µl of 1x egg buffer.
3. Place the sample to liquid nitrogen to freeze.
4. Make a glass pestle that fills the bottom of the tube to grind the worms. Clean the pestle with Ethanol. Break worms with pestle.
5. Spin down at maximum speed for 1 min. Remove the supernatant.
6. Add 500 µl of cold methanol and mix properly. Incubate for 1 minute and spin down. Remove methanol.
7. Add 500 µl of PBST (1x PBS, 0.1% Tween) and mix properly. Incubate rotating at room temperature for 5 min.
8. Add 500 µl of 1x PBST containing 4% paraformaldehyde and incubate in a nutator for 30 minutes.
9. Spin down and remove the fix, wash 2 times for 3 min in 500 µl PBST. Incubate in nutator while washing.
10. Incubate in blocking solution: PBST, 1% BSA. Incubate at room temperature for 1 h in nutator.
11. Spin down and remove the blocking solution. Add the antibody to be cleaned in a 1:10 dilution in PBST. Incubate in nutator over night at room temperature.
12. Spin down. Save the liquid = cleaned antibody. Add BSA (1mg/ml final).
13. Aliquot and store the antibody at -20°C.

5.5 Microscopy and Imaging

Gonads were imaged as 3D z-stacks using Delta Vision system equipped with 60x/1.42 and 100x/1.40 oil 391 immersion objective lenses and an Ultra Delta Vision microscope equipped with a 4-Megapixel 391 sCMOS camera. Stacks were acquired with 0.2 µm spacing between stack layers. Using SoftWoRx images were deconvolved in 32-bit range or border rolloff settings (dependent on the microscope). Deconvolved stacks were aligned in ImageJ and optimally processed in Adobe Photoshop CS.

5.6 Quantification of foci

Based on protein to be analyzed, gonads were divided in 4 or 7 zones. Amount of foci was evaluated for each zone either manually or automatically using following method:

5.6.1 Automatic quantification of foci (a protocol developed by Antoine Baudrimont)

1. Save every channel as single TIF file including zones.
2. Open the pictures with ImageJ.
3. Open ROI manager in ImageJ.
4. Using circle selection mark nuclei in the DAPI channel by placing a circle on the nuclei and pressing T. Select representative number of nuclei for each zone.
5. Select one nucleus in the ROI manager and run following script (using macro in ImageJ):

    - for(r=1; r<100; r++) {
      run("Find Maxima...", "noise=r output=Count"); }

6. Repeat for all selected nuclei and plot the results. The first plateau of the curve is the value of noise tolerance which detects the foci in a significant manner. Add this value to the script:

    - selections = roiManager("count");
      for(r=1; r<selections; r++) {
      roiManager("Select", r);
      run("Find Maxima...", "noise= //add here the value of noise tolerance// output=Count"); }

7. Using the ROI manager select all nuclei within zones and count amount of foci running the above described script.

5.6.2 Quantification of colocalization (a protocol developed by Antoine Baudrimont)

Colocalization of two proteins was analyzed using automated method. Projected gonads were divided in 4 or 7 zones (dependent on proteins to be analyzed) and channels were saved as single TIF files. Using the ROI manager (ImageJ) nuclei were selected for each zone. Colocalization was calculated for each zone by running the script:

- selections = roiManager("count");
  newImage("red_q", "8-bit black", 400, 400, 1);
  newImage("green_q", "8-bit black", 400, 400, 1);
  for(r=0; r<selections; r++){
  selectWindow("red.png");
  roiManager("Select", r);
  run("Copy");
  selectWindow("red_q");
  run("Paste");
  selectWindow("green.png");
  roiManager("Select", r);
  run("Copy");
  selectWindow("green_q");
  run("Paste");
  run("Colocalisation Threshold", "channel_1=red_q channel_2=green_q use_roi=None
  channel_combination=[Red : Green]");
  selectWindow("red_q");
  run("Clear", "slice");
  selectWindow("green_q");
  run("Clear", "slice");
  }

5.7 Western Blot

5.7.1 Preparation of samples

1. Select 200 L4 hermaphrodites for each genotype and incubate them for 24h at 20°C.
2. Clean worms from bacteria by transferring them on unseeded plate.
3. Place worms to a solution containing 32µl of 1xTE + 3.2µl of 10X Proteinase inhibitor Roche (stock solution of proteinase: 10X with 1 tab in 1ml water).
4. Freeze the samples in liquid nitrogen for 5 min and defrost them. Repeat 3 times.
5. Add 8µl of 5X Laemli Buffer and lock the tubes.
6. Boil the samples at 99°C for 10 min.
7. At this step, samples can be stored at -20°C or blotted.

5.7.2 Western Blot procedure

Prepare following media:

1. 1 liter of 1X Running Buffer (from 10X stock solution)
2. Ladder
3. 1 liter of Transfer Buffer (200 ml Methanol, 600 ml water, 200ml 5X TrisGlyc) and store it in the cold room.
4. 1 liter TBST-T.

Day 1

1. Assemble the poly-acrylamide gel (10%) and put it in the tank. Fill the tank with the 1X Running Buffer.
2. Add 6µl of Ladder and load 40µl of each sample using extra thin long crystal tips.
3. Run the gel at 65 mA for 20 to 40 min.
4. Prepare the transfer as described below and assemble it on the black side of the cassette:
    - Sponge
    - 2X WhiteMan paper
    - Gel
    - Membrane (activate it in Methanol for 20s)
    - 2X WhiteMan paper
    - Sponge
5. Put it in the tank and fill the tank with Transfer Buffer. Run at 4°C for one h with 400 mA or 100V. When recovering the membrane cut one corner to keep the orientation.
6. Rinse the membrane in TBS-T.
7. Block it for at least 20 min in Blocking Buffer (5% milk in 1X TBS-T).
8. Add the primary antibody diluted in Blocking Buffer and hybridize at 4°C overnight in the black tank (min Vol 10ml).

Day 2

1. Wash 3 times in 1X TBS-T (5 to 10 min).
2. Apply secondary antibody diluted in Blocking Buffer for 1.5 h at room temperature.
3. Wash 3 times in 1X TBS-T (5 to 10 min).
4. Proceed with ECL detection for 1 min.
5. Image the membrane.

Table 8: *Primary antibodies including with dilution factor.*

internal number	primary antibody	provider	dilution
1457	mouse anti HA	Cell Signaling	1:1000
1522	goat anti actin	Santa Cruz Biotechnology	1:3000

Table 9: *Secondary antibodies including their conjugate and dilution factor.*

internal number	secondary antibody	conjugate	provider	dilution
1428	goat anti-mouse	HRP	Cell Signaling	1:2500
1435	donkey anti-goat	HRP	Santa Cruz Biotechnology	1:8000

5.8 SNP-based mapping of crossovers

The frequency of crossovers was tested in *rmh-2* and *top-3_ZnF* mutants. For this, I took advantage of the Hawaiian wild type strain (Hw), which contains SNPs in a high frequency that deviate from the Bristol wild type strain (N2) (Bazan and Hillers 2011). These phenotypically neutral differences were detected by PCR and consecutive endonuclease restriction was performed. First, we applied CRISPR to generate *top-3_ZnF* and *rmh-2* in the Hawaii strain (#2097 and #2201 strain numbers in table 1) which were subsequently crossed to same mutations in N2 wild type (#2075 and #2200 strain numbers in table 1) to produce strains that were homozygous for mutation of interest and heterozygous for the introgressed "Hawaii chromosomes", focusing specifically on the chromosomes IV and V. Recombination events were allowed to take place in F1 worms that were crossed to a wild type strain carrying the tomato marker (#1417 strain number in table 1) which is visible by microscopy allowing

us to easily control the cross, to introduce a wt paternal chromosome and allow the exclusive monitoring of the recombination event in oogenesis. After laying eggs, F1 mums were lysed and then genotyped to ensure that the first cross worked using the presence of Hawaiian SNPs as a read-out. The F2 hermaphrodites were used for detection of the recombination events. Primers listed in tables 10 and 11 were designed to detect positions corresponding to the SNPs in Hw and N2 along chromosomes IV and V. Restriction (with DraI for 2h at 37°C) and gel electrophoresis (2% agarose gel) showed fragments (table 12 and 13) revealing the distribution of crossovers along tested chromosomes.

Table 10: *Primers used to detect SNPs on specific positions along chromosome IV.*

SNP	genetic position	internal number	primer sequence	T_m	T_a	extension time
N°2	-16	**VJ769**	cgcataaatccaacgttctctg	64	60	1’
		VJ770	aatccataagtttcgtgttgg	58	60	
N°4	1	**VJ1208**	aaaatgggaagcgtaccaaa	56	60	1’
		VJ1209	tgcttgtagcgtttccaaga	58	60	
N°5	8	**VJ775**	gacacgactttagaaacaaca	58	60	1’
		VJ776	tggtatggagtccctattttg	60	60	
N°6	14	**VJ1159**	gaatttcaggtgttggaagg	58	60	1’
		VJ1160	tgctctgaaaaaattggctg	56	60	

Table 11: *Primers used to detect SNPs on specific positions along chromosome V.*

SNP	genetic position	internal number	primer sequence	T_m	T_a	extension time
N°1	-17.5	**VJ944**	tttcggaaaattgcgactgt	56	60	1’
		VJ945	cgcgttttggagaattgttt	56	60	
N°3	-5	**VJ948**	gagattctagagaaatggacaccc	70	60	1’
		VJ949	aaaaatcgactacaccacttttagc	68	60	
N°4	1	**VJ950**	agaaatgatccgatgaaaaagc	60	60	1’
		VJ951	ccgatagtgttcatagcatccc	66	60	
N°5	5.8	**VJ1157**	agccacataagcgccataac	60	60	1’
		VJ1158	gtgacggaacaaactcatctgc	66	60	
N°8	17.8	**VJ1155**	gccactgatgggacagaacc	64	60	1’
		VJ1156	cagaaaattgccaaaactaccg	62	60	

Table 12: *Restriction fragments on tested genetic positions along chromosome IV.*

SNP	genetic position	N2	HW
N°2	-16	cut	uncut
N°4	1	uncut	cut
N°5	8	cut	uncut
N°6	14	cut	uncut

Table 13: *Restriction fragments on tested genetic positions along chromosome V.*

SNP	genetic position	N2	HW
N°1	-17.5	uncut	cut
N°3	-5	uncut	cut
N°4	1	uncut	cut
N°5	5.8	uncut	cut
N°8	17.8	cut	uncut

5.10 Heterologous recombination assay

Heterologous recombination can occur between non-identical sequences and is extremely rare in wild type (Ortiz et al. 2018). Worms that were scored for the occurrence of heterologous recombination carried chromosome inversion on chromosome II shown in figure 9. Chromosome copies are heterologous in the region of *mln1* balancer, since one copy carries the inversed balancer version. Different genetic markers flanking the region (*dpy-25, rol-1* and GFP) were used to distinguish between non-recombinant (figure 10) and recombinant (figure 11) progeny.

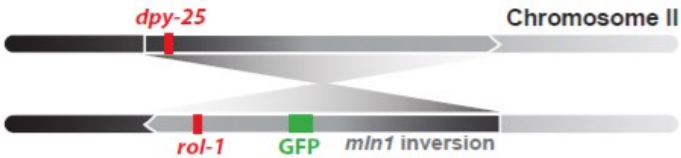

Figure 9: *Chromosome II with genetic markers applied to test the occurrence of heterologous recombination (Ortiz et al., 2018).*

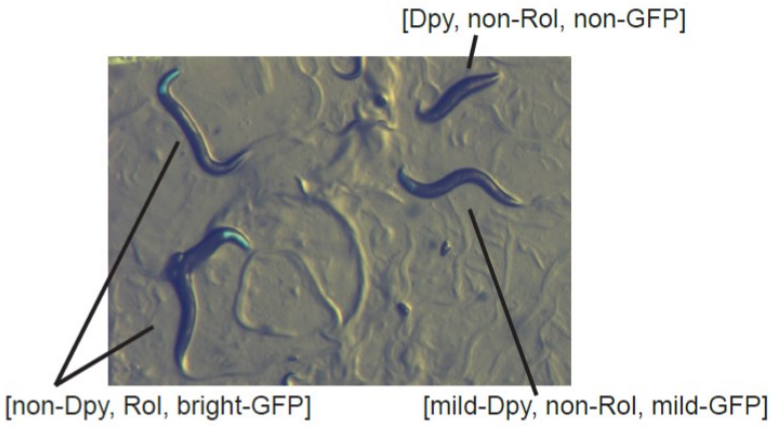

Figure 10: *Phenotypes of non-recombinant progeny (Ortiz et al., 2018).*

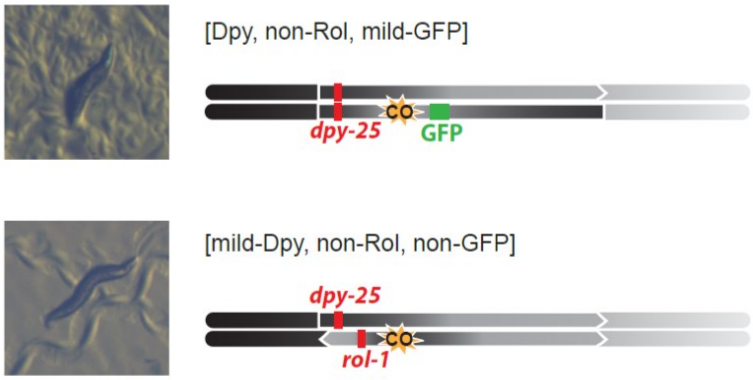

Figure 11: *Example of recombinant progeny after crossover in the heterologous region (Ortiz et al., 2018).*

5.11 Statistic tests

I applied the Mann-Whitney t-test (unpaired and nonparametric data) to see the difference between diakinesis and localization of BTR complex members between single zones of meiotic prophase I.

6. Results

6.1 Generation of the *top-3_ZnF* mutant and crude characterization of the new strains

The ZnF motif was deleted in the TOP-3 protein by using CRISPR/Cas9 to introduce a stopcodon directly after the first amino acid of the motif (schematic illustration in figure 12). First, I examined the hatch rate and embryonic lethality and found that the *top-3_ZnF* mutant is as viable as the wild type (table 14). Larval arrest and the incidence of males were slightly increased compared to the wild type (table 14), however all these increases are very subtle and within the range of the standard deviation.

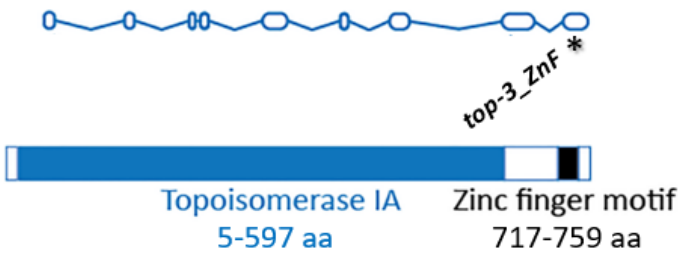

***Figure 12: Schematics of TOP-3 with Topoisomerase IA domain (5-597 aa) and Zinc finger motif (717-759 aa)**. Truncated version of TOP-3, the TOP-3_ZnF was generated by inserting a stopcodon directly after the first amino acids of the motif.*

***Table 14: Viability counts of top-3_ZnF compared to the wild type.** In total (N), 16 hermaphrodites were analyzed for viability rate, brood size, larval arrest and incidence of males. Displayed numbers are average values for single hermaphrodite including standard deviation.*

	wt	***top-3_ZnF***
Viability	99,75 ± 0,5 %	98,72 ± 0,7 %
Brood size	229 ± 28	248 ± 34
Larval arrest	0%	1,8 ± 1,3%
Incidence of males	0,06 ± 0,2 %	0,8 ± 1,1 %
N	16	16

Western Blot analysis demonstrated that TOP-3_ZnF is indeed a truncated protein version, since it ran at smaller molecular weight (80.8kDa) than TOP-3 full length (85.4kDa) (figure 13A). Nevertheless, the expressed amount of truncated protein was comparable to the amount of TOP-3 full length, as shown by quantifying the band intensities of the two proteins visualized by Western Blot (figure 13B).

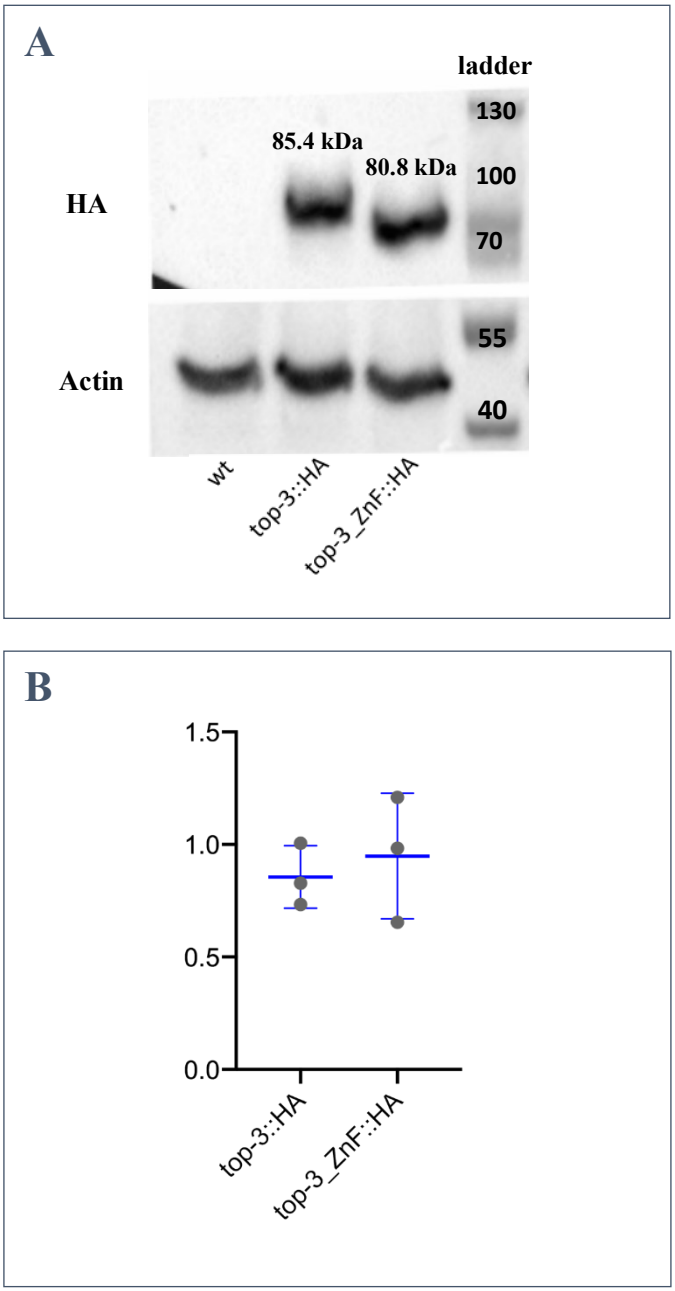

Figure 13: (A) Western Blot of TOP-3_ZnF compared to TOP-3. *Both proteins were tagged with HA to facilitate their detection. Every genotype was represented by triplicates containing 200 worms. Actin was applied to control that every sample contained the same amount of worm material.* ***(B) Intensity values calculated for all tested triplicates.*** *Measurements indicated that both genotypes produced similar total amount of protein.*

6.2 Analysis of diakinesis chromosomes in *top-3_ZnF* mutant

By quantifying DAPI-stained bodies in *top-3_ZnF* diakinesis, I started to investigate the function of the ZnF motif during meiotic recombination. Diakinesis represents the last stage of meiotic prophase I by containing bivalent chromosomes that underwent recombination. Most of the defects that occur during recombination lead to changes in specific organization and number of bivalents. Therefore, by quantifying the diakinesis, I received the first hint that ZnF motif may be important during recombination. The number of DAPI bodies was screened in the most mature oocytes that were prior to fertilization and are often referred to as -1 oocytes. In wild type, all diakinesis stages showed 6 bivalents (figure 14A). In *top-3_ZnF*, the majority of observed oocytes displayed 6 bivalents. However, 3% of diakinesis had 7 DAPI bodies and about 6% exhibited a chromatin bridge between two bivalents corresponding to 5 bodies (figure 14B). Additionally, 31% of oocytes displayed round shaped bivalents (figure 14C).

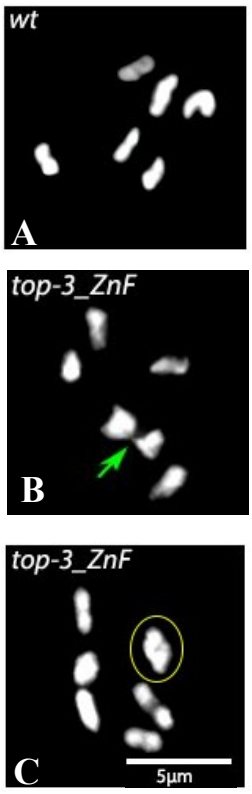

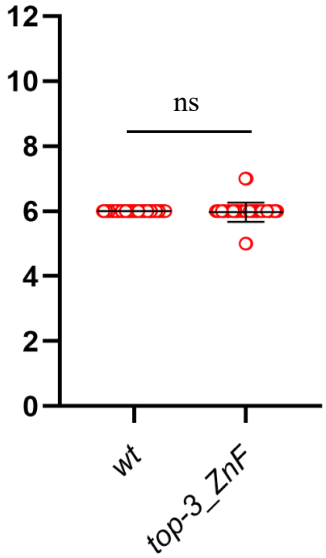

number of DAPI bodies	5	6	7	N
wt	0	100	0	50
top-3_ZnF	5,8	91,3	2,9	103

Figure 14: Quantitative analysis of DAPI bodies in diakinesis oocyte nuclei in top-3_ZnF compared to the wild type in %. *Genotypes are represented by* ***(A)*** *6 bivalents in wild type* ***(B)*** *5 DAPI bodies with one chromatin connection between two bivalents (green arrow) in top-3_ZnF* ***(C)*** *6 bodies with one round shaped bivalent (yellow circle) in top-3_ZnF. Table depicts the relative percentage of diakinesis counts for the given number of DAPI bodies for each indicated genotype. N is the total number of quantified oocyte nuclei for indicated genotypes.*

In order to understand whether the diakinesis phenotype of *top-3_ZnF* is dependent on meiotic recombination initiation, I generated a *spo-11; top-3_ZnF* double mutant. SPO-11 is known to introduce DSBs that start the process of meiotic recombination leading to formation of 6 bivalents (Dernburg et al. 1998) (explained in more detail in the introduction chapter 4.3.3). If this initiation doesn´t occur, as it was the case in *spo-11* worms, oocytes show 12 univalents (figure 15A). The double mutant *spo-11; top-3_ZnF* exhibited exactly the same phenotype, where all 50 diakinesis displayed 12 univalents (figure 15B), implying that the defects in *top-3_ZnF* diakinesis are *spo-11* dependent.

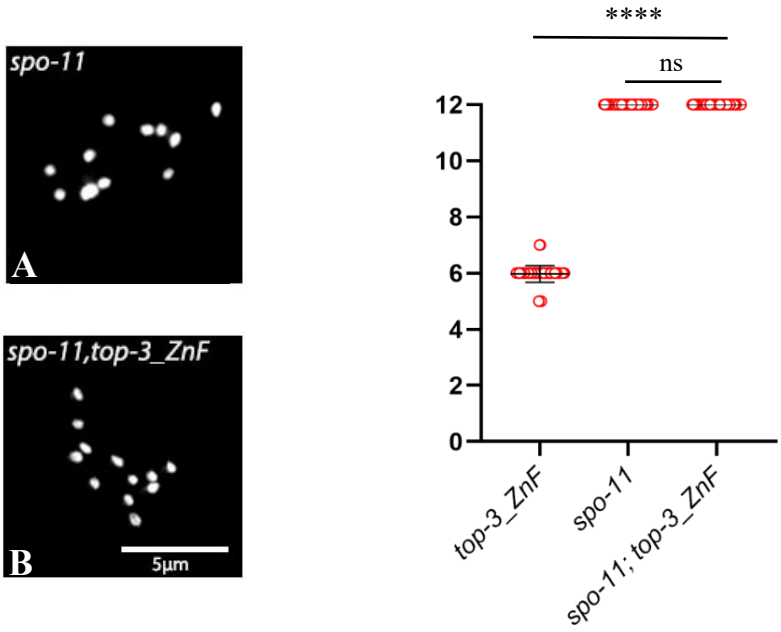

***Figure 15**: **Quantitative analysis of DAPI bodies in diakinesis oocyte nuclei in spo-11; top-3_ZnF compared to the spo-11 and top-3_ZnF in %.** All 50 examined oocytes displayed 12 univalents in **(A)** spo-11 and **(B)** spo-11; top-3_ZnF. Mann-Whitney test calculated top-3_ZnF vs. spo-11; top-3_ZnF **** p<0.000.*

6.3 Quantification of RAD-51 recombination foci in *top-3_ZnF* mutant

As next, I analyzed the RAD-51 kinetics that allowed us to understand, whether the phenotype of *top-3_ZnF* diakinesis is caused by defects during early repair of DSBs. RAD-51 mediates the process of strand invasion and marks ongoing recombination (Alpi et al. 2003; Colaiácovo et al. 2003). I quantified the protein by dividing the stained gonad in 7 zones of equal length. In wild type, RAD-51 started localizing in distinct foci in transition zone nuclei (z3 in figures 16-17) whose number rapidly accumulated upon entering early pachynema (z4 in figures 16-17). When nuclei moved to mid pachynema, RAD-51 started to be disengaged from chromatin (z5 in figures 16-17) and became almost completely removed by the end of late pachynema (z6-z7 in figures 16-17). Similar dynamics

was observed also for *top-3_ZnF*, but the number of foci was increased, mostly from the beginning of the transition zone to mid pachynema (z3-z5 in figures 16-17). Additionally, RAD-51 appeared in form of stretches (yellow arrow in figure 16), where many foci localized in such close proximity that it was impossible to distinguish them as distinct foci. Nevertheless, RAD-51 was resolved by late pachynema (z6-z7 in figures 16-17).

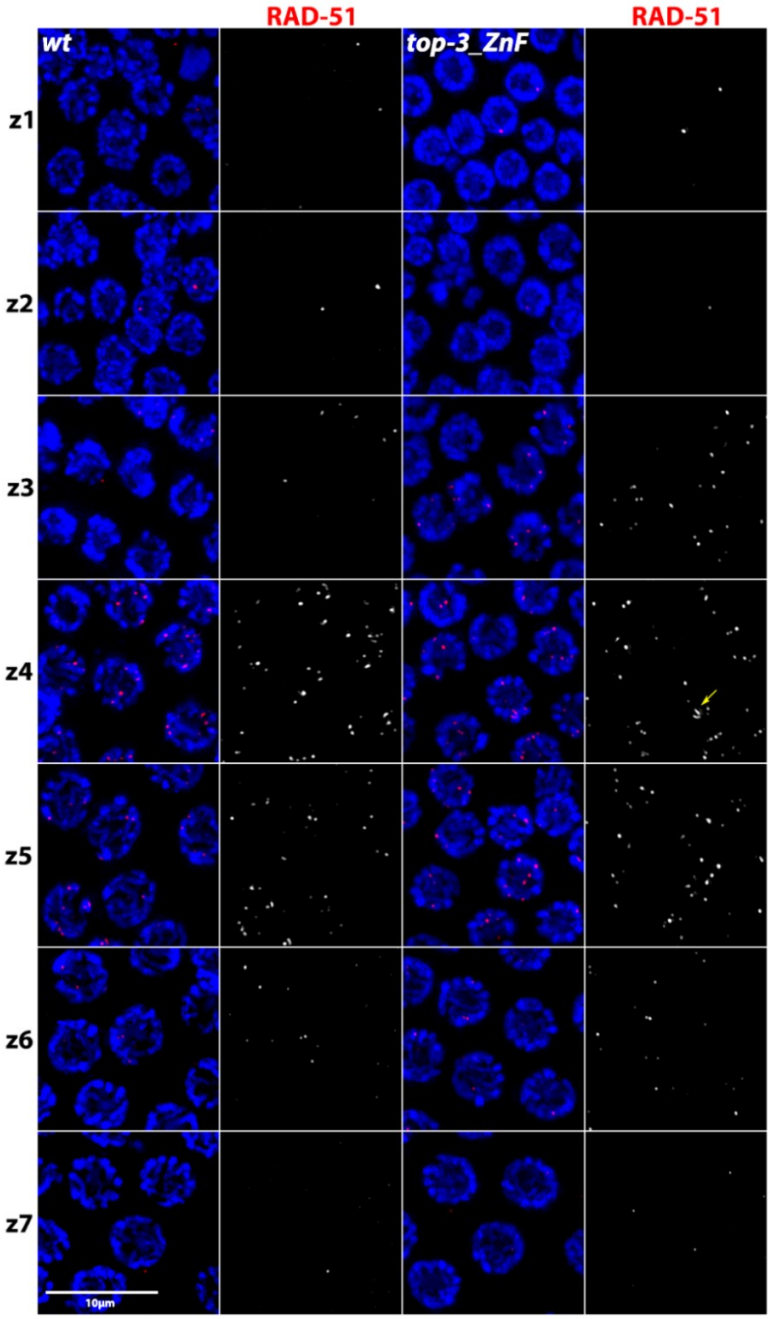

Figure 16: Localization of RAD-51 recombination foci in top-3_ZnF compared to the wild type. *Images display the RAD-51 localization in 7 zones of RAD-51 stained gonads of indicated genotypes. Zones represent mitotic zone (z1-z2) and stages of meiotic prophase I: transition zone (z3), early pachynema (z4), mid pachynema (z5) and late pachynema (z6-z7). Yellow arrow in top-3_ZnF z4 points to RAD-51 marked stretches.*

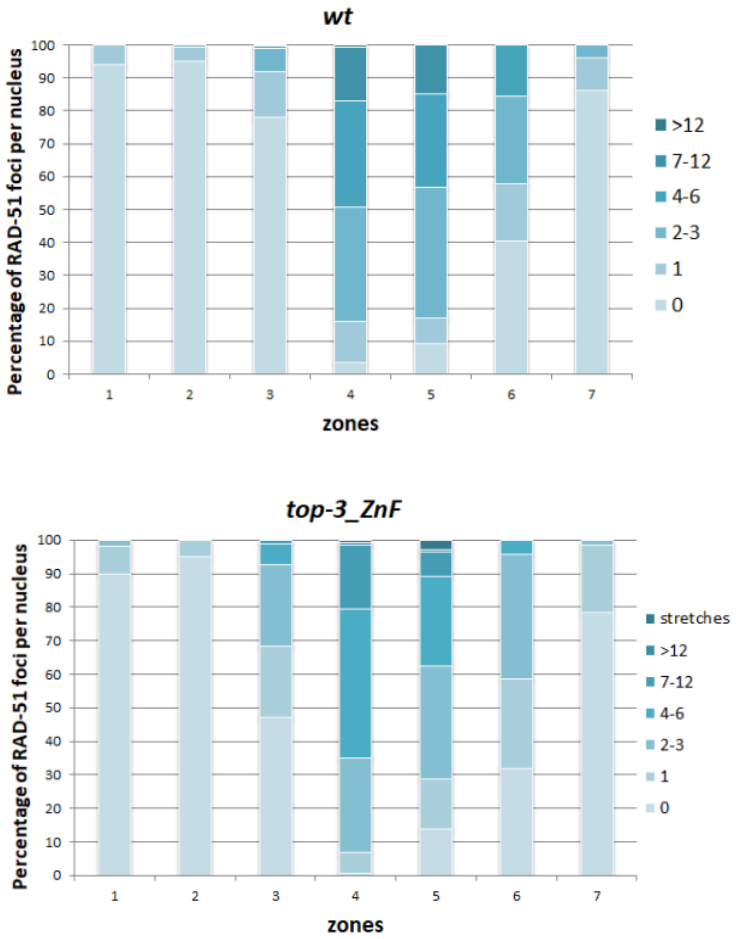

Figure 17: Quantification of RAD-51 foci dynamics in top-3_ZnF compared to the wild type. *Categories with percentage of RAD-51 foci per nucleus are plotted for every zone of indicated genotypes. Zones represent mitotic zone (z1-z2) and stages of meiotic prophase I: transition zone (z3), early pachynema (z4), mid pachynema (z5) and late pachynema (z6-z7). In total, 6 gonads with 1203 nuclei were evaluated for the top-3_ZnF and 6 gonads with 1143 nuclei were evaluated for the wild type.*

Furthermore, I wanted to know, whether the RAD-51 deviations from the wild type were meiosis specific. The double mutant *spo-11; top-3_ZnF* phenocopied the single mutant *spo-11*, where RAD-51 localized only as one or two foci in all stages of meiotic prophase I (figures 18-19).

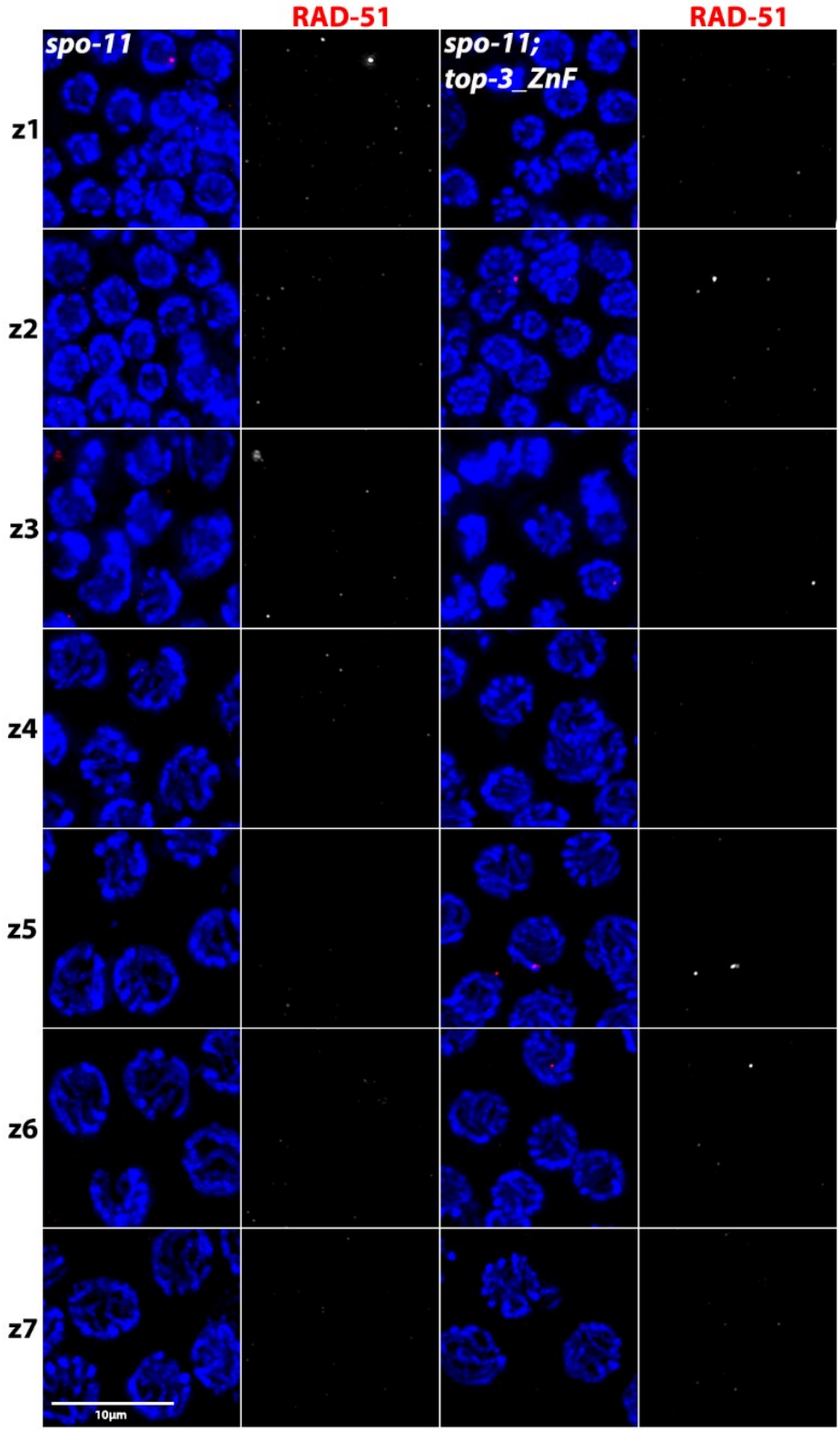

Figure 18: Localization of RAD-51 recombination foci in spo-11; top-3_ZnF compared to the spo-11. *Images display the RAD-51 localization in 7 zones of RAD-51 stained gonads of indicated genotypes. Zones represent mitotic zone (z1-z2) and stages of meiotic prophase I: transition zone (z3), early pachynema (z4), mid pachynema (z5) and late pachynema (z6-z7).*

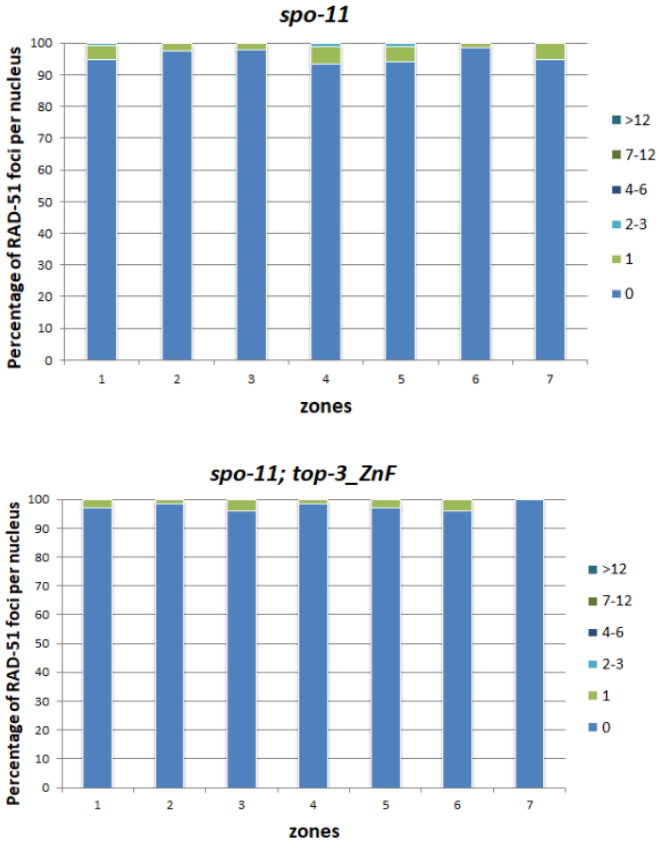

Figure 19: Quantification of RAD-51 foci dynamics in spo-11; top-3_ZnF compared to the spo-11. *Categories with percentage of RAD-51 foci per nucleus are plotted for every zone of indicated genotypes. Zones represent mitotic zone (z1-z2) and stages of meiotic prophase I: transition zone (z3), early pachynema (z4), mid pachynema (z5) and late pachynema (z6-z7). In total, 3 gonads with 513 nuclei were evaluated for the spo-11; top-3_ZnF and 3 gonads with 673 nuclei were evaluated for the spo-11.*

The RAD-51 profile of *top-3_ZnF* and its *spo-11* dependency indicates that *top-3_ZnF* generates meiotic defects which most likely disrupt the early kinetics of DSB repair based on the localization of RAD-51 protein. However, the fact that RAD-51 marked recombination foci are not present in late pachynema of *top-3_ZnF*, exactly as in the wild type, suggests that despite the defects in early DSBs kinetics, intermediates are resolved. Moreover, since *top-3_ZnF* diakinesis did not display any joint structures, I can conclude that the topoisomerase activity which is necessary for resolving joint intermediates is not compromised or that alternative redundant pathways remove any joint structures. Those results propose a potential role of the ZnF motif during early steps of recombination, perhaps during the D-loop formation, function that has been already suggested for the STR complex in yeast in 2015 (Kaur et al. 2015; Tang et al. 2015).

6.4 Are defects in *top-3_ZnF* compensated by other nucleases?

In *C. elegans* meiosis, two major pathways mediate the resolution of DNA joint molecules: MUS-81 cooperates with SLX-1, and HIM-6 with XPF-1 (Agostinho et al. 2013). Additionally, MUS-81 works together with LEM-3 by processing joint molecules during early steps of recombination (Hong et al., 2018). Since it was shown in other systems that aberrantly joint DNA molecules produced due to the lack of the STR complex (Kaur et al. 2015; Tang et al. 2015; Séguéla-Arnaud et al. 2016; Dorn et al. 2018) need "non-canonical resolvases" for their processing, I wanted to examine how the double mutant *top-3_ZnF* with *mus-81* or *top-3_ZnF* with *lem-3* would look like. I generated *lem-3; top-3_ZnF* and *mus-81; top-3_ZnF* double mutants and *mus-81 lem-3; top-3_ZnF* triple mutant and subjected those to the same basic phenotype analysis as discussed above in chapters 6.1 to 6.3. Those include viability tests, diakinesis chromosome inspection and RAD-51 quantification to detect defects during meiotic recombination.

6.4.1 *lem-3; top-3_ZnF*

Viability rate of double mutant *lem-3; top-3_ZnF* was only slightly reduced in contrast to single mutants or wild type. Larval arrest resembled the numbers found in the *lem-3* single mutant and the incidence of males was about 2-fold reduced compared to *top-3_ZnF*, but only slightly higher when compared to *lem-3* (table 15).

Diakinesis quantification revealed (figure 20), that in *lem-3; top-3_ZnF*, most mature oocytes showed 98% of 6 bivalents. The remaining 2% exhibited 7 DAPI bodies (not shown). Interestingly, about 29% of examined oocytes displayed bivalents with round shaped structures as observed in *top-3_ZnF*. Double mutant *lem-3*; *top-3_ZnF* didn't exhibit the phenotype with two bivalents connected by a chromosomal bridge found in *top-3_ZnF.*

Table 15: Viability counts of lem-3; top-3_ZnF compared to the lem-3 and top-3_ZnF single mutants and wild type. *N is the total number of hermaphrodites tested for viability, brood size, larval arrest and incidence of males. Displayed numbers are average values for single hermaphrodite including standard deviation.*

	wt	***top-3_ZnF***	***lem-3***	***lem-3; top-3_ZnF***
Viability	99,75 ± 0,5 %	98,72 ± 0,7 %	97,53 ± 2,5%	96 ± 2,1 %
Brood size	229 ± 28	248 ± 34	199 ± 35	218 ± 18
Larval arrest	0%	1,8 ± 1,3%	3 ± 1,8 %	3,9 ± 1,6 %
Incidence of males	0,06 ± 0,2 %	0,8 ± 1,1 %	0%	0,38 ± 0,5%
N (total worms)	16	16	8	8

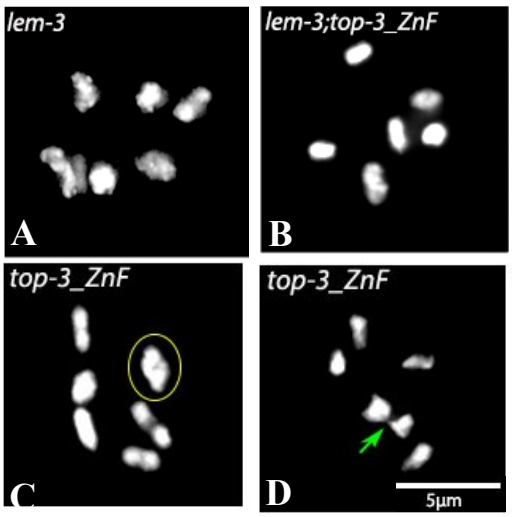

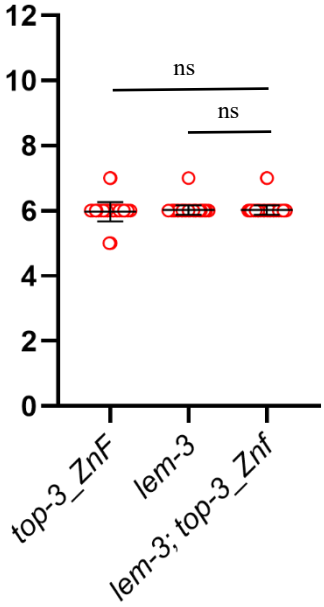

number of DAPI bodies	5	6	7	N
top-3_ZnF	5,8	91,3	2,9	103
lem-3	0	100	0	50
lem-3; top-3_ZnF	0	97,9	2,1	95

Figure 20: Quantitative analysis of DAPI bodies in diakinesis oocyte nuclei in lem-3; top-3_ZnF compared to the lem-3 and top-3_ZnF single mutants in %. *Genotypes are represented by* ***(A)*** *6 bivalents in lem-3* ***(B)*** *6 bivalents in lem-3; top-3_ZnF* ***(C)*** *6 bivalents with round shaped structure (yellow circle) in top-3_ZnF and* ***(D)*** *5 bodies due to the connection between two bivalents (green arrow) in top-3_ZnF. Table depicts the relative percentage of diakinesis counts for the given number of DAPI bodies for each indicated genotype. N is the total number of quantified oocyte nuclei for indicated genotypes.*

Furthermore, the double mutant showed a similar RAD-51 profile as the single mutants: it localized in distinct foci in transition zone (z3 in figures 21-22) and reached the peak in early pachynema (z4 in figures 21-22). RAD-51 foci started disengaging from chromatin, when nuclei moved to mid pachynema (z5 in figures 21-22) and were almost completely resolved in late pachynema (z6-z7 in figures 21-22). Stretches were found mainly in mid pachynema and they were resolved in a manner similar to *top-3_ZnF*. Numbers of quantified foci and stretches did not exceed the quantity of RAD-51 counted for *top-3_ZnF* or *lem-3*.

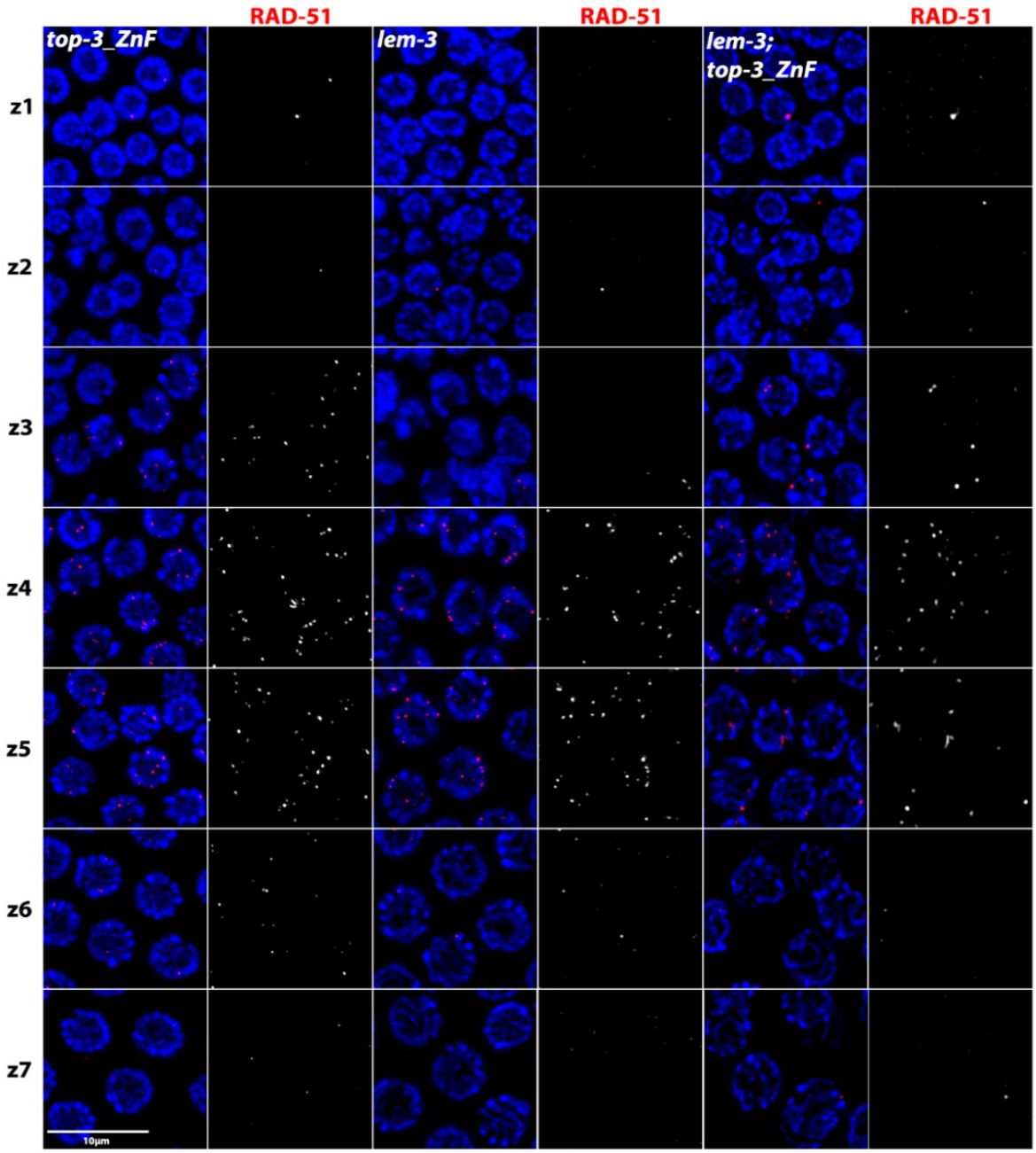

Figure 21: Localization of RAD-51 recombination foci in lem-3; top-3_ZnF compared to the lem-3 and top-3_ZnF single mutants. *Images display the RAD-51 localization in 7 zones of RAD-51 stained gonads of indicated genotypes. Zones represent mitotic zone (z1-z2) and stages of meiotic prophase I: transition zone (z3), early pachynema (z4), mid pachynema (z5) and late pachynema (z6-z7).*

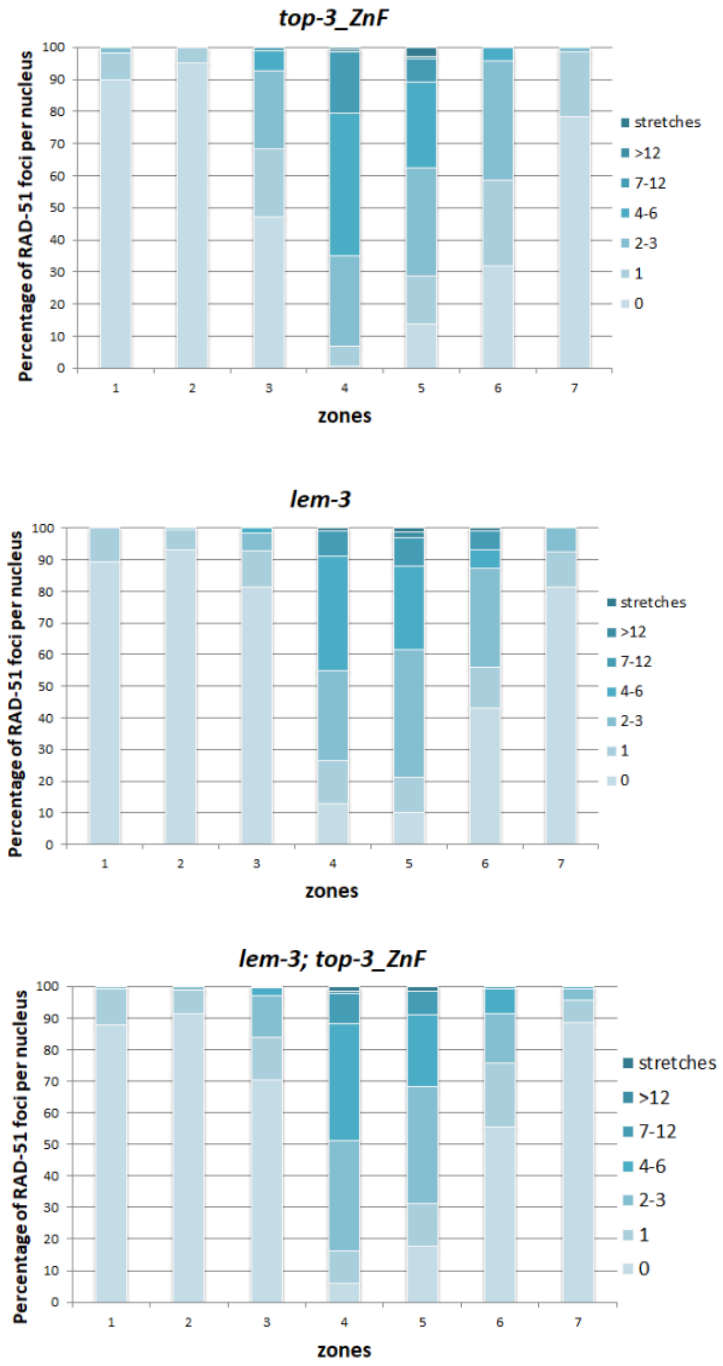

Figure 22: Quantification of RAD-51 foci dynamics in lem-3; top-3_ZnF compared to the lem-3 and top-3_ZnF single mutants. *Categories with percentage of RAD-51 foci per nucleus are plotted for every zone of indicated genotypes. Zones represent mitotic zone (z1-z2) and stages of meiotic prophase I: transition zone (z3), early pachynema (z4), mid pachynema (z5) and late pachynema (z6-z7). In total, 3 gonads with 835 nuclei were evaluated for lem-3; top-3_ZnF and 3 gonads with 800 nuclei were evaluated for lem-3 and 6 gonads with 1203 nuclei were evaluated for the top-3_ZnF.*

Both the diakinesis phenotypes and RAD-51 profile of *lem-3; top-3_ZnF* indicate that removal of LEM-3 does not generate defects enhancing the *top-3_ZnF* phenotype. These findings suggest that LEM-3 is not a resolvase which functions in parallel to TOP-3 in early recombination events or is a nuclease required to remove *top-3* mediated aberrant recombination intermediates.

6.4.2 *mus-81; top-3_ZnF*

The removal of *mus-81* from *top-3_ZnF* displayed more defects compared to the double mutant with *lem-3*. Only 75% of laid eggs hatched, representing a quite large reduction, compared to 98,7% viability of *top-3_ZnF* or 95% viability of *mus-81* (table 16). Hermaphrodites laid reduced amount of eggs and larval arrest was increased to 9,5%, which corresponds to a 2-fold increase compared to *mus-81* and 5-fold increase compared to *top-3_ZnF*. The incidence of males was only slightly increased in contrast to wild type but similar to the single mutants.

Table 16: Viability counts of mus-81; top-3_ZnF compared to the mus-81 and top-3_ZnF single mutants and wild type. *N is the total number of hermaphrodites analyzed for viability, brood size, larval arrest and incidence of males. Depicted numbers are average values for single hermaphrodite including standard deviation.*

	wt	***top-3_ZnF***	***mus-81***	***mus-81; top-3_ZnF***
Viability	99,75 ± 0,5 %	98,72 ± 0,7 %	94,6 ± 5,4 %	75,52 ± 24,5%
Brood size	229 ± 28	248 ± 34	187 ± 27	162 ± 45
Larval arrest	0%	1,8 ± 1,3%	4,25 ± 3 %	9,5 ± 7,2%
Incidence of males	0,06 ± 0,2 %	0,8 ± 1,1 %	0,1 ± 0,3%	0,3 ± 0,8%
N	16	16	7	8

In total, 50 oocytes were evaluated for the number of DAPI bodies in *mus-81; top-3_ZnF* (figure 23). Among these oocytes, 80% exhibited 6 bivalents, 18% showed 7 bodies and the remaining 2% were counted as 5 bodies (figure 23).

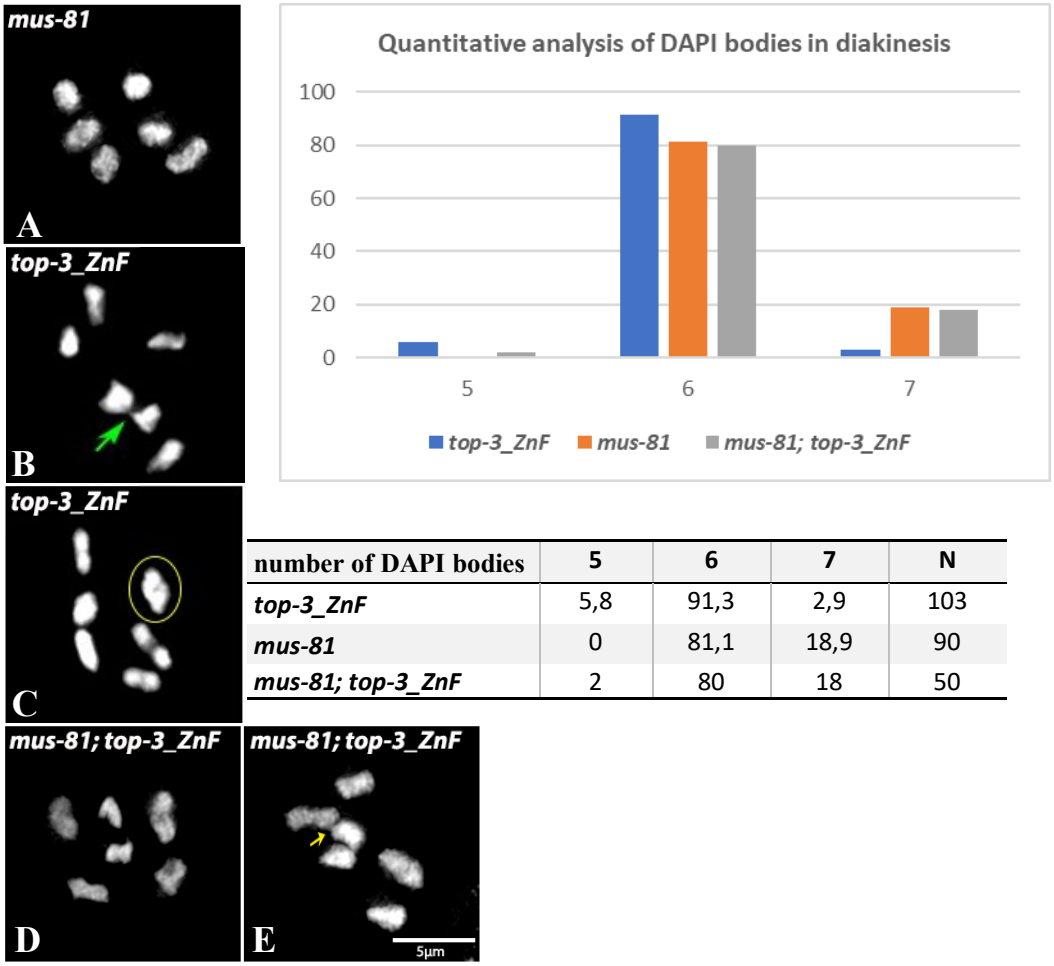

number of DAPI bodies	5	6	7	N
top-3_ZnF	5,8	91,3	2,9	103
mus-81	0	81,1	18,9	90
mus-81; top-3_ZnF	2	80	18	50

Figure 23: Quantitative analysis of DAPI bodies in diakinesis oocyte nuclei in mus-81; top-3_ZnF compared to the mus-81 and top-3_ZnF single mutants in %. *Genotypes are represented by* ***(A)*** *6 bivalents in mus-81* ***(B)*** *5 bodies due to chromatin connection (green arrow) between two bivalents in top-3_ZnF* ***(C)*** *6 bivalents with round shaped structure (yellow circle) in top-3_ZnF* ***(D)*** *6 bivalents in mus-81; top-3_ZnF* ***(E)*** *5 bodies with chromatin bridge (yellow arrow) between two bivalents in mus-81; top-3_ZnF. Table depicts the relative percentage of diakinesis counts for the given number of DAPI bodies for each indicated genotype. N is the total number of quantified oocyte nuclei for indicated genotypes.*

Many oocytes displayed abnormal structures in contrast to the shape of the wild-type bivalents, so they were classified qualitatively to describe the different shapes of bodies (figures 24-25). The first and most common category was 6 bivalents (figure 24A). Fragments were defined as DAPI signals smaller than univalents (figure 24B and 24D). The n.d. category (figure 24B) described fused bodies, where the connection was not as visible as in case of a bridge (figure 24E). The term atypical classified shapes that appeared to be aggregates of bivalents with univalents/fragments (figure 24B). The category dissociated bivalents (figure 24C) described two univalents connected by a chromatin bridges (the term mentioned by Jagut et al. 2016 and Hong et al. 2018).

In the double mutant, only 45% of all oocyte nuclei could be qualitatively categorized as 6 bivalents in contrast to 70% in *mus-81* and 92% in *top-3_ZnF* (figure 25). The rest of chromosome structure in the

oocyte nuclei can be classified to all other categories, which I described above. Fragments and univalents occurred to an extent similar to *mus-81*, but the amount of n.d. bodies was greatly increased from 1,1% in *mus-81* to 9,5% in the double mutant. The categories dissociated bivalents and atypical bodies represent the highest difference. The occurrence of dissociated bivalents was almost doubled in the double mutant and the classification of atypical bodies was only observed in the double mutant (9,5%) and not in the single mutant (figure 25).

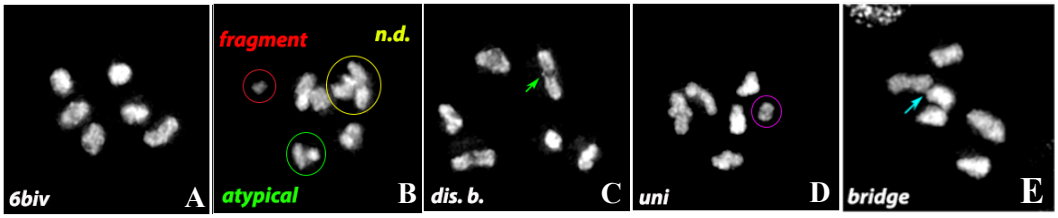

Figure 24: Categories of DAPI bodies' shapes in diakinesis oocyte nuclei. ***(A)*** *6 bivalents* ***(B red)*** *fragments* ***(B green)*** *atypical body* ***(B yellow)*** *n.d. category* ***(C)*** *dissociated bivalents* ***(D)*** *univalents* ***(E)*** *bridge.*

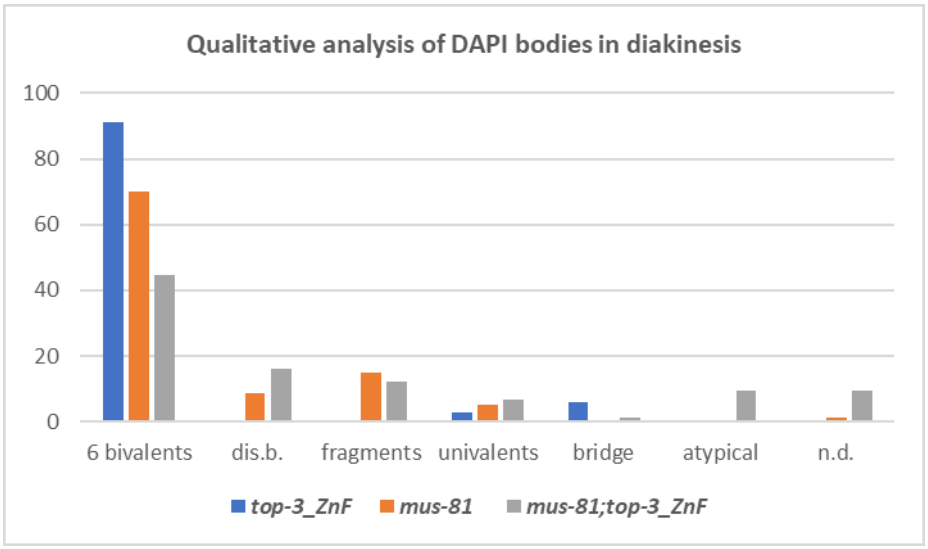

category	6 bivalents	dis. b.	fragments	univalents	bridge	atypical	n.d.	N
top-3_ZnF	91,3	0,0	0	2,9	5,8	0	0	103
mus-81	70,2	8,5	14,9	5,3	0,0	0	1,1	90
mus-81; top-3_ZnF	44,6	16,2	12	6,8	1,4	9,5	9,5	50

Figure 25: Qualitative analysis of DAPI bodies in diakinesis oocyte nuclei in mus-81; top-3_ZnF compared to the mus-81 and top-3_ZnF single mutants in %. *Table depicts the relative percentage of diakinesis counts for the given category for each indicated genotype. N is the total number of quantified oocyte nuclei for indicated genotypes.*

The other notable phenotypic difference between the single mutants and the double mutant was the appearance of the RAD-51 foci localization (figures 26-27). In the double mutant, RAD-51 appeared in form of bright foci and stretches already in the mitotic zone (z1-z2 in figure 26-27). Those

accumulated upon entering the transition zone (z3 in figures 26-27) and became most abundant during early pachynema (z4 in figures 26-27). They started to disappear from beginning of mid pachynema (z5 in figures 26-27), but more than 50% were not resolved at the end of meiotic prophase I (z6-z7 in figures 26-27). RAD-51 localized in a similar manner as seen in *mus-81*, but both the number of foci and stretches was much smaller in the single mutant and around 60% to 70% of them became resolved in contrast to the double mutant (figures 26-27).

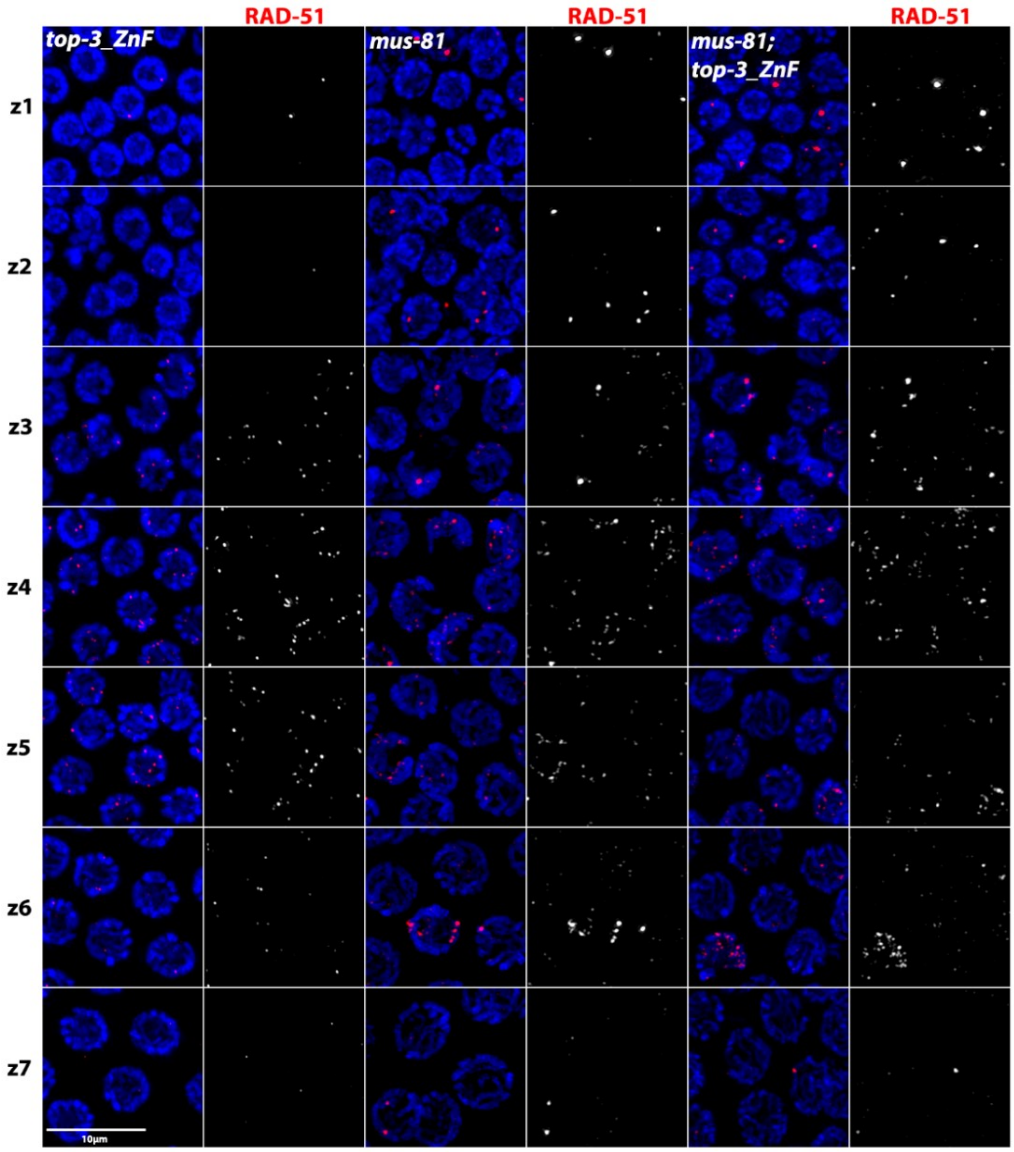

Figure 26: Localization of RAD-51 recombination foci in mus-81; top-3_ZnF compared to the mus-81 and top-3_ZnF single mutants. *Images display the RAD-51 localization in 7 zones of RAD-51 stained gonads of indicated genotypes. Zones represent mitotic zone (z1-z2) and stages of meiotic prophase I: transition zone (z3), early pachynema (z4), mid pachynema (z5) and late pachynema (z6-z7).*

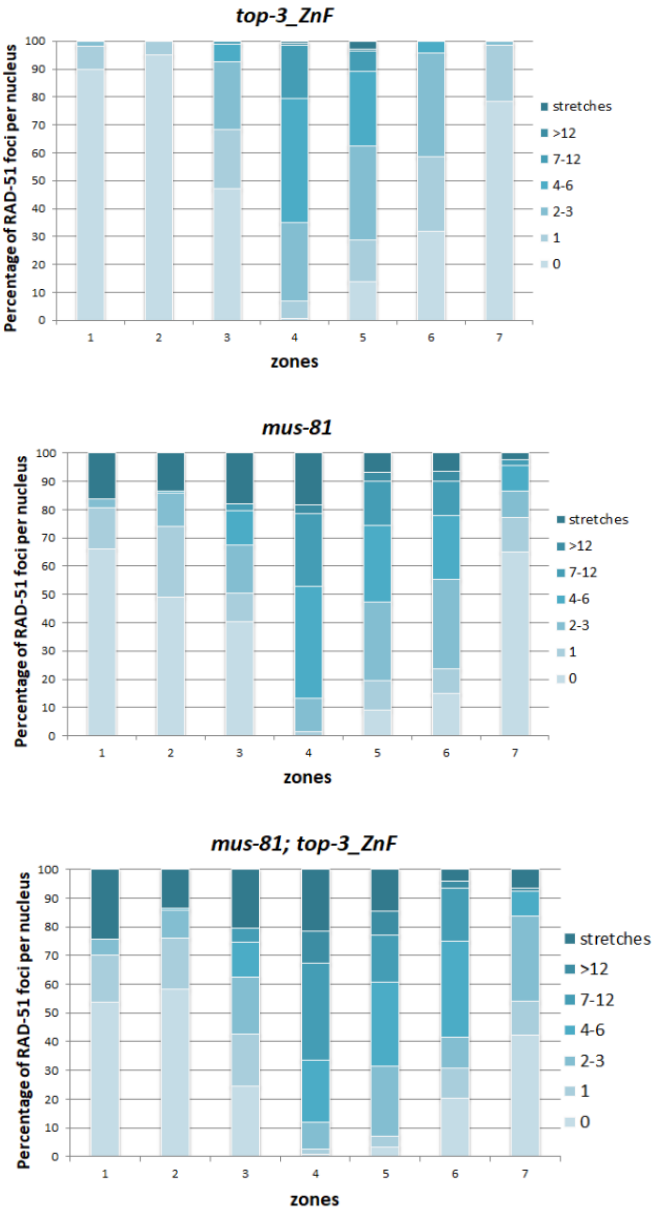

Figure 27: Quantification of RAD-51 foci dynamics in mus-81; top-3_ZnF compared to the mus-81 and top-3_ZnF single mutants. *Categories with percentage of RAD-51 foci per nucleus are plotted for every zone of indicated genotypes. Zones represent mitotic zone (z1-z2) and stages of meiotic prophase I: transition zone (z3), early pachynema (z4), mid pachynema (z5) and late pachynema (z6-z7). In total, 4 gonads with 793 nuclei were evaluated for mus-81; top-3_ZnF and 3 gonads with 589 nuclei were evaluated for mus-81 and 6 gonads with 1203 nuclei were evaluated for the top-3_ZnF.*

The double mutant *mus-81; top-3_ZnF* expressed the highest number of RAD-51 foci and stretches in contrast to *mus-81* and *top-3_ZnF* over all stages of meiotic prophase I. This and the severe diakinesis defects display a worsening of the phenotype of the double mutant compared to the two single mutants indicating that MUS-81 and TOP-3 ZnF motif might work in a parallel pathway to resolve recombination intermediates or that MUS-81 is needed to resolve the intermediates that are generated upon loss of the ZnF motif in TOP-3.

6.4.3 *mus-81 lem-3; top-3_ZnF*

The removal of the two above mentioned resolvases from *top-3_ZnF* background did not display much difference compared to the already severely affected double mutant *mus-81 lem-3*. The brood size of the triple mutant was unexpectedly higher than in the double mutant (table 17). Nevertheless, both mutants were 100% lethal since the laid eggs did not hatch.

Table 17: Viability counts of mus-81 lem-3; top-3_ZnF compared to wild type and mus-81 lem-3. *In total (N), 22 hermaphrodites were analyzed and averaged to define the hatch rate and brood size per single worm. Averages for brood size include standard deviation.*

	wt	***mus-81 lem-3***	***mus-81 lem-3; top-3_ZnF***
Lethality	0,3%	100%	100%
Brood size	229 ± 28	6 ± 5	42 ± 29
N	16	21	22

Quantification of DAPI bodies (figure 28) revealed that 82% of analyzed oocyte nuclei exhibited 6 bivalents and 9% showed 7 bodies thereby resembling the findings for *mus-81 lem-3*. However, 3,6% of observed diakinesis demonstrated 8 bodies and 5,4% displayed 5 bivalents in the triple mutant (figure 28).

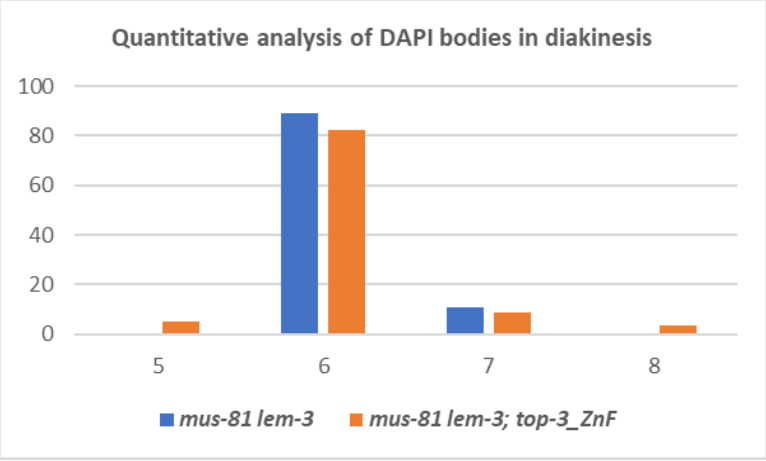

number of DAPI bodies	**5**	**6**	**7**	**8**	**N**
mus-81 lem-3	0	89,3	10,7	0	56
mus-81 lem-3; top-3_ZnF	5,4	82,1	8,9	3,6	56

Figure 28: Quantitative analysis of DAPI bodies in diakinesis oocyte nuclei in mus-81 lem-3; top-3_ZnF compared to the mus-81 lem-3 in %. *Table depicts the relative percentage of diakinesis counts for the given number of DAPI bodies for each indicated genotype. N is the total number of quantified oocyte nuclei for indicated genotypes.*

Diakinesis chromosomes were also examined qualitatively (figure 29). Only 35% of the examined oocyte nuclei exhibited 6 bivalents. The occurrence of dissociated bivalents was increased compared to *mus-81, top-3_ZnF*, but reduced when compared to *mus-81 lem-3*. Fragments were found only in 9% of nuclei representing little reduction in contrast to 11% in *mus-81 lem-3* or 12% in *mus-81; top-3_ZnF*. However, the number of univalents observed in triple mutant corresponded roughly to 3-fold increase over *mus-81 lem-3*. The most striking difference is the severely increased amount of atypical (11,5%) and n.d. bodies (10,3%) (figure 29).

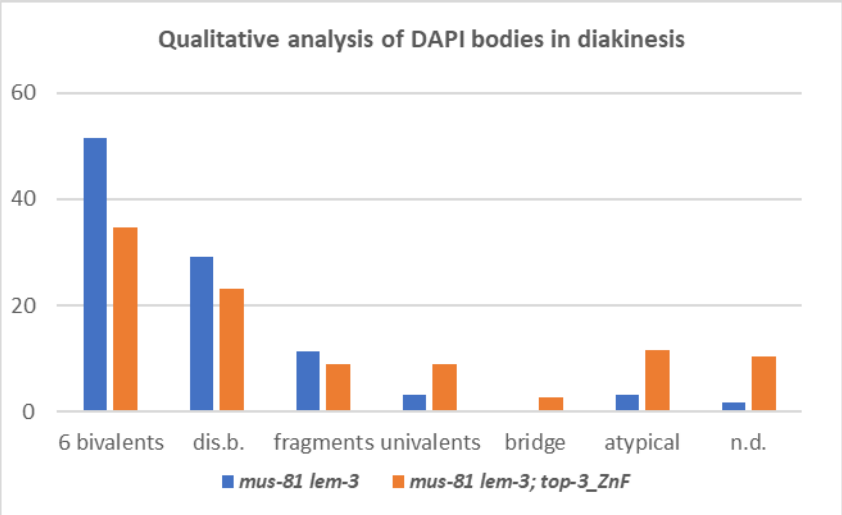

category	6 biv	dis. b.	fragments	univalents	bridge	atypical	n.d.	N
mus-81 lem-3	51,6	29,0	11,3	3,2	0,0	3,2	1,6	56
mus-81 lem-3; top-3_ZnF	34,6	23,1	9,0	9,0	2,6	11,5	10,3	56

Figure 29: Qualitative analysis of DAPI bodies in diakinesis oocyte nuclei in mus-81 lem-3; top-3_ZnF compared to the mus-81 lem-3 in %. *Table depicts the relative percentage of diakinesis counts for the given category for each indicated genotype. N is the total number of quantified oocyte nuclei for indicated genotypes.*

The triple mutant *mus-81 lem-3; top-3_ZnF* accumulated RAD-51 foci in a manner similar to the *mus-81 lem-3* (figures 26-27). It appeared in form of foci as well as stretches already in the mitotic zone (z1-z2 in figures 30-31), started to accumulate in the transition zone (z3 in figure 30-31) and peaked in early pachynema (z4 in figures 30-31). Both started to disappear when nuclei moved to mid pachynema (z5 in figures 30-31) and at least 50% became dissolved in the last zone of late pachynema (z7 in figures 30-31). The triple mutant showed more RAD-51 foci from the beginning of transition zone to the end of mid pachynema, whereas the double mutant *mus-81 lem-3* accumulated more foci and stretches in the mitotic zone and in late pachynema (z1-z2 and z6-z7 in figures 30-31). The triple mutant didn't accumulate more RAD-51 than *mus-81; top-3_ZnF* (figure 26-27), but showed more pyknotic nuclei, indicating an increased occurrence of apoptosis.

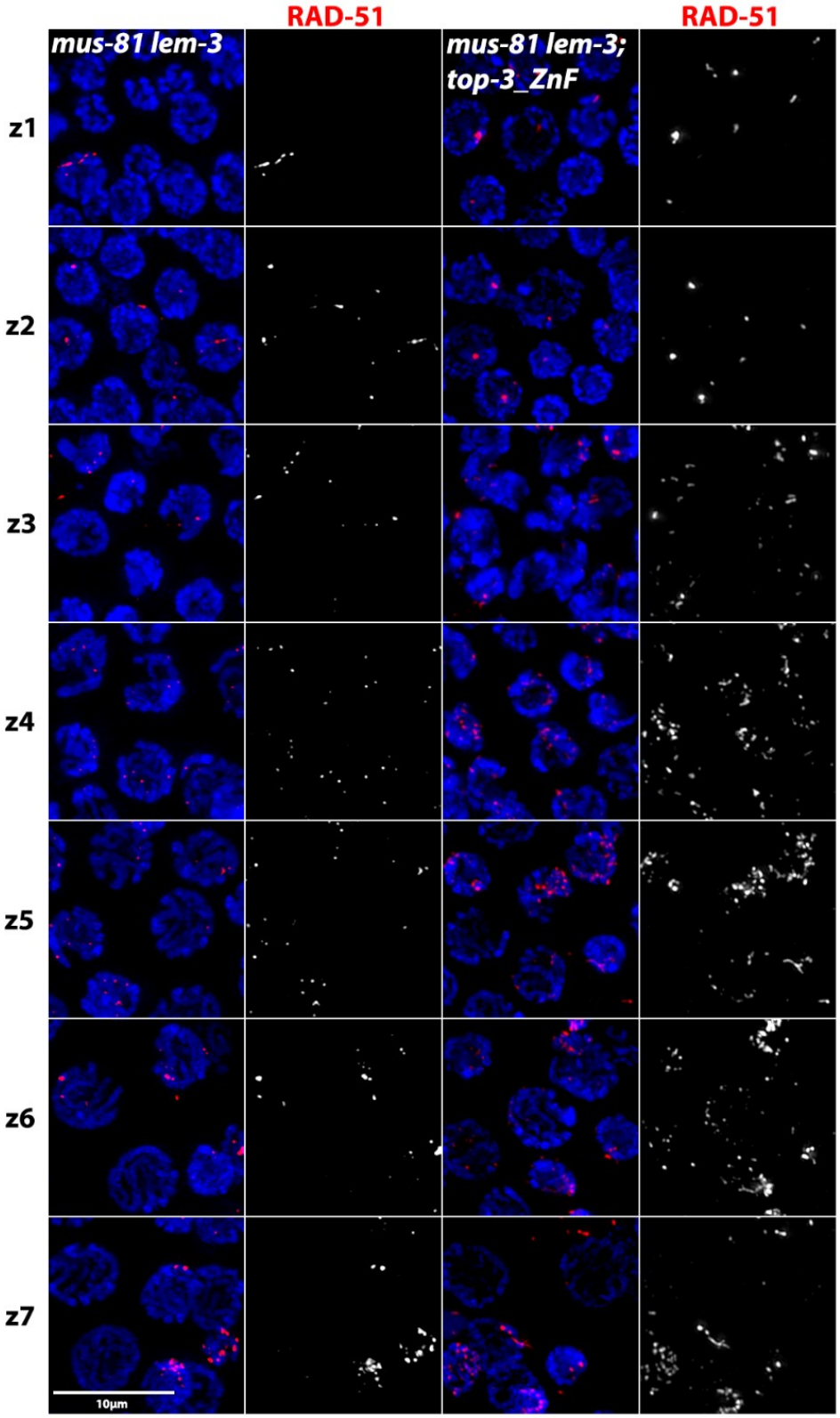

Figure 30: Localization of RAD-51 recombination foci in mus-81 lem-3; top-3_ZnF compared to the mus-81 lem-3 double mutant. *Images display the RAD-51 localization in 7 zones of RAD-51 stained gonads of indicated genotypes. Zones represent mitotic zone (z1-z2) and stages of meiotic prophase I: transition zone (z3), early pachynema (z4), mid pachynema (z5) and late pachynema (z6-z7).*

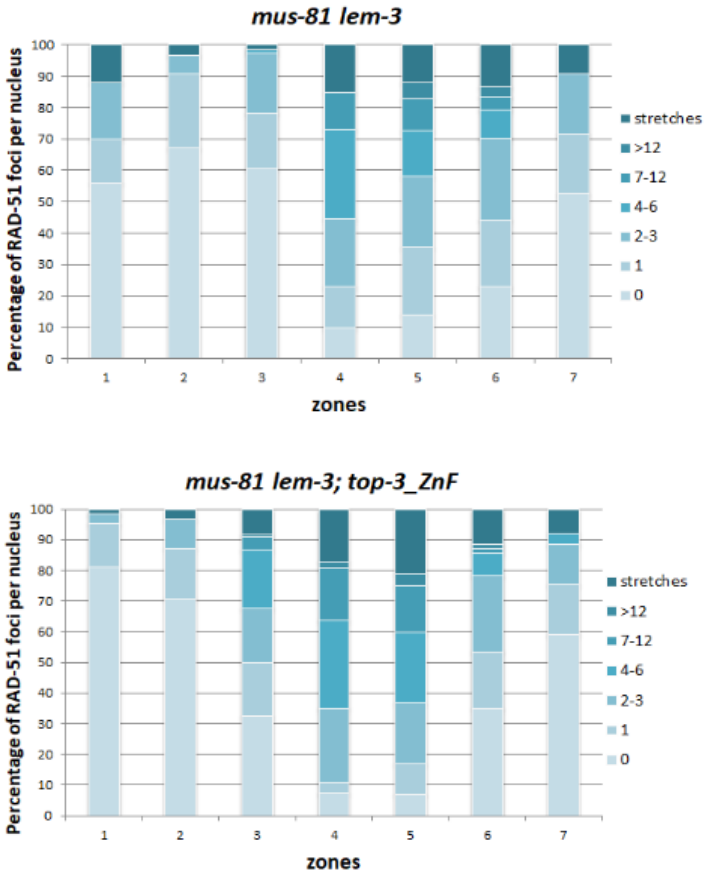

Figure 31: Quantification of RAD-51 foci dynamics in mus-81 lem-3; top-3_ZnF compared to the mus-81 lem-3 double mutant. *Categories with percentage of RAD-51 foci per nucleus are plotted for every zone of indicated genotypes. Zones represent mitotic zone (z1-z2) and stages of meiotic prophase I: transition zone (z3), early pachynema (z4), mid pachynema (z5) and late pachynema (z6-z7). In total, 6 gonads with 907 nuclei were evaluated for mus-81 lem-3; top-3_ZnF and 3 gonads with 407 nuclei were evaluated for mus-81 lem-3.*

At the resolution of above mentioned assays I found that *mus-81; top-3_ZnF* showed severe diakinesis defects and the highest increase of RAD-51 recombination foci form which more than 50% were not resolved at the end of the meiotic prophase I. On the contrary, the double mutant *lem-3; top-3_ZnF* displayed only a slight worsening of the *top-3_ZnF* phenotype. Comparing these double mutants to the triple mutant *mus-81 lem-3; top-3_ZnF,* I observed that removal of the ZnF motif worsened the severe meiotic and mitotic defects already displayed in the double mutant *mus-81; lem-3,* indicating the possibilities that in the absence of both resolvases TOP-3 supports the resolution of some early recombination intermediates.

6.5 Localization of the axial proteins HTP-3 and HTP-1 on diakinesis chromosomes

Crossover formation triggers chromosome remodeling which becomes apparent especially in the bivalents in diakinesis (Martin-Perez et al. 2008). During the remodeling process, specific axial elements become localized to different parts of bivalent arms in response to a yet undetermined crossover intermediate (Nabeshima et al.,2005; Martin-Perez et al. 2008). The re-distribution of those markers is often applied as a cytological readout for bivalent organization. The organization of abnormally shaped bivalents, that were observed in the double mutant *mus-81; top-3_ZnF* and in the triple mutant *mus-81 lem-3; top-3_ZnF*, were further examined by this technique and are displayed below.

6.5.1 *top-3_ZnF*

Localization of axial elements revealed that *top-3_ZnF* generated bivalents (DAPI in figure 32) that had the typical features of axial proteins seen in the wild type, where HTP-3 localized both along the short and long arms and HTP-1 concentrated to long arms (figure 32). No differences were detected in oocytes displaying 5 or 7 DAPI bodies (not shown).

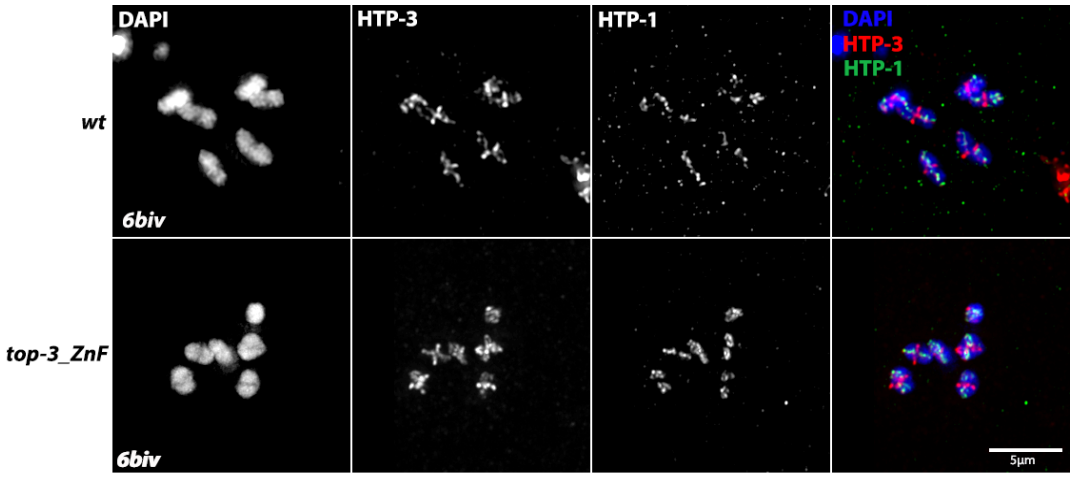

Figure 32: Localization of HTP-3 and HTP-1 in diakinesis of top-3_ZnF compared to the wild type. *The displayed oocytes show representative pictures of the localization of HTP-3 and HTP-1 in top-3_ZnF.*

6.5.2 *mus-81; top-3_ZnF*

The organization of abnormally shaped diakinesis described for *mus-81; top-3_ZnF* (figure 25) were analyzed by immunofluorescence and are depicted in figure 33. Oocytes with 6 bivalents displayed HTP-3 along both arms and HTP-1 only on long arms in the double as well as single mutants. Dissociated bivalents of the double mutant and *mus-81* single mutant (not shown) phenocopied this localization. HTP-3 and HTP-1 co-localized on univalents, whereas fragments displayed the proteins partially separately. In bodies of the n.d. category, that seem to be fused but the connection between them is not as visible as in case of a bridge, both proteins resembled the wild type. They did not reveal any fusion or abnormal organization. The atypical bodies, that occurred for the first time in the *mus-81; top-3_ZnF* double mutant and appeared as aggregates of bivalents and univalents/fragments, localized the HTP-3 and HTP-1 as well, however, the HTP-3 didn't appear in the cruciform way as observed usually for a bivalent. Most of the aggregates co-localized HTP-3 and HTP-1, however a small fraction localized them separately. Additionally, HTP-3 and HTP-1 didn't localize at the chromatin connection between two bodies generating a bridge.

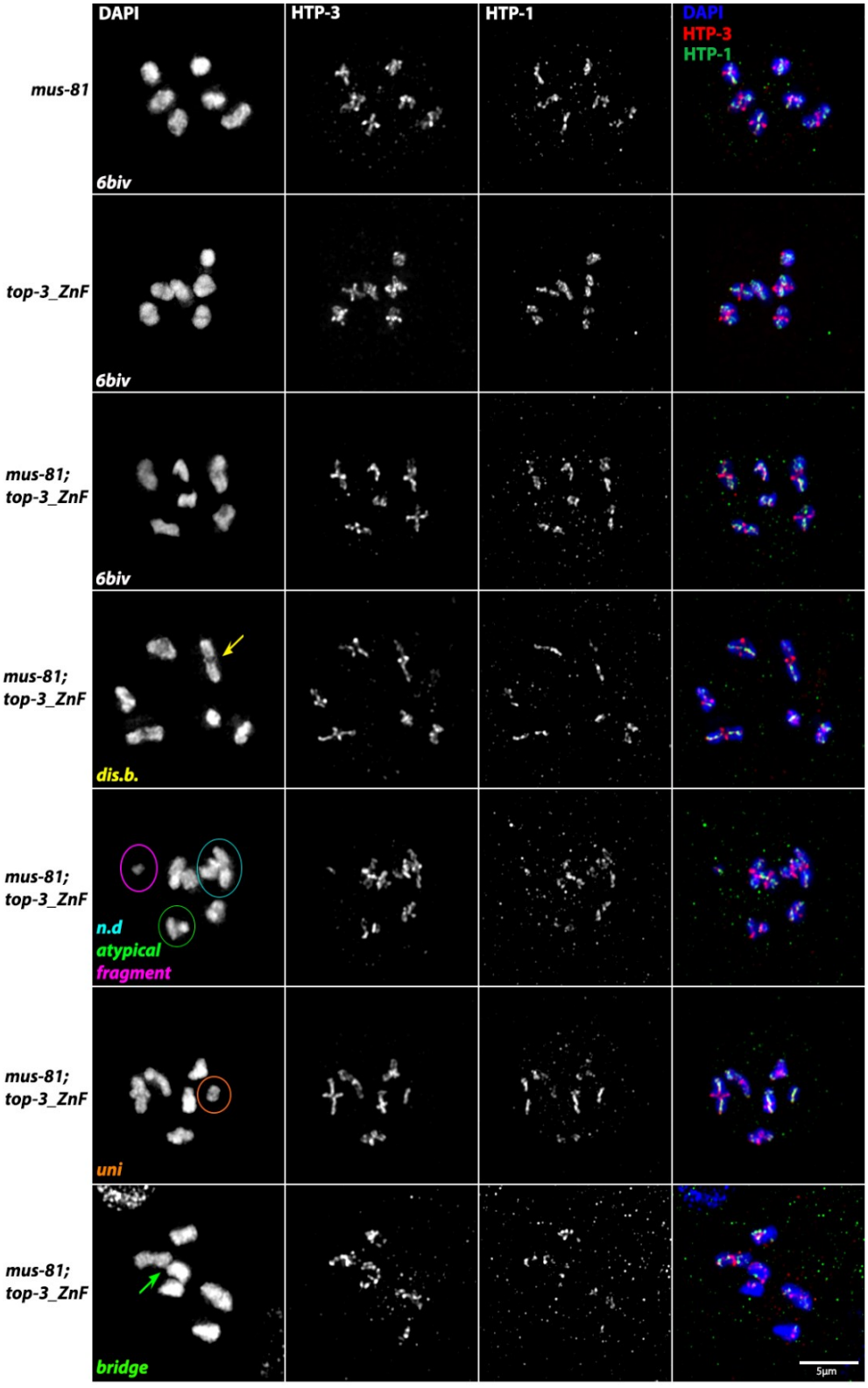

Figure 33: Localization of HTP-3 and HTP-1 in diakinesis of mus-81; top-3_ZnF double mutant compared to the mus-81 and top-3_ZnF single mutants. *The depicted oocytes show representative categories of DAPI bodies seen in the double mutant and the most frequent category of 6 bivalents in single mutants. Apart from the atypical and bridge, all categories occurred also in mus-81 and expressed HTP-3 and HTP-1 in a manner similar to the mus-81; top-3_ZnF double mutant.*

6.5.3 *mus-81 lem-3; top-3_ZnF*

DAPI bodies that were classified in the category of 6 bivalents displayed the localization of axial elements as known for the wild type: HTP-3 was localized on both arms whereas HTP-1 only on long arms. This was observed in the triple mutant as well as in *mus-81 lem-3* (figure 34). In the triple mutant, fragments and univalents resembled HTP-3 and HTP-1 localization observed in *mus-81; top-3_ZnF* or *mus-81 lem-3*. Two other categories localized both proteins in a manner similar to *mus-81; top-3_ZnF*: the bridge was visualized only by DAPI and dissociated bivalents showed HTP-1 on long bivalent arms and cruciform HTP-3. The triple mutant showed atypical bodies with following organization (figure 34): One seemed to be a bivalent aggregated with univalents. The bivalent showed cruciform HTP-3 and HTP-1 locating on long arms, while the two univalents co-localized axial elements HTP-3 and HTP-1. The other two resembled the atypical bodies found in *mus-81; top-3_ZnF*, where aggregates partially co-localized HTP-3 and HTP-1.

I analyzed the localization of HTP-3 and HTP-1 in order to examine the organization of the chromosomes at diakinesis stage in *mus-81; top-3_ZnF* and *mus-81 lem-3; top-3_ZnF* (figure 32 and 33). The qualitative analysis of the axial proteins displayed a similar localization in those mutants. Bivalents and dissociated bivalents concentrated HTP-3 along both arms, whereas HTP-1 only on long arms. Univalents showed a co-localization of the proteins in 6,8% of observed oocyte nuclei in *mus-81; top-3_ZnF* and 9% in *mus-81 lem-3; top-3_ZnF*. This differs from *rmh-1* which manage to designate crossovers but fails sometimes to keep the connections between homologous, since it localizes the axial proteins to reciprocal domains (Jagut et al., 2016). Therefore, I conclude, that not only the crossover designation but also the maturation is affected in absence of the ZnF motif of TOP-3 and the resolvases MUS-81 and LEM-3. Organization of the n.d. or atypical bodies, which seemed to be aggregates of bivalents with fragments/univalents, were not revealed by the localization of HTP-3 and HTP-1.

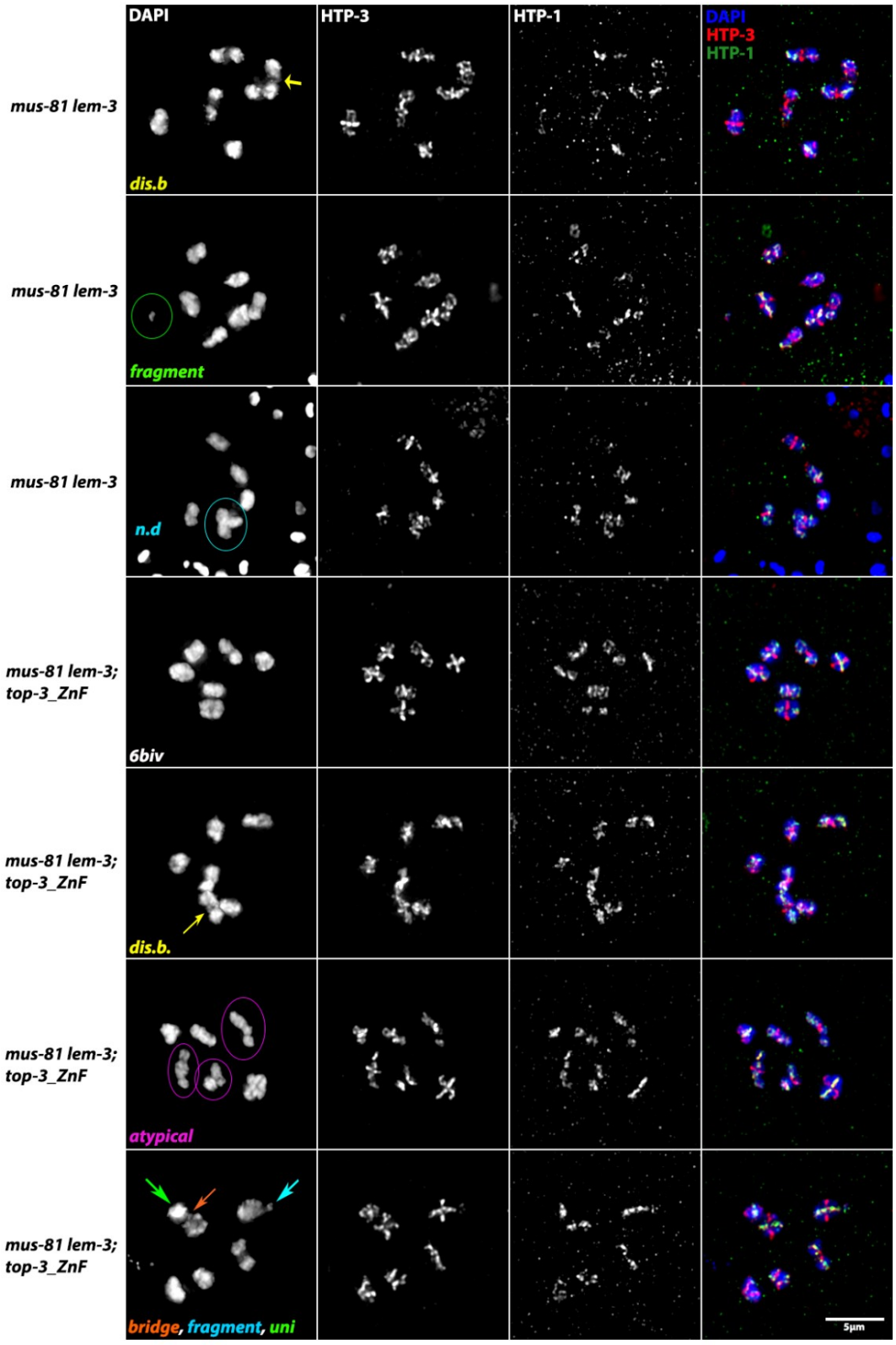

Figure 34: Localization of HTP-3 and HTP-1 in diakinesis of mus-81 lem-3; top-3_ZnF triple mutant compared to the mus-81 lem-3 double mutant. *The depicted oocytes display representative categories of DAPI bodies. Apart from bridge, all categories occurred also in the double mutant and expressed HTP-3 and HTP-1 in a manner similar to the triple mutant.*

6.6 Heterologous recombination assay in *top-3_ZnF*

In order to further analyze the role of the TOP-3 ZnF motif in early steps of recombination, I assessed illegitimate recombination between non-identical sequences. This allowed me to examine, whether the ZnF of TOP-3 is necessary to discourage the strand invasion event into heterologous non-matching sequences, which can potentially lead to genome rearrangements. I analyzed the illegitimate recombination in progenies of *top-3_ZnF* parents, that carried a specifically customized chromosome II from the strain *mIn1[mIs14 (GFP)rol-1(e91)]/[dpy-25(e817)]*. In the *mln-1* balancer a large region is inverted and thus creates a big region of heterology encompassing the balancer (Ortiz et al. 2018). The phenotypic screening of the progeny serves as a read-out whether heterologous recombination has taken place in the parental germ cells. In the case of illegitimate recombination, markers give rise to different recombinant-phenotypes (explained in detail in the method section, see chapter 5.10).

In wild type, only 3 of 4123 examined progenies showed recombinant phenotypes. On the contrary, with 11 recombinants of 4103 observed worms, *top-3_ZnF* increased the occurrence of heterologous recombination almost 4 times (table 18).

Table 18: Numbers of progenies in the wild type and top-3_ZnF showing non-recombinant and recombinant phenotypes demonstrated by different combinations of visible genetic markers. *Percentage of heterologous recombination is indicated for each genotype.*

phenotypes	***wt***	***top-3_ZnF***
mild dpy, non rol, mild GFP	2275	2192
dpy, non rol, non GFP	661	788
non dpy, rol, bright GFP	1184	1112
total non-recombinant worms	**4120**	**4092**
dpy, non rol, mild GFP	3	9
mild dpy, non rol, bright GFP	0	1
mild dpy, non rol, non GFP	0	0
non dpy, rol, mild GFP	0	1
total recombinant worms	**3**	**11**
% heterologous recombination progeny	3/4123 **0,07%**	11/4103 **0,27%**

Ortiz et al. 2018 showed that removal of HIM-6 increased the heterologous recombination to 6,6% (Ortiz et al. 2018). We measured 0,27% of ectopic invasions in *top-3_ZnF,* that corresponds to a 4-fold increase over the wild type but, when compared to the number for illegitimate recombination in *him-6* mutants, the small increase suggests that the *top-3_ZnF* mutant is still proficient to discourage heterologous recombination, although not to 100%.

6.7 Localization of the TOP-3 protein, without the ZnF motif

Using CRISPR/Cas9 genome editing, I inserted an HA tag into the TOP-3 wild-type protein and the TOP-3_ZnF protein to analyze whether the lack of the ZnF affects the localization of TOP-3. Worms were immune-stained and processed as described in the method section (see chapters 5.4 to 5.6). Images of representative gonads were divided into 4 zones of equal length from beginning of the transition zone to the end of late pachynema. Those zones represent the transition zone, early, mid and late pachynema of meiotic prophase I. Figure 35 shows representative pictures with nuclei from each zone stained with DAPI and anti-HA, depicting the recombination foci which contain TOP-3 or TOP-3_ZnF.

Automated quantification revealed bright and faint populations of foci (figures 36 to 38). TOP-3 started to form few distinct foci (0,2 bright and 1,8 foci) in transition zone (z1 in figures 35-38). The abundance of both populations rapidly increased in the next two zones, on average, about 15 foci, ranging from 3 to 35 (z2-z3 in figures 35-38). Faint foci (9 per nucleus) reached their maximal abundance in early and late pachynema, whereas bright foci (8,6 per nucleus) peaked during mid pachynema (figure 37 and 38). When entering the fourth zone (z4 in figures 35-38), the bright population of foci decreased to an average of 5 bright foci per nucleus (figure 37). TOP-3 didn't further localize into foci in nuclei of diplonema and at the proximal end of the gonad (not shown).

TOP-3_ZnF showed a comparable dynamic distribution of foci as seen in the wild-type TOP-3: it appeared as foci, on average 0,2 bright and 2 faint foci in transition zone (z1 in figures 35-38), accumulated in early and mid pachynema (z2-z3 in figures 35-38), decreased in late pachynema (z4 in figures 35-38) and was removed in diplotene nuclei and at the proximal end of the gonad (not shown). The amounts of foci for both populations were however reduced: in early pachynema there were on average only 6,4 foci ranging from 0 to 20. In mid pachynema the number increased to 14,2 foci, ranging from 5 to 25 per nucleus. With a 4-fold reduction of bright and a 2-fold reduction of faint foci early pachynema represents the region with the most prominent difference of TOP-3_ZnF foci compared to TOP-3 foci (figures 36-38). The peak of TOP-3 faint foci that occurred in early and late pachynema was not observed for TOP-3_ZnF (figure 38).

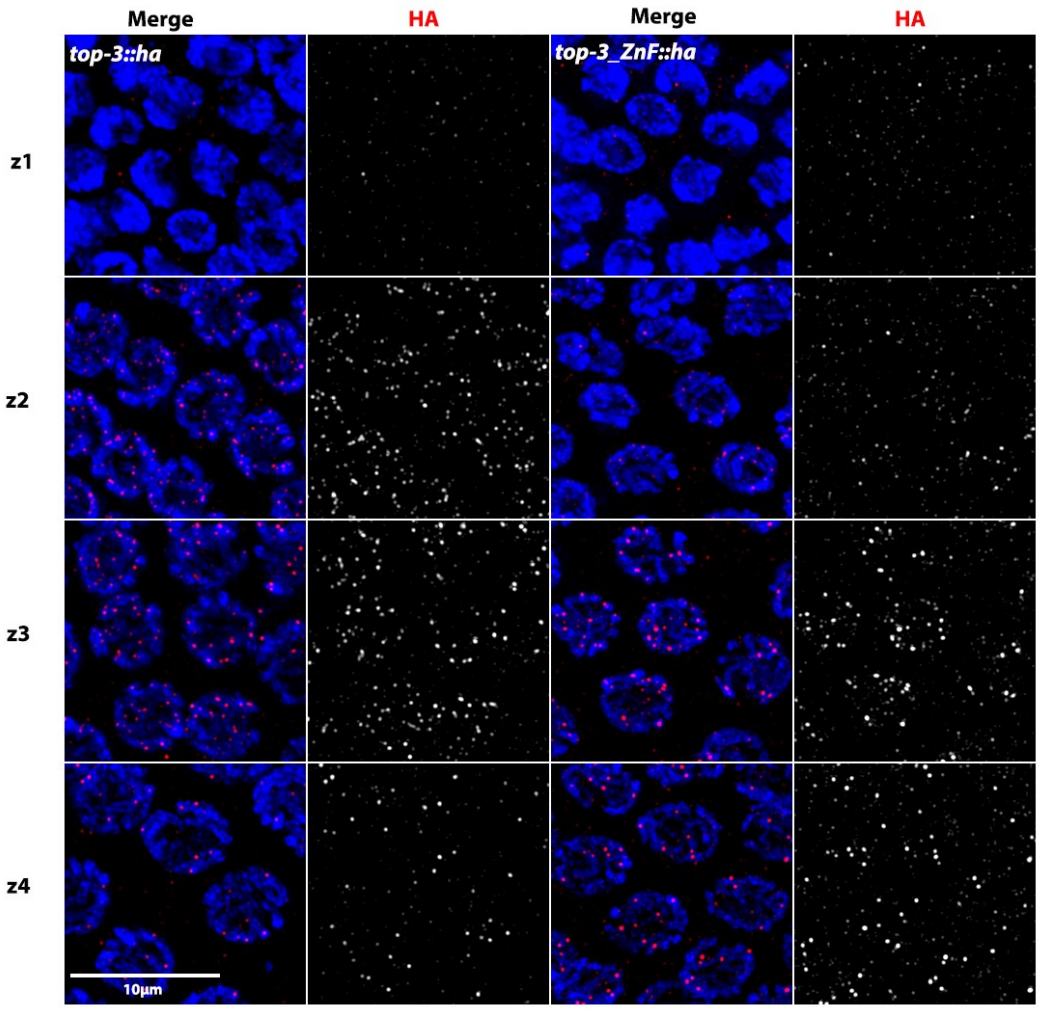

Figure 35: Localization of HA foci in top-3::ha and top-3_ZnF::ha. *Zones represent the transition zone (z1), early pachynema (z2), mid pachynema (z3) and late pachynema (z4) of meiotic prophase I.*

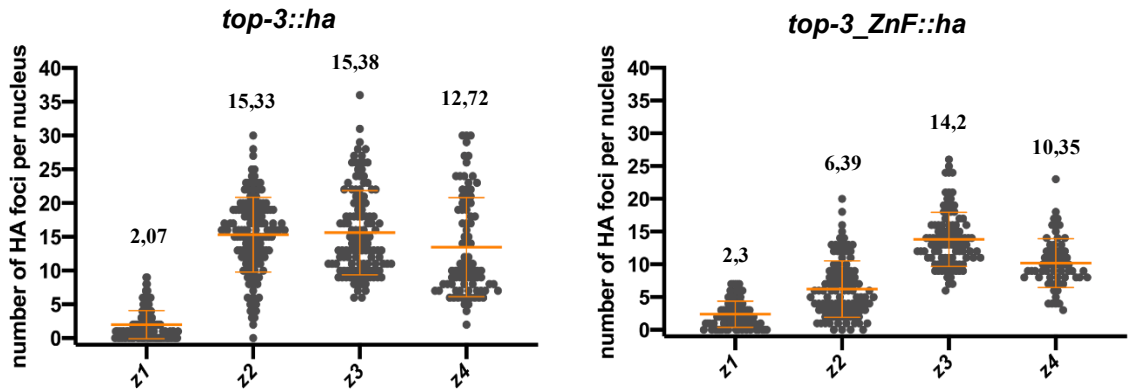

Figure 36: Combined counts of bright and faint HA foci automatically quantified in top-3::ha and top-3_ZnF::ha*. Every zone displays the average number of combined counts of bright and faint foci. In total, 3 gonads with 502 nuclei were evaluated for top-3::ha and 3 gonads with 435 nuclei for top-3_ZnF::ha. Mann-Whitney test calculated following difference in transition zone: top-3::ha vs. top-3_ZnF:: ha p>0.05; early pachynema: top-3:: ha vs. top-3_ZnF::ha p<0.0001; mid pachynema: top-3::ha vs. top-3_ZnF::ha p>0.05; late pachynema: top-3::ha vs. top-3_ZnF::ha p>0.05.*

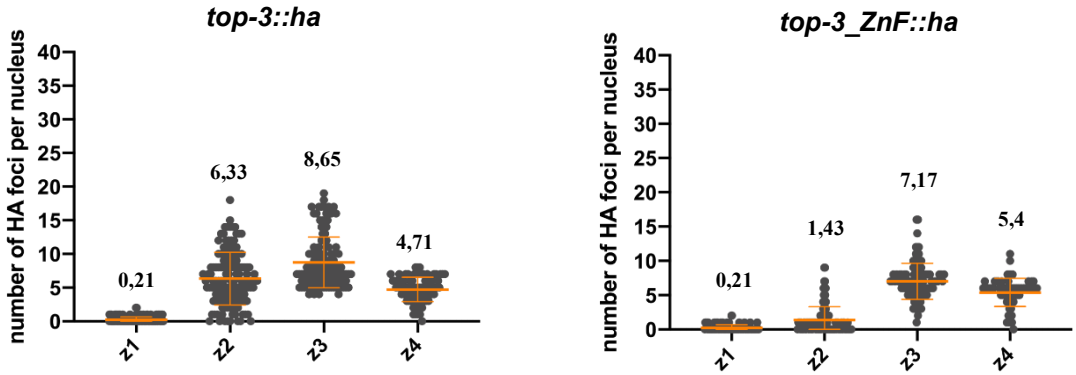

Figure 37: Automatic quantification of HA bright foci in top-3::ha and top-3_ZnF::ha*. Zones represent the transition zone (z1), early pachynema (z2), mid pachynema (z3) and late pachynema (z4) of meiotic prophase I. Every zone displays the average number of bright foci.*

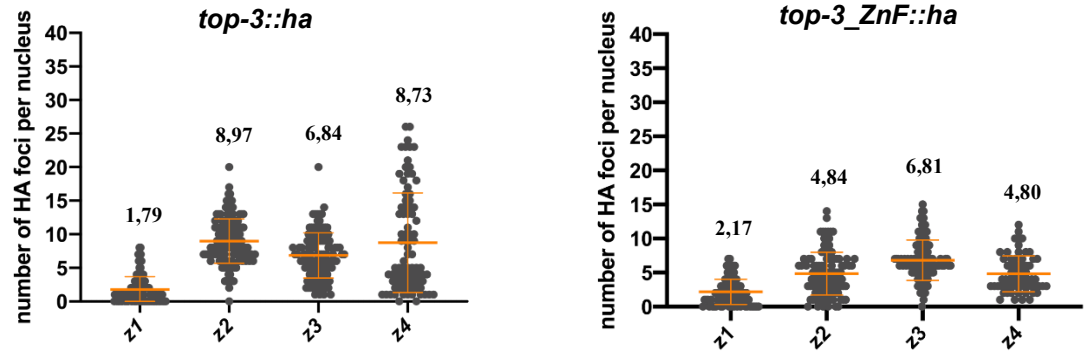

Figure 38: Automatic quantification of HA faint foci in top-3::ha and top-3_ZnF::ha. *Zones represent the transition zone (z1), early pachynema (z2), mid pachynema (z3) and late pachynema (z4) of meiotic prophase I. Every zone displays the average number of faint foci.*

I conclude that the removal of the ZnF motif reduced both populations of TOP-3 foci over all zones and shifted the peak of localization on pachytene chromatin, indicating the important role of the ZnF motif for localization of TOP-3. The largest reduction was observed during early pachynema, supporting the hypothesis, that the ZnF motif has an important role during early steps of recombination.

6.8 Localization of the BTR complex members in *top-3_ZnF*

In order to analyze whether the deletion of the ZnF motif affects the localization of the complex members HIM-6 and RMH-1, I crossed the tagged versions of HIM-6 and RMH-1 with HA and GFP tags respectively into the *top-3_ZnF* mutant. After immunostainings to detect the tagged proteins (see materials and methods chapter 5.4), I analyzed the images in the following way: I divided the gonads

into 4 zones of equal length as previously described for the TOP-3 and TOP-3_ZnF localization (see chapter 6.7). Figures 39 to 42 show the localization of HIM-6 and RMH-1 in the following meiotic stages: transition zone (figure 39), early pachynema (figure 40), mid pachynema (figure 41) and late pachynema (figure 42). Every figure depicts the comparison of RMH-1 and HIM-6 localization in the wild type and *top-3_ZnF* mutant. RMH-1 was quantified using the automated method (figure 43). HIM-6 was analyzed only qualitatively since it localizes as a combination of nucleoplasmic haze and recombination foci.

In the transition zone (figure 39), RMH-1 started to localize into foci, on average 1,8 in wild type and 0,7 in *top-3_ZnF*. HIM-6 appeared mostly as nucleoplasmic haze with small amounts of distinct foci in both, wild type and *top-3_ZnF*.

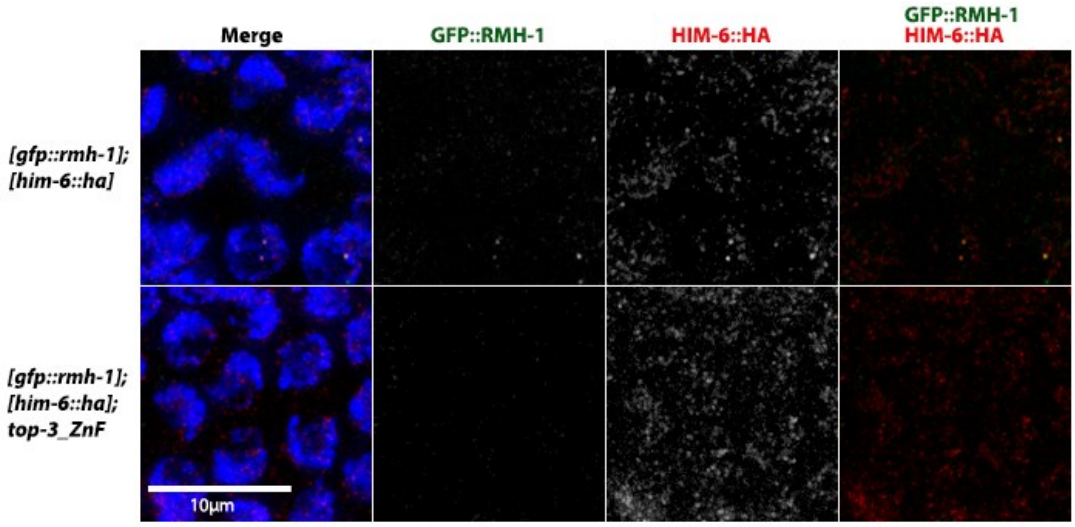

Figure 39: Localization of GFP and HA foci in transition zone of gfp::rmh-1; him-6::ha compared to gfp::rmh-1; him-6::ha; top-3_ZnF.

At the beginning of early pachynema (figure 40), RMH-1 accumulated rapidly, localizing on average as 15,2 foci per nucleus, ranging from 3 to 32 (figure 43). HIM-6 was harder to detect in foci and rather seen as a nucleoplasmic haze, but the number of foci markedly increased compared to the transition zone. Both complex members showed similar increasing trends in the mutant. However, RMH-1 was reduced to only 10,5 foci per nucleus, ranging from 0 to 28 (figure 43). HIM-6 continued localizing as nucleoplasmic haze but also seemed to be reduced in foci abundance.

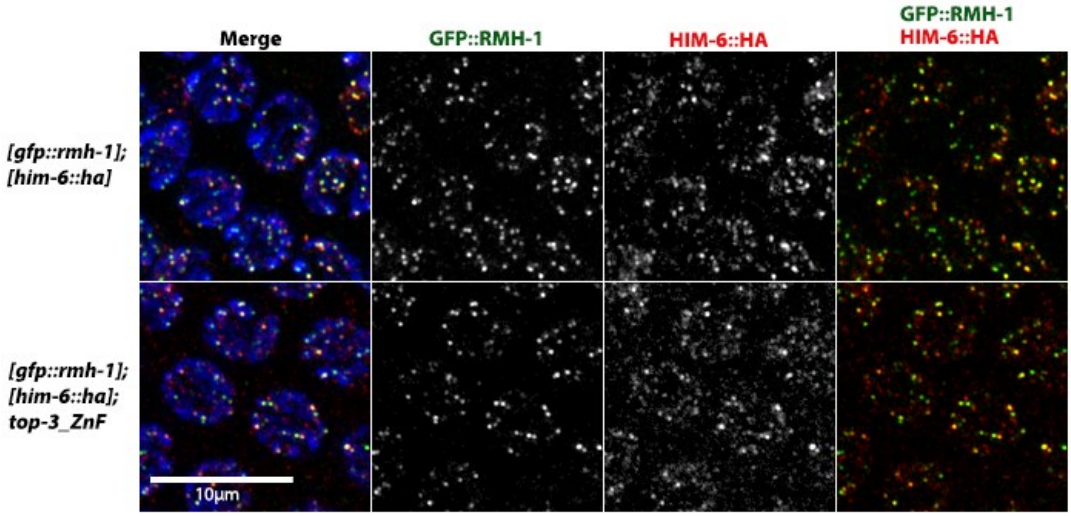

Figure 40: Localization of GFP and HA foci in early pachynema of gfp::rmh-1; him-6::ha compared to gfp::rmh-1; him-6::ha; top-3_ZnF.

Localization during mid pachynema (figure 41) can be described as a further increase in abundance and intensity of RMH-1 foci as well as HIM-6 foci and nucleoplasmic haze. With an average of 18,64 the amount of RMH-1 is the highest during meiotic prophase I. This amount was reduced in *top-3_ZnF*, where RMH-1 concentrated into an average of 12,8 foci per nucleus (figure 43). Again, the HIM-6 signal was reduced in abundance and intensity of foci as well as nucleoplasmic haze when compared to the wild type.

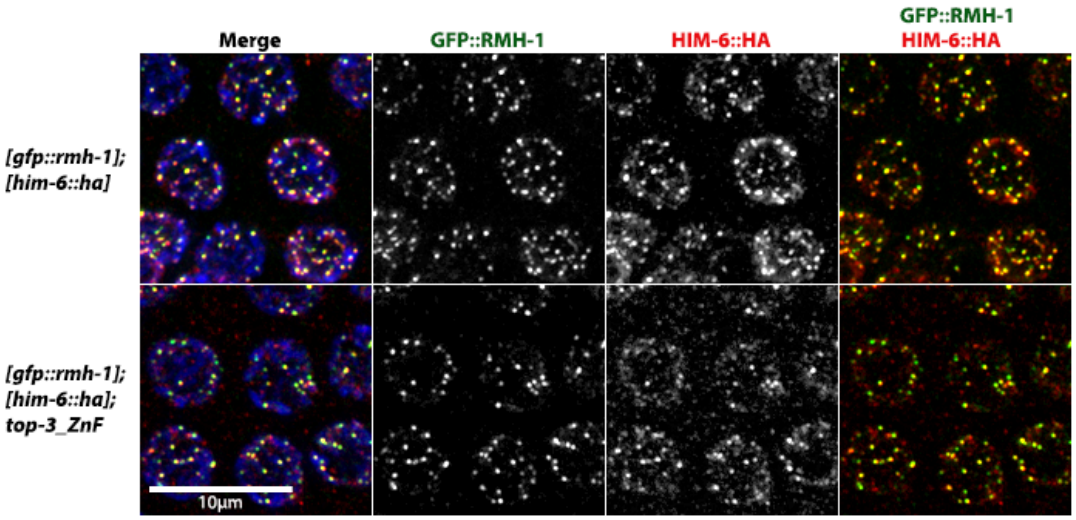

Figure 41: Localization of GFP and HA foci in mid pachynema of gfp::rmh-1; him-6::ha compared to gfp::rmh-1; him-6::ha; top-3_ZnF.

In late pachynema (figure 42), RMH-1 and HIM-6 foci were detected in reduced numbers in both the wild type and the mutant, nevertheless the foci were larger and more intense. HIM-6 localized again as nucleoplasmic haze. In *top-3_ZnF*, the quantity of foci was reduced. RMH-1 localized on average as 6,9 foci in *top-3_ZnF* in contrast to 8,5 in wild type (figure 43) and HIM-6 appeared to be reduced in intensity and abundance. Upon entering diplonema (not shown), RMH-1 and HIM-6 disengaged from the chromatin in wild type and *top-3_ZnF*.

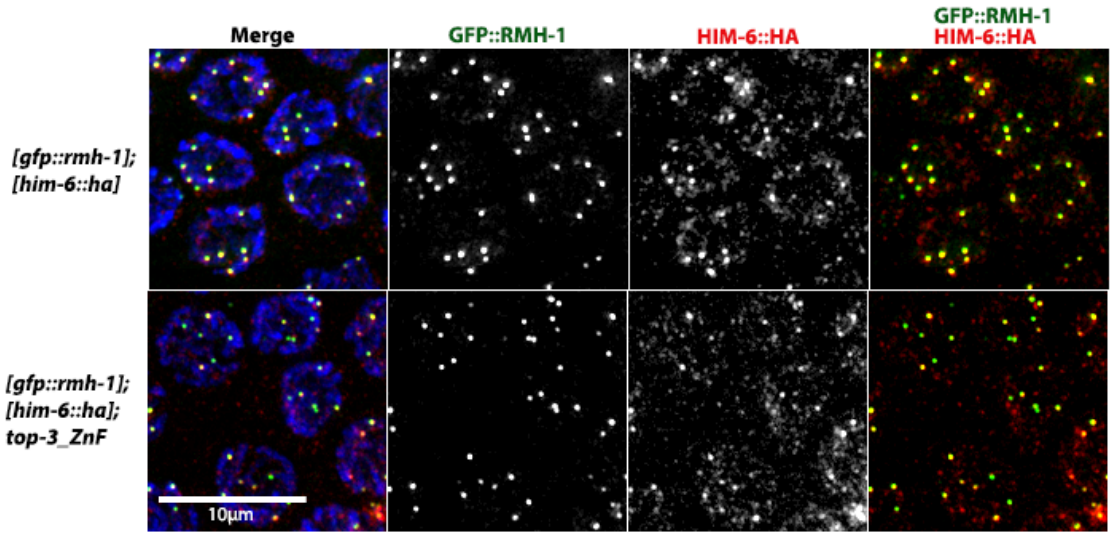

Figure 42: Localization of GFP and HA foci in late pachynema of gfp::rmh-1; him-6::ha compared to gfp::rmh-1; him-6::ha; top-3_ZnF.

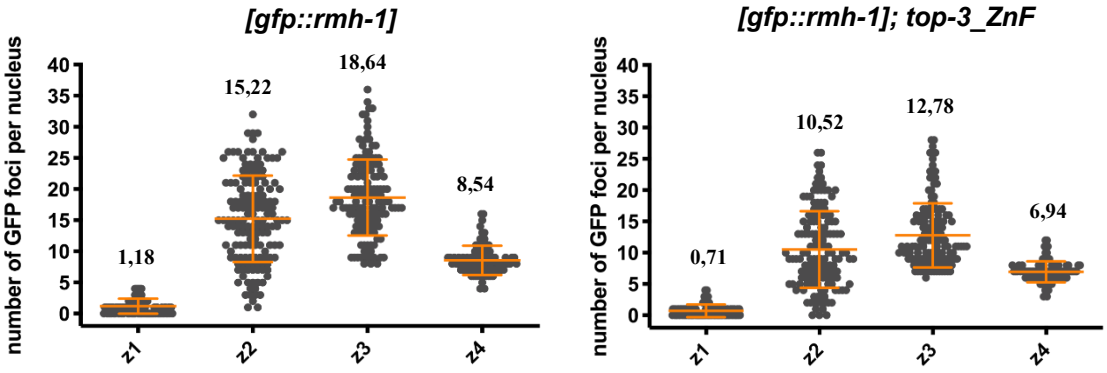

Figure 43: Automated quantification of GFP foci in gfp::rmh-1; him-6::ha compared to gfp::rmh-1; him-6::ha; top-3_ZnF. *Zones represent transition zone (z1), early pachynema (z2), mid pachynema (z3) and late pachynema (z4) of meiotic prophase I. Each zone displays the average number of GFP foci. In total, 3 gonads with 502 nuclei were evaluated for gfp::rmh-1; him-6::ha and 3 gonads with 570 nuclei were evaluated for gfp::rmh-1; him-6::ha; top-3_ZnF. Mann-Whitney test calculated following difference in transition zone: gfp::rmh-1 vs. gfp::rmh-1; top-3_ZnF p=0.0005; early pachynema: gfp::rmh-1 vs. gfp::rmh-1; top-3_ZnF p<0.0001; mid pachynema: gfp::rmh-1 vs. gfp::rmh-1; top-3_ZnF p<0.0001; late pachynema: gfp::rmh-1 vs. gfp::rmh-1; top-3_ZnF p<0.0001.*

Overall, the reduction of RMH-1 and HIM-6 foci implies, that additionally to TOP-3 localization, the TOP-3 ZnF motif also affects the localization of the other complex members. The most prominent difference is represented by RMH-1 localization in early pachynema and thereby resembles the reduction of TOP-3.

6.9 Co-localization of the BTR complex members in *top-3_ZnF*

Localization assays revealed similar expression patterns of RMH-1 and TOP-3 suggesting the possibility of co-localization. Additionally, these patterns seemed to be affected by the deletion of the ZnF motif. To investigate the co-localization of RMH-1 with TOP-3 and whether it is affected by *top-3_ZnF* mutation, gonads were immune stained and processed as described in the previous chapters 6.7 and 6.8.

As shown in figure 44, RMH-1 and TOP-3 localized in a similar manner: appeared as few bright foci in the transition zone, accumulated during early and mid pachynema and decreased during late pachynema. When looking at the localization in *top-3_ZnF*, it was clear that RMH-1 and TOP-3_ZnF followed the same dynamics across the four zones, however, the amount of foci was reduced with the biggest reduction in early pachynema.

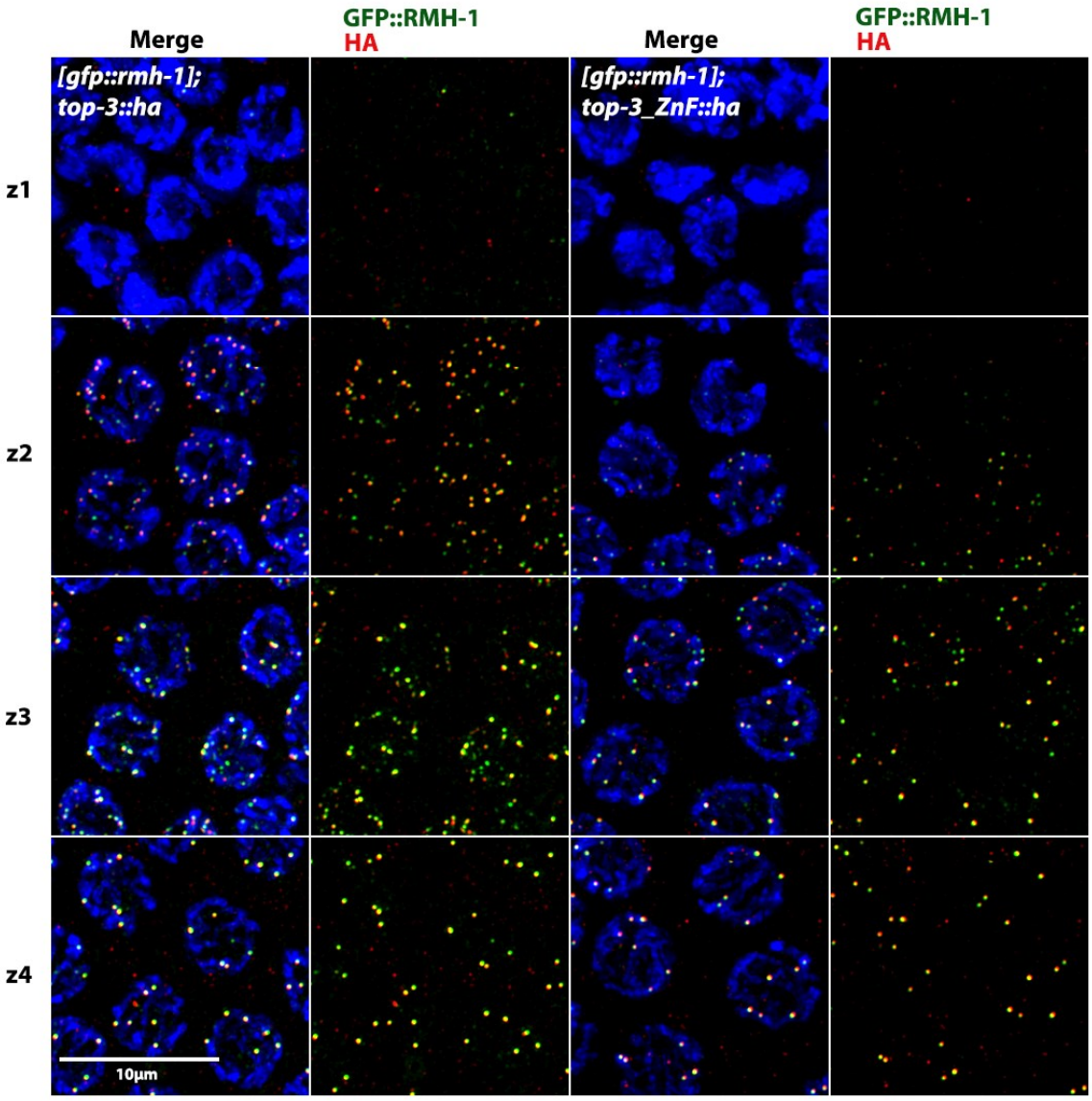

Figure 44: Localization of GFP and HA foci in gfp::rmh-1; top-3::ha compared to gfp::rmh-1; top-3_ZnF::ha. *Zones represent transition zone (z1), early pachynema (z2), mid pachynema (z3) and late pachynema (z4) of meiotic prophase I.*

Co-localization was analyzed by applying an automated script that calculates the percentage of HA foci colocalizing with GFP foci versus percentage of GFP foci colocalizing with HA foci in wild type and *top-3_ZnF*.

In wild type, the percentage of HA foci increased from 15,5% in transition zone to almost 70% in mid pachynema and slightly decreased to 65% in late pachynema (figure 45). RMH-1 foci followed the same trend with a slightly smaller percentage of co-localization from zone 2 to zone 4. Upon entering late pachynema, only 48% of GFP foci co-localized with HA foci representing quite a difference to 66% of HA co-localization (figure 45).

gfp::rmh-1; top-3::ha	ZONE 1	ZONE 2	ZONE 3	ZONE 4
% HA foci ± SD	15,5 ± 3,8	59,6 ± 3,6	69,91 ± 6,4	66,54 ± 7,4
% GFP foci ± SD	17,4 ± 5,7	53,4 ± 3,6	62,10 ± 6,1	48,19 ± 11,2

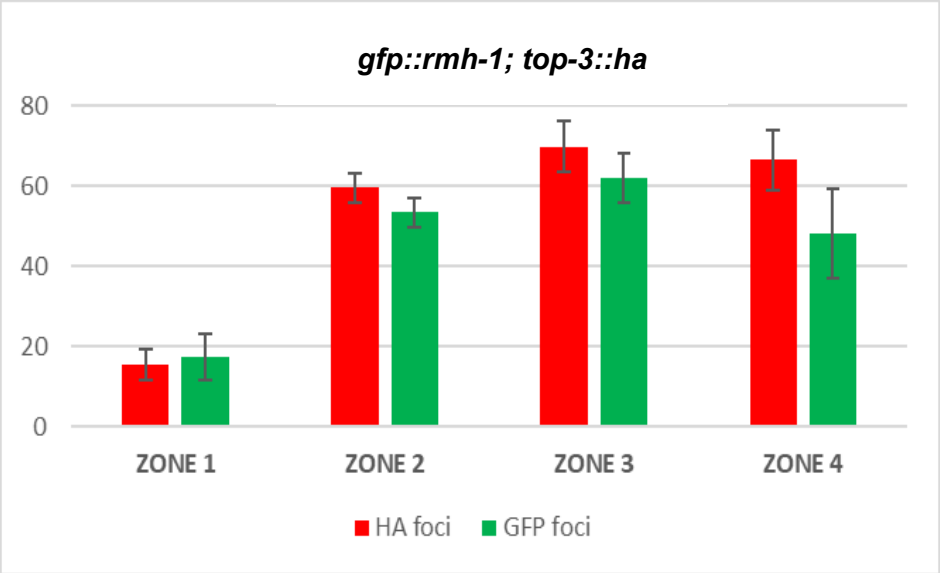

Figure 45: Co-localization of GFP and HA foci in gfp::rmh-1; top-3::ha in 4 zones of meiotic prophase I. *Percentages of HA foci (red) colocalizing with GFP foci versus percentages of GFP foci (green) colocalizing with HA foci were calculated by automated quantification. All averages include standard deviation. In total, 4 gonads with 547 nuclei were evaluated for gfp:rmh-1; top-3::ha.*

Co-localization in *top-3_ZnF* contradicted the findings for the wild type. TOP-3_ZnF showed a reduced percentage of co-localization throughout all zones, ranging from 2,8% in transition zone to 55% in late pachynema (figure 46). RMH-1 displayed a similar extent of co-localization starting as well with 2,2% in transition zone and ending with 54% in late pachynema. The last zone showed, however, that there were more RMH-1 foci which co-localized with TOP-3_ZnF than with TOP-3 wild type (figure 46).

gfp::rmh-1; top-3_ZnF::ha	ZONE 1	ZONE 2	ZONE 3	ZONE 4
%HA foci ± SD	2,68 ± 0,8	25,15 ± 5,1	53,71 ± 14,9	54,94 ± 9,1
%GFP foci ± SD	2,20 ± 1,4	21,07 ± 7,4	45,66 ± 12,8	53,41 ± 18,3

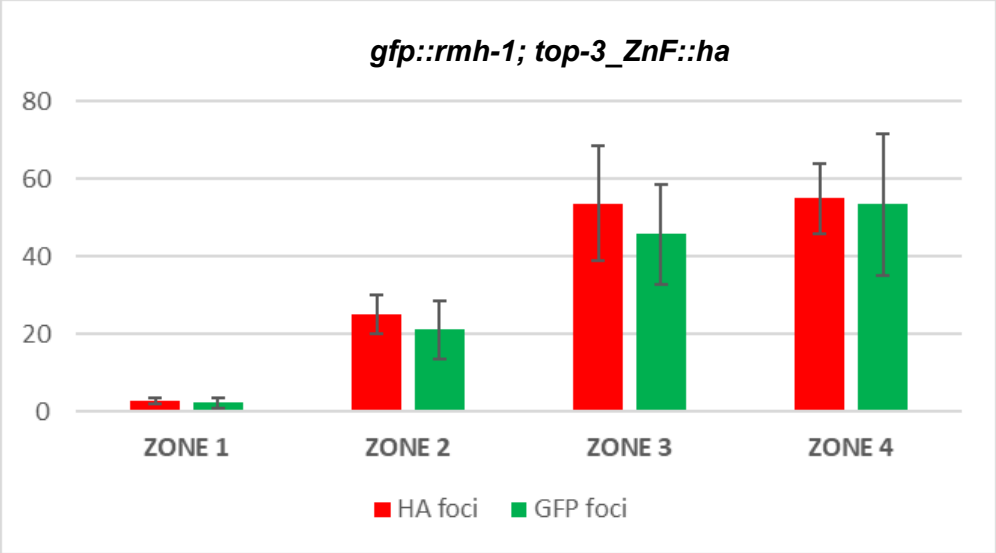

Figure 46: Co-localization of GFP and HA foci in gfp::rmh-1; top-3_ZnF::ha in 4 zones of meiotic prophase I. *Percentages of HA foci (red) colocalizing with GFP foci versus percentages of GFP foci (green) colocalizing with HA foci were calculated by automated quantification. All averages include standard deviation. In total, 4 gonads with 392 nuclei were evaluated for gfp:rmh-1; top-3_ZnF::ha.*

The ZnF motif of TOP-3 has an important role, because its removal affected the localization of RMH-1 and TOP-3 to such an extent that it alters their co-localization. The fact that both TOP-3 and RMH-1 foci are altered in the early stages of meiosis (transition zone and early pachynema) supports the idea that the ZnF motif has already a function in the early recombination intermediates. The lower amount of co-localization in the *top-3_ZnF* mutant could be caused by the overall fainter signals in this genetic background.

6.10 Analysis of *rmh-2; top-3_ZnF* mutant

Previous biochemical studies conducted in lab showed a potential interaction between TOP-3 and RMH-2 raising the questions of an interdependent role in meiosis. RMH-2 is the second homolog of RMI1. It is considered to act redundantly with the first RMI1 homolog RMH-1, since the *rmh-1(jf54); rmh-2(jf94)* double mutant was inviable (Jagut et al. 2016). However, its exact function is unknown. In order to investigate, whether the ZnF motif is required for a potential functional collaboration, the *top-3_ZnF* mutant was combined with the *rmh-2* deletion and analyzed for possible defects on meiotic

recombination using following methods: inspection of diakinesis chromosomes and quantification of RAD-51 recombination foci.

Diakinesis quantification (figure 47) revealed that in *rmh-2*, 90% of examined oocytes showed 6 bivalents and the rest displayed 7 bodies. Removal of *rmh-2* from *top-3_ZnF* reduced the amount of 6 bivalents to only 39,2% and increased greatly the occurrence of univalents and DNA fragments. In 2% of cases, oocytes displayed up to 11 DAPI bodies. However, 7 or 8 bodies were with 31,4% and 17,6%, the most frequently found categories (figure 47B and 47C). Apart from univalents, 5,9% of all examined oocytes phenocopied the occurrence of 5 bodies detected in *top-3_ZnF*. In addition, the double mutant displayed fused DAPI bodies (figure 47D) that were not found in the single mutants.

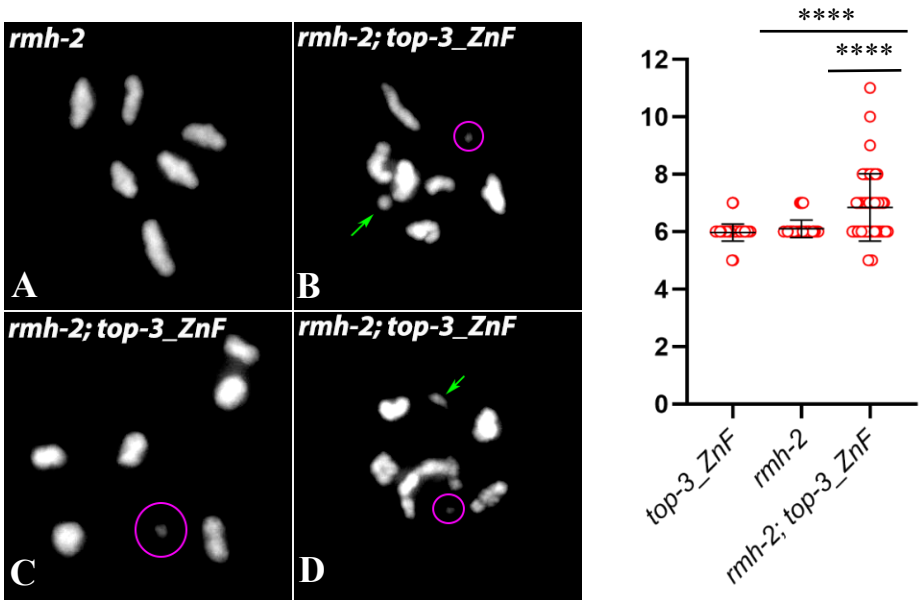

number of DAPI bodies	5	6	7	8	9	10	11	N
top-3_ZnF	5,8	91,3	2,9	0	0	0	0	103
rmh-2	0	90	10	0	0	0	0	50
rmh-2; top-3_ZnF	5,9	39,2	31,4	17,6	2	2	2	51

Figure 47: Quantitative analysis of DAPI bodies in diakinesis oocyte nuclei in rmh-2; top-3_ZnF compared to the rmh-2 and top-3_ZnF single mutants in %. *Representative examples are shown for the following genotypes* ***(A)*** *6 bivalents in rmh-2* ***(B)*** *8 bodies with two fragments (circle and arrow) in rmh-2; top-3_ZnF* ***(C)*** *7 bodies showing one fragment (circle) rmh-2; top-3_ZnF* ***(D)*** *7 bodies with round shaped bivalent and fused bodies in rmh-2; top-3_ZnF. Table depicts the relative percentage of diakinesis counts for the given number of DAPI bodies for each indicated genotype. N is the total number of quantified oocytes. Mann-Whitney test calculated top-3_ZnF vs. rmh-2; top-3_ZnF **** $p<0.0001$ and rmh-2 vs. rmh-2; top-3_ZnF **** $p<0.0001$.*

The recombination protein RAD-51 formed distinct foci as well as stretches in *rmh-2; top-3_ZnF* in all stages in the premeiotic region and meiotic prophase I (figures 48-49). Both forms occurred already in the mitotic zone (z1-z2 in figures 48-49) and accumulated very rapidly, when nuclei entered the transition zone (z3 in figures 48-49). Foci reached their maximum amount in early pachynema (z4 in figure 48-49), whereas stretches were most abundant in mid pachynema (z4 in figures 48-49). In late pachynema (z6 in figures 48-49) RAD-51 started to be unloaded from the chromatin and was almost completely removed in zone 7. When compared to the single mutants, *rmh-2; top-3_ZnF* accumulated higher number of foci and stretches throughout all examined zones.

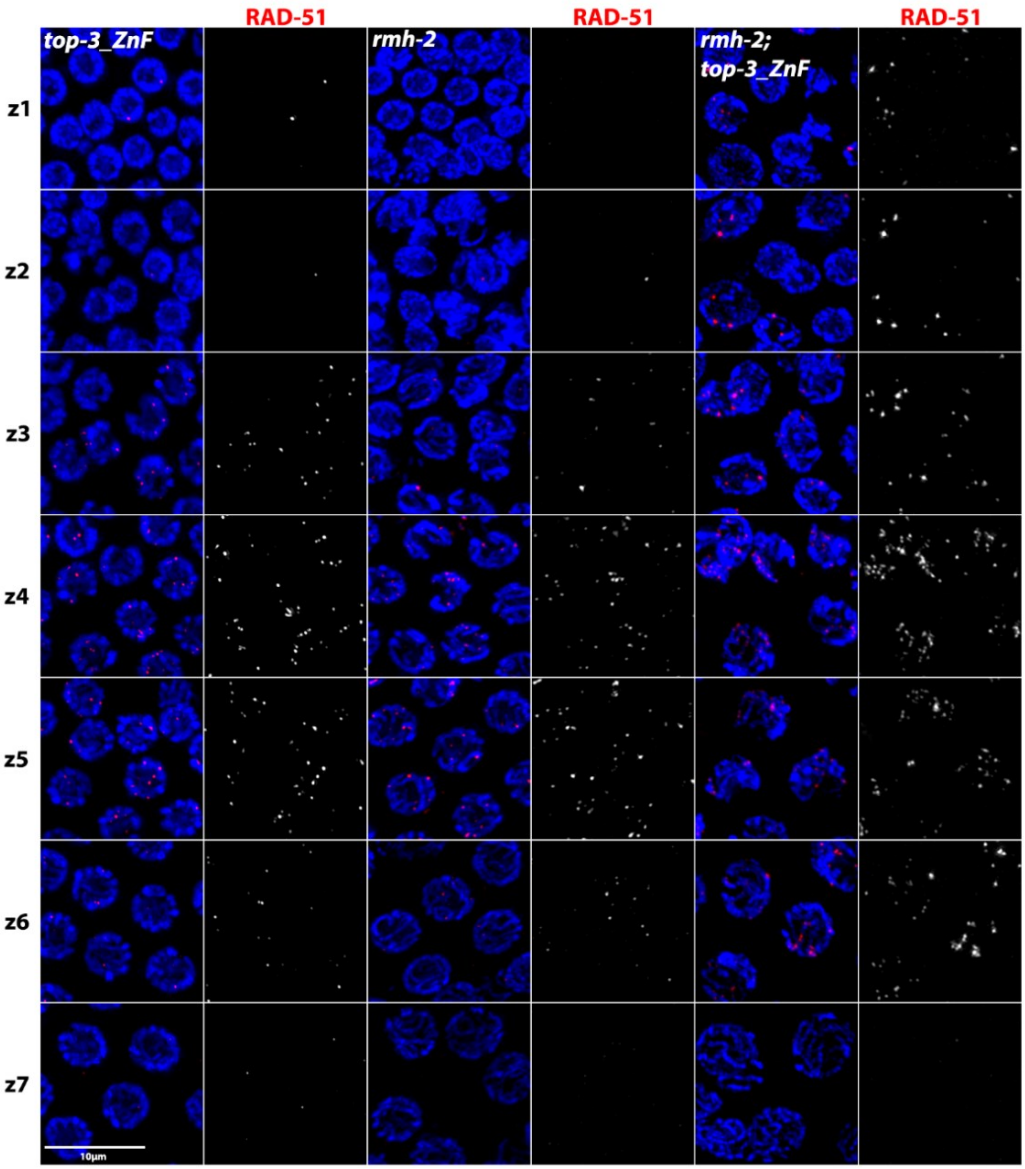

Figure 48: Localization of RAD-51 recombination foci in rmh-2; top-3_ZnF compared to the rmh-2 and top-3_ZnF single mutants. *Images display the RAD-51 localization in 7 zones of RAD-51 stained gonads of indicated genotypes. Zones represent mitotic zone (z1-z2) and stages of meiotic prophase I: transition zone (z3), early pachynema (z4), mid pachynema (z5) and late pachynema (z6-z7).*

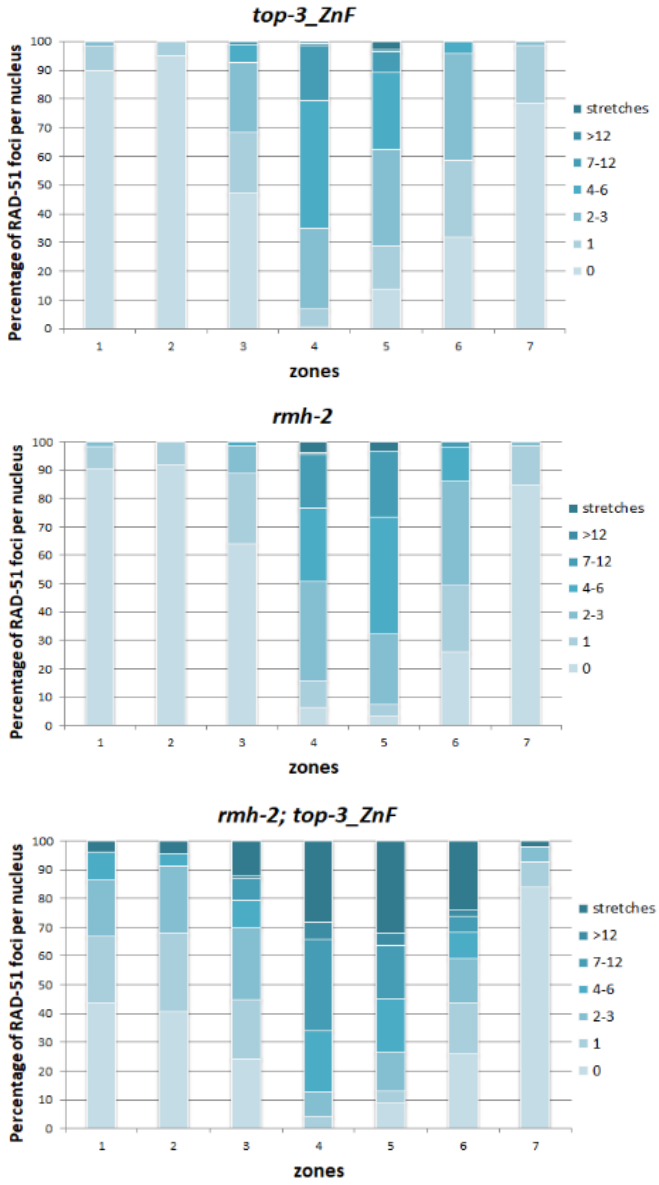

Figure 49: Quantification of RAD-51 foci dynamics in rmh-2; top-3_ZnF compared to the rmh-2 and top-3_ZnF single mutants. *Categories with percentage of RAD-51 foci per nucleus are plotted for every zone of indicated genotypes. Zones represent mitotic zone (z1-z2) and stages of meiotic prophase I: transition zone (z3), early pachynema (z4), mid pachynema (z5) and late pachynema (z6-z7). In total, 3 gonads with 717 nuclei were evaluated for rmh-2; top-3_ZnF and 3 gonads with 853 nuclei were evaluated for rmh-2 and 6 gonads with 1203 nuclei were evaluated for the top-3_ZnF.*

Severe defects in *rmh-2; top-3_ZnF* oocytes indicate that RMH-2 activity cooperates with the function of the ZnF motif at early stages of recombination. The altered profile of RAD-51 supports the observation that they act synergistically, and that DNA repair is severely affected. Furthermore, RAD-51 foci already accumulated in the mitotic zone in the double mutant *rmh-2; top-3_ZnF*, suggesting that the diakinesis phenotype and the aberrant RAD-51 profile may result from meiotic as well as mitotic defects.

6.11 Localization of TOP-3 and TOP-3_ZnF in *rmh-2*

HA tagged versions of TOP-3 and TOP-3_ZnF were crossed into the *rmh-2* deletion in order to examine, whether RMH-2 affects the localization of the wild type TOP-3 and / or of the ZnF mutant.

As previously shown, automated quantification of TOP-3 foci demonstrated that TOP-3 localized as faint and bright populations of foci (figures 35-38). However, when looking at the TOP-3 profile in *rmh-2* (figures 50-53), I detected a few differences. In early pachynema (z2 in figure 50), TOP-3 localized on average as 12,4 foci, ranging from 0 to 28 in *rmh-2*, whereas in the wild type, it reached the average number of 15 foci, ranging from 2 to 35 (figure 50-53). This reduction was most likely a consequence of a decreased amount of the faint population of foci from about 9 foci in the wild type to 7 in *rmh-2* (figure 53). A much greater reduction was, however, found for the faint population in late pachynema (z4 in figures 50 and 53). In the wild type, TOP-3 formed almost 9 faint foci per nucleus, whereas in *rmh-2*, it localized on average, only as 4 foci.

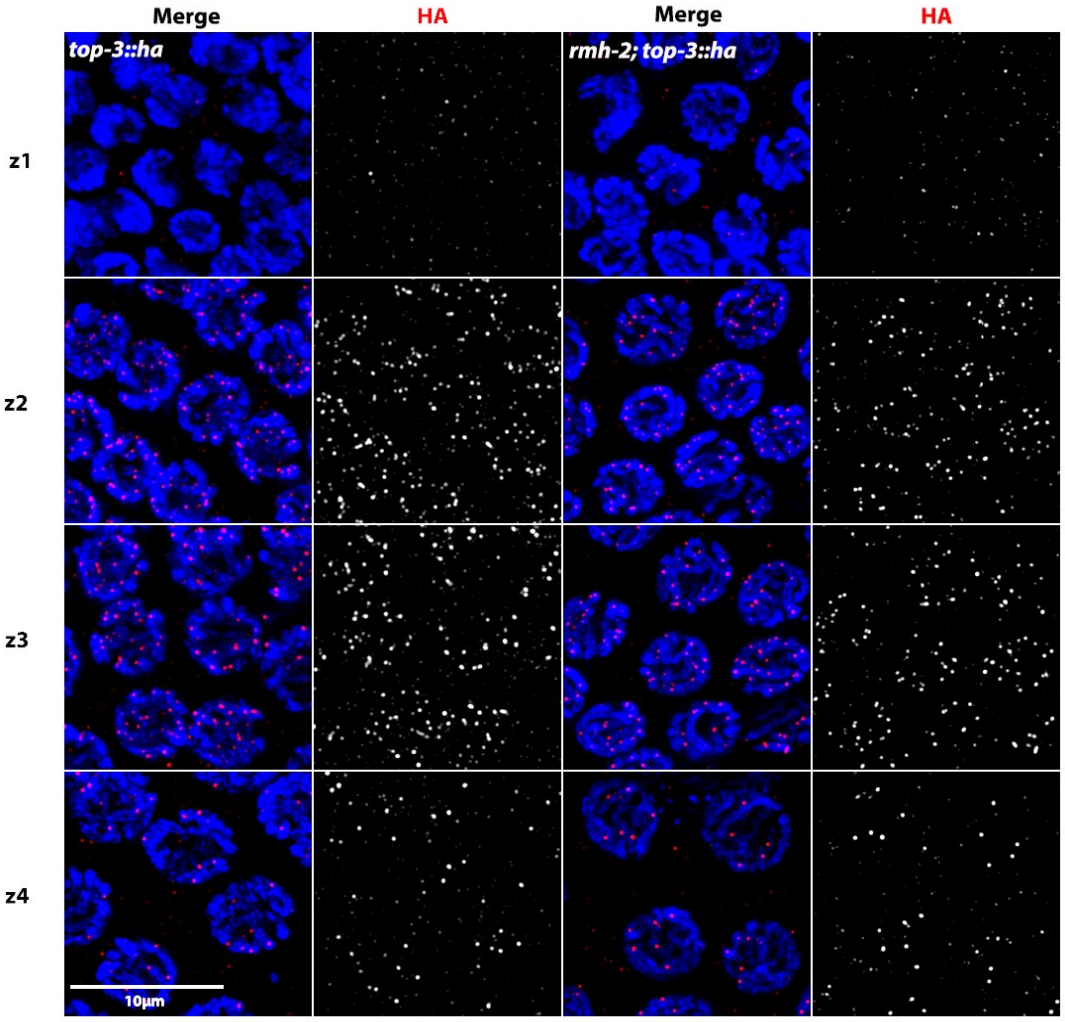

Figure 50: Localization of HA foci in top-3::ha compared to rmh-2; top-3::ha. *Zones represent transition zone (z1), early pachynema (z2), mid pachynema (z3) and late pachynema (z4) of meiotic prophase I.*

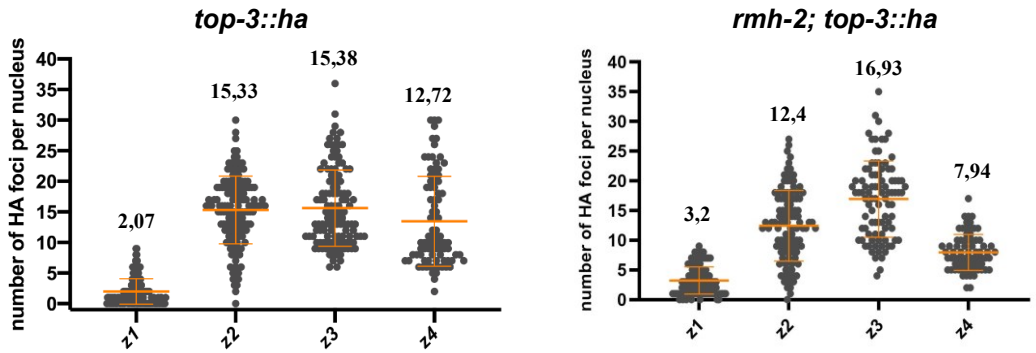

Figure 51: Combined counts of bright and faint HA foci automatically quantified in top-3::ha compared to rmh-2; top-3::ha. *Each zone is defined by average number of combination of bright and faint foci. In total, 3 gonads with 502 nuclei were evaluated for top-3::ha and 3 gonads with 400 nuclei were evaluated for rmh-2; top-3::ha. Mann-Whitney test calculated following difference in transition zone: top-3::ha vs. top-3::ha; rmh-2 p<0.0001; early pachynema: top-3::ha vs. top-3::ha; rmh-2 p<0.0001; mid pachynema: top-3::ha vs. top-3::ha; rmh-2 p>0.05; late pachynema: top-3::ha vs. top-3::ha; rmh-2 p<0.0001.*

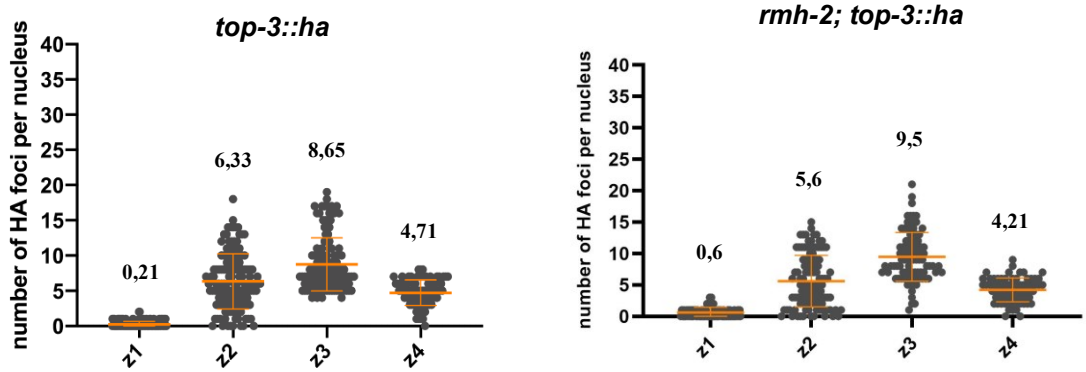

Figure 52: Automated quantification of bright HA foci in top-3::ha compared to rmh-2; top-3::ha. *Zones represent transition zone (z1), early pachynema (z2), mid pachynema (z3) and late pachynema (z4) of meiotic prophase I. Average number of bright foci is defined for every zone.*

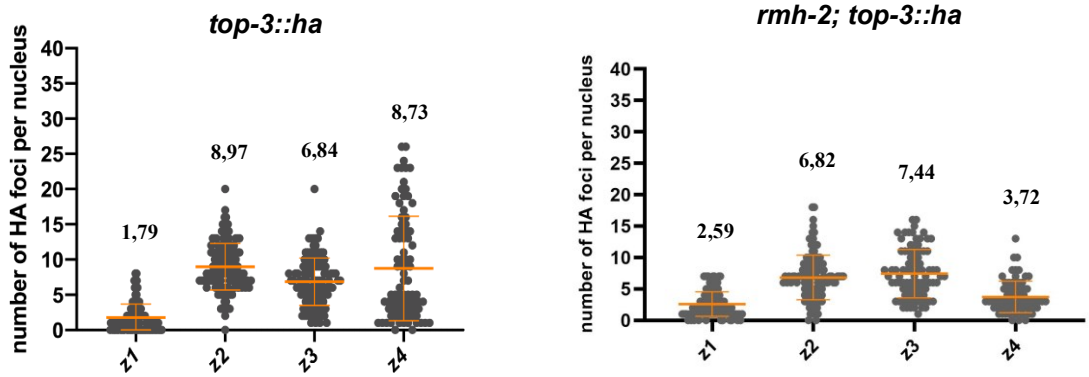

Figure 53*: Automated quantification of faint HA foci in top-3::ha compared to rmh-2; top-3::ha.* *Zones represent transition zone (z1), early pachynema (z2), mid pachynema (z3) and late pachynema (z4) of meiotic prophase I. Average number of faint foci is defined for every zone.*

On the contrary to TOP-3 wild type, localization of TOP-3_ZnF (figure 54) in the *rmh-2* mutant was disrupted to such an extent that foci in some zones were impossible to be quantified. The localization of TOP-3_ZnF in transition zone (z1 in figure 54) was not affected by the absence of RMH-2. But, upon entering early pachynema (z2 in figure 54), TOP-3_ZnF localized as many faint foci that showed similar intensity as those in the cytoplasmatic region between nuclei. In the next two stages (mid pachynema (z3 in figure 54) and late pachynema (z4 in figure 54)), we could still detect few bright foci in the nuclei, but faint population located in nuclei as well as in the cytoplasm.

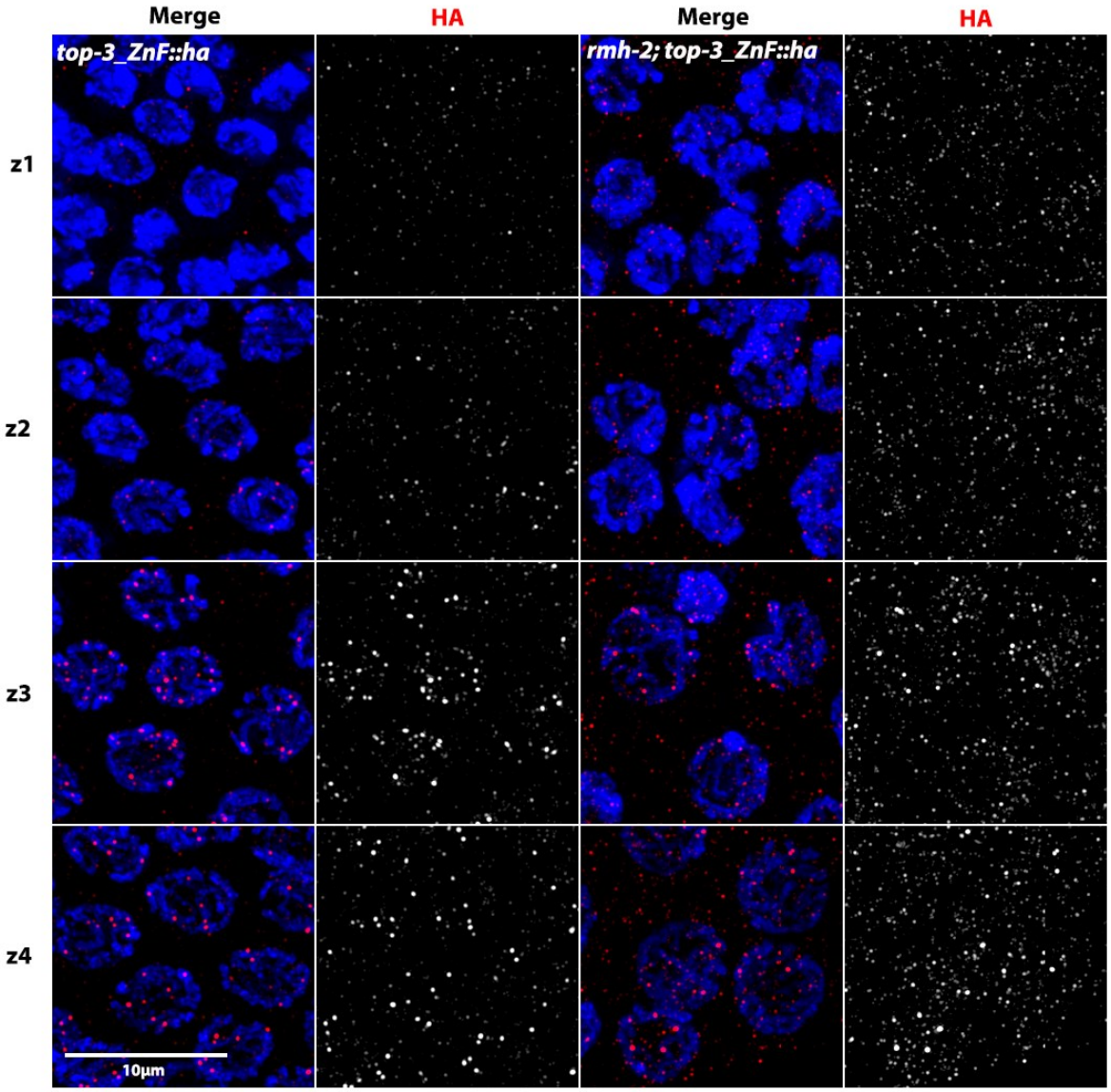

Figure 54: Localization of HA foci in top-3_ZnF::ha compared to rmh-2; top-3_ZnF::ha. *Zones represent transition zone (z1), early pachynema (z2), mid pachynema (z3) and late pachynema (z4) of meiotic prophase I.*

Removal of RMH-2 altered the localization of both wild type TOP-3 as well as TOP-3_ZnF. While wild type TOP-3 was reduced only slightly in the number of foci, TOP-3_ZnF was not concentrated into foci on the chromatin and with this the protein was misplaced into the cytoplasm. The localization results together with the above described defects at diakinesis indicate that RMH-2 and the ZnF motif of TOP-3 may cooperate for the loading of the complex onto the recombination intermediates and their processing.

6.12 Localization of crossover-promoting factors in *top-3_ZnF and rmh-2*

Given the highly aberrant diakinesis structures with numerous chromosomes fragments and the accumulating RAD-51 foci in the *top-3_ZnF; rmh-2* double mutant, I wanted to asses to which extent meiotic crossover recombination can occur in the *top-3_ZnF* and *rmh-2* single mutant. Therefore, I choose to analyze the localization dynamics of MSH-5 and COSA-1 pro-crossover factors (Winand et al. 1998; Zalevsky et al. 1999; Nguyen et al. 2018).

6.12.1 Quantification of MSH-5

The expression of the MSH5::GFP transgene was quantified manually by dividing the gonad into 4 equal zones from transition zone to late pachynema. In wild type, it began forming distinct foci in early pachynema (z2 in figure 55), on average about 8,6 per nucleus (figure 56). Mid pachytene nuclei (z3 in figure 55) displayed a slightly higher number of foci, on average, almost 11 (figure 56). But upon entering late pachynema (z4 in figure 55), this number was reduced to about 6 bright foci per nucleus (figure 56).

In *top-3_ZnF* and *rmh-2,* the localization of MSH-5 foci displayed the same trend as in the wild type, but with fewer foci in the early zones (z2 in figure 55). The number of foci was greatly reduced from 8,6 foci in wild type to 2,7 in *top-3_ZnF* and 2,2 in *rmh-2* (figure 56). The increasing trend during mid pachynema (z3 in figure 55) could be observed in both mutants, but the quantity of foci was again reduced compared to wild type displaying on average 11 foci in contrast to 7,3 in *top-3_ZnF* and 8,5 in *rmh-2* (figure 56). Interestingly, at the time of late pachynema (z4 in figure 55), nuclei displayed identical numbers: there were on average 6 foci in *top-3_ZnF* and *rmh-2*, exactly the same quantity as in the wild type (figure 56).

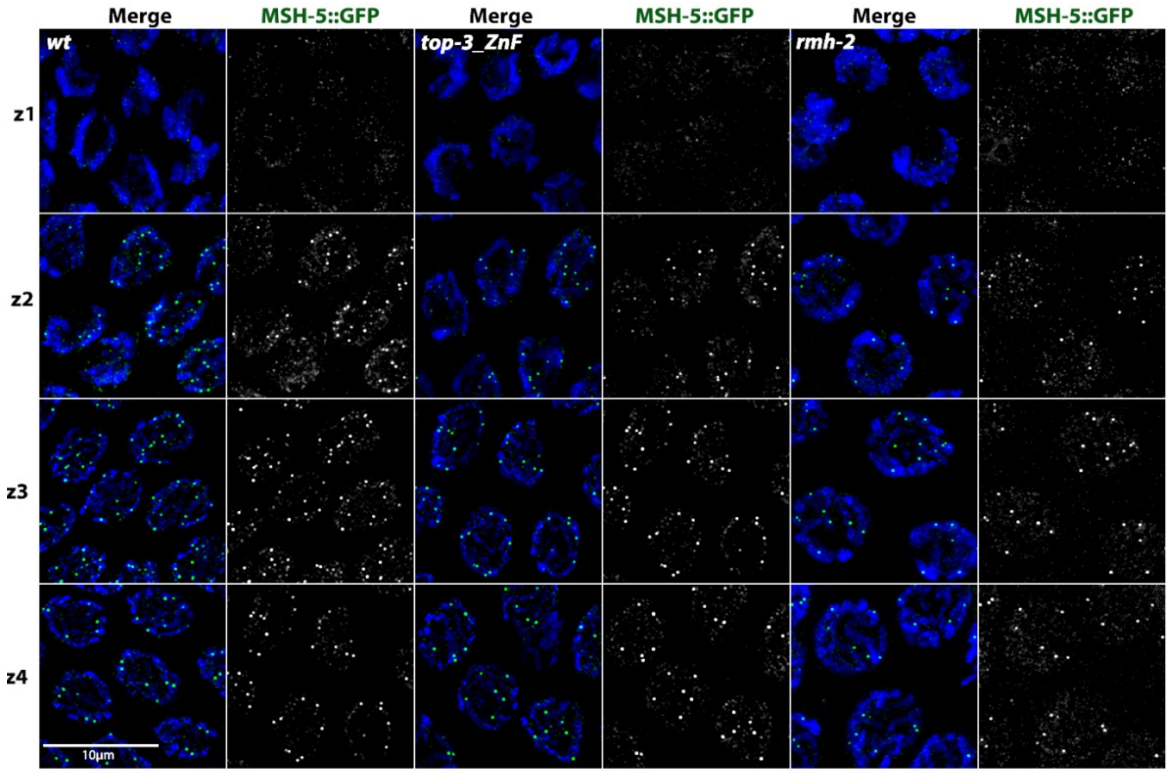

Figure 55: Localization of GFP foci in msh-5::gfp wild type compared to msh-5::gfp; top-3_ZnF and msh-5::gfp; rmh-2. *Zones represent transition zone (z1), early pachynema (z2), mid pachynema (z3) and late pachynema (z4) of meiotic prophase I.*

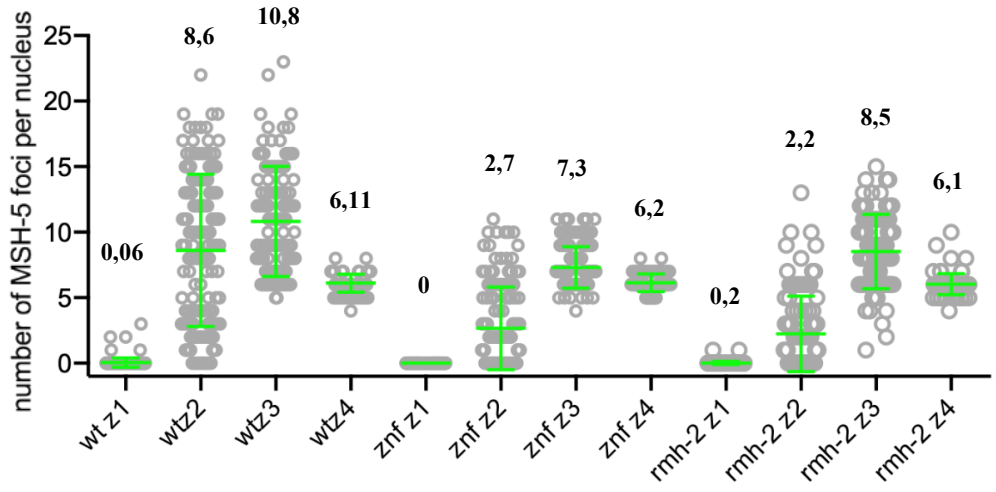

Figure 56**: **Manual quantification of GFP foci in msh-5::gfp wild type compared to msh-5::gfp; top-3_ZnF and msh-5::gfp; rmh-2. *Zones represent stages of meiotic prophase I: transition zone (z1), early pachynema (z2), mid pachynema (z3) and late pachynema. Numbers display the average quantity of foci calculated for every zone in indicated genotypes. In total, 3 gonads with 520 nuclei were evaluated for wild type, 3 gonads with 491 nuclei were evaluated for top-3_ZnF and 3 gonads with 409 nuclei were evaluated for rmh-2.*

6.12.2 Quantification of COSA-1

The COSA-1 factor is usually applied to label intermediates in late pachynema of meiotic prophase I (Yokoo et al. 2012). Manual quantification of N-terminally OLLAS tagged COSA-1 showed that *rmh-2* and *top-3_ZnF* displayed the same average of 6 foci per nucleus as found in wild type (figure 57 and 58).

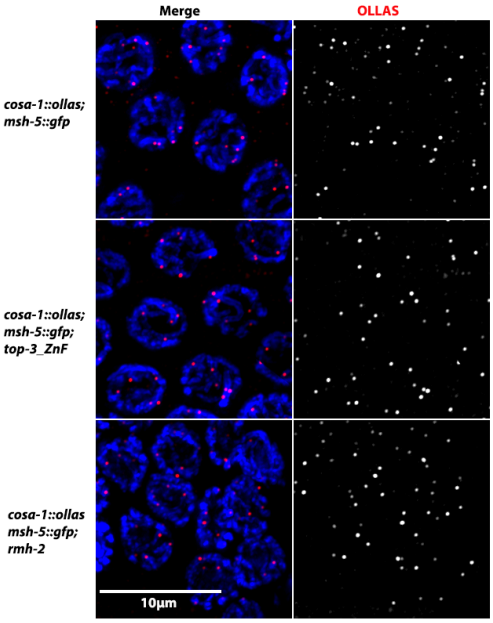

Figure 57: Localization of OLLAS foci in cosa-1::ollas; msh-5::gfp compared to cosa-1::ollas; msh-5::gfp; top-3_ZnF and cosa-1::ollas; msh-5::gfp; rmh-2 single mutants in late pachynema of meiotic prophase I.

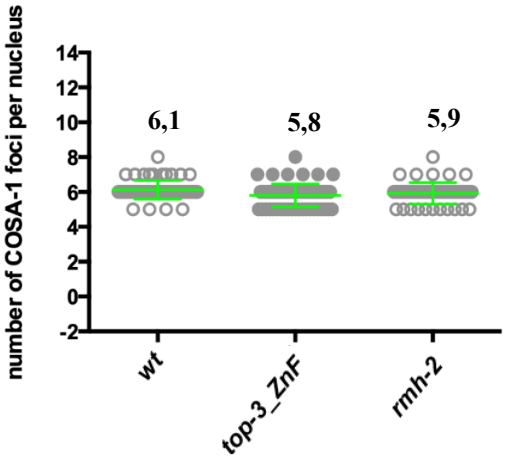

Figure 58: Manual quantification of OLLAS foci in cosa-1::ollas; msh-5::gfp wild type compared to cosa-1::ollas; msh-5::gfp; top-3_ZnF and cosa-1::ollas; msh-5::gfp; rmh-2 single mutants in late pachynema of meiotic prophase I. *Numbers display the average quantity of foci for indicated genotypes. In total, 3 gonads with 61 nuclei were evaluated for wild type and 3 gonads with 67 nuclei were evaluated for top-3_ZnF and 3 gonads with 52 nuclei for rmh-2.*

The localization of MSH-5 and COSA-1 indicate that the *top-3_ZnF* and *rmh-2* mutants manage to establish the same number of class I crossovers in late pachynema as the wild type, although, especially from the localization of MSH-5, but also from the localization patterns shown for RMH-1 and HIM-6, I deduce that the processing/maturation of early recombination intermediates is affected.

6.13 SNP-based mapping of crossovers in *top-3_ZnF* and *rmh-2*

Beside the cytological approach, formation of crossovers can be investigated by mapping methods that reveal the number of crossovers and their position across chromosomes (Bazan and Hillers 2011). This method is based on single nucleotide polymorphisms between Bristol wild type (#1 strain number in table 1) and Hawaii wild type (#1481 strain number in table 1). Polymorphisms were detected by a PCR-based approach to measure crossovers at specifically selected genetic positions (explained in detail in the materials and methods, see chapter 5.8) on chromosomes IV and V.

Four SNP positions generated the following intervals AB, BC and CD along chromosome IV (figure 59). AB and CD correspond to chromosomal ends, whereas BC represents the central region. Wild type showed 29,5% of recombination rate with the highest occurrence of crossovers at the AB interval. The central region (BC) and the chromosomal end (CD) exhibited similar numbers of crossovers in the wild type. The total recombination rate of *rmh-2* is with 26 % slightly smaller than the one observed in wild type, even though *rmh-2* generated 2 double crossovers and increased the CO frequency at the CD interval in contrast to wild type (8,5% to 5,5%). Apart from that, the tendency to generate most of the crossovers within the AB interval could be observed also for *rmh-2.* The highest rate, in total 39% was measured for *top-3_ZnF,* where the AB interval represents again a position of the most frequent recombination. Additionally, *top-3_ZnF* generated 3 double crossovers and increased the recombination rate in the central region corresponding roughly to a 2-fold increase over the wild type and a 3-fold increase over the *rmh-2* single mutant (figure 59).

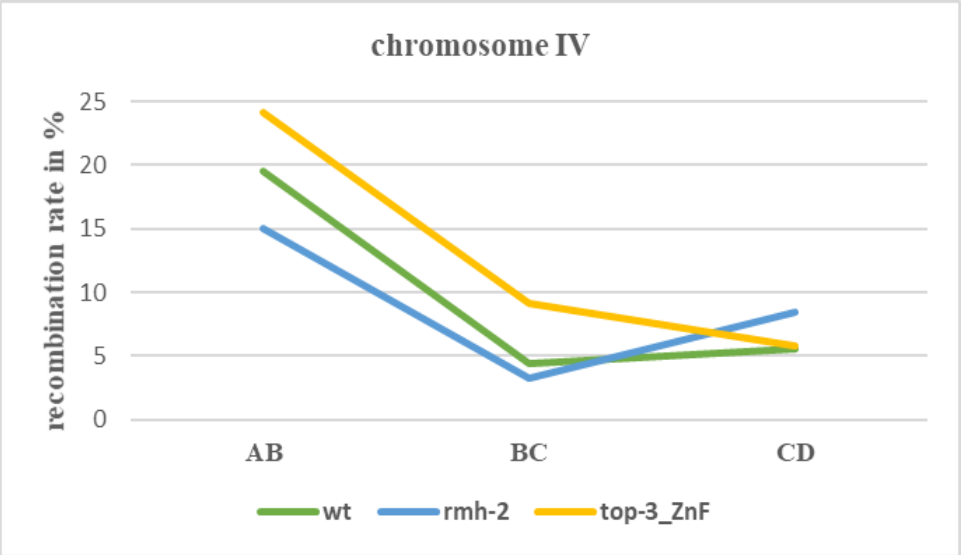

	AB	BC	CD	total %	2CO	3CO	N
wt	19,6	4,4	5,5	29,5	0	0	271
rmh-2	15	3,3	8,5	26,8	2	0	213
top-3_ZnF	24,1	9,1	5,8	39	3	0	272

Figure 59: Recombination rate in % and the number of 2CO and 3CO on chromosome IV in top-3_ZnF and rmh-2 compared to wild type. *Intervals AB and CD correspond to chromosomal ends, whereas BC represents central region. Table depicts the relative percentage of recombination rate for each interval in indicated genotypes and the amount of double and triple crossovers. N is the total number of analyzed hermaphrodites.*

Chromosome V was analyzed at 4 intervals: AB and DE were measured for crossovers occurring at the ends, whereas BC and CD represent the central region (figure 60). In the wild type, crossovers were measured at a frequency of 35,6%. Similar to chromosome IV, they were formed mostly at the chromosomal ends with a preference for one interval. This preference for the DE interval was observed for all tested genotypes. The highest recombination rate, in total 48,6% was measured for *top-3_ZnF* with a markedly higher frequency in the central region. This increase is even higher than the rate measured in the central region for chromosome IV. Moreover, *top-3_ZnF* generated 10 double and 2 triple crossovers. In contrast to *top-3_ZnF,* the lowest recombination rate was calculated for *rmh-2* (figure 60).

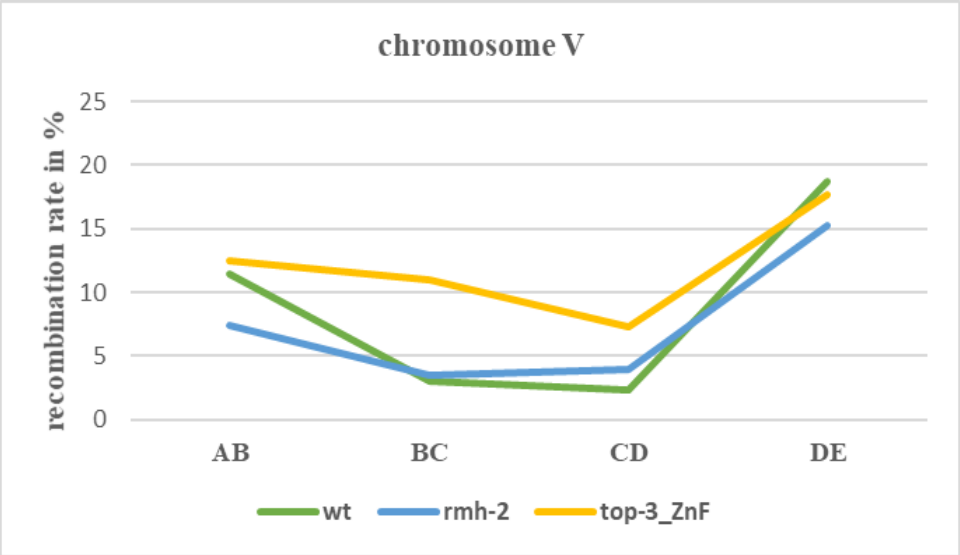

	AB	BC	CD	DE	total %	2CO	3CO	N
wt	11,5	3,1	2,3	18,8	35,6	0	1	261
rmh-2	7,4	3,5	3,9	15,2	30 %	1	0	230
top-3_ZnF	12,5	11	7,4	17,6	48,6	10	2	272

Figure 60: Recombination rate in % and the number of 2CO and 3CO on chromosome V in top-3_ZnF and rmh-2 compared to wild type. *Intervals AB and DE correspond to chromosomal ends whereas BC and CD represent central region. Table depicts the relative percentage of recombination rate for each interval in indicated genotypes and the amount of double and triple crossovers. N is the total number of analyzed hermaphrodites.*

The absence of the ZnF domain in TOP-3 increased the overall recombination rate on both analyzed chromosomes indicating the occurrence of additional exchange. Several extra double crossovers (on chromosome V also triple crossovers) were observed. However, these extra crossovers appear to be cytologically distinct from canonical class I crossovers, since the factors MSH-5 and COSA-1 localized in wild-type numbers during late pachynema of *top-3_ZnF*. Furthermore, the removal of the ZnF motif increased the crossover rate also at chromosome centers suggesting the lack of CO interference and the suppression of central placement of crossovers, normally seen in the wild type. In contrast to *top-3_ZnF*, *rmh-2* did not generate more crossovers than wild type, indicating that RMH-2 might be not/or be less involved in a TOP-3 mediated recombination activity for which the ZnF is important.

7. Discussion

In this master project I investigated the role of the zinc finger motif in the TOP-3 protein during prophase I of *C. elegans* meiosis. By applying the CRISPR/Cas9 technique I generated a specific allele, where I deleted the ZnF motif and thereby generated the *top-3_ZnF* allele expressing a truncated form of TOP-3 protein. I subjected this mutation to various analysis to understand its contribution to meiotic recombination.

7.1 The dynamic localization of TOP-3 into recombination foci reflects its activity on DNA joint molecules during recombination

Different types of DNA joint molecules have been observed to arise during meiotic recombination. They are referred to as nascent/extended D-loops, Holliday junctions or more complex intermediates such multichromatid or inter-sister JMs (Schwacha and Kleckner 1995; Hunter and Kleckner 2001; Oh et al. 2007; Bzymek et al. 2010). Their structures require the regulated action of various enzymes and factors that are essential for the accurate outcome of recombination. One of such factors is the dissolvasome complex as recently proposed by two extensively detailed studies in yeast (Kaur et al. 2015; Tang et al. 2015) which suggest that the BTR/TR complex secures normal occurrence of recombination pathways by resolving different types of joint molecules and channeling them towards crossover or noncrossover fates.

Taking this into consideration I suggest that the localization of TOP-3 with a highly dynamic behavior throughout the gonad, which includes stages of meiotic prophase I, reflects that TOP-3 function is important during several steps of recombination. I think that the early population of TOP-3 foci could represent the unwinding activity which has been proposed to cooperate with HIM-6 and RMH-1 by disassembling aberrant D-loops that arise during early repair of DBSs. As already stated, this may indirectly promote and antagonize crossovers, since dissociated strands can be repaired by SDSA to become noncrossovers or engage in another round of recombination that can result in crossover resolution (Kaur et al. 2015; Tang et al. 2015). But, to confirm this hypothesis, it might be useful to analyze the localization of TOP-3 foci in mutants with dysfunctional D-loop resolution such as *rtel-1* or *mus-81* to see whether the early population of TOP-3 foci is affected.
During mid and late pachynema, a fraction of TOP-3 foci could decorate the intermediates where dissolution takes place (Karrow et al. 2000; Wu and Hickson, 2003; Bussen et al. 2007; Bocquet et al. 2014; Bizard and Hickson 2014) or intermediates such as inter-sister or multi-chromatid entanglements whose topology requires topoisomerase activity as reported in the yeast studies (Kaur et

al. 2015; Tang et al. 2015). In addition, a subset of foci may represent a fraction of repair intermediates where TOP-3 or RMH-1 might have a potential role in crossover reinforcement/ maturation. Similar to the intermediates that Jagut et al., 2016 observed containing HIM-6, RMH-1 and MSH-5 signal. Moreover, late foci of RMH-1 and HIM-6 localized at sites labeled by MSH-5 and COSA-1 implying their role in promoting of the crossover fate for those recombination intermediates in late pachynema (Jagut et al.2016). I suggest that TOP-3 as a member of the BTR complex might be involved in this late activity as well, since the late population of TOP-3 foci displayed strong co-localization with RMH-1 and HIM-6 foci. However, in order to understand this better, it is necessary to analyze the localization of TOP-3 in mutants lacking conserved crossover factors, in the *msh-5* and *cosa-1,* and to examine whether TOP-3 locates on crossover sites labeled by MSH-5. On the other hand, diakinesis of *top-3 delta*, a mutant defective in the topoisomerase domain, displays masses of fused bivalents which differ from diakinesis of *him-6* and *rmh-1* that showed partially achiasmate bodies indicating defects in crossover maturation (Schvarzstein et al. 2014; Jagut et al. 2016). It is therefore possible, that the primary function of TOP-3 is not related to promoting crossover formation or that the highly aberrant "over-connected" chromosome masses in *top-3* mutants mask the univalent chromosome structures seen in *him-6* and *rmh-1* mutants.

Since Rmi1 has been observed to form a stable complex with Top3 in yeast (Chen and Brill 2007), I investigated their cooperation in *C. elegans* by analyzing the co-localization of TOP-3 and RMH-1 foci and *vice versa*. TOP-3 co-localized with RMH-1 only up to 60-70% during the pachynema stages, whereas RMH-1 co-localized with TOP-3 only to 50-60%, suggesting that a fraction of TOP-3 found in foci as well as RMH-1 might act outside of the BTR/TR complex. However, it is important to note that co-localization studies might be prone to inaccuracies resulting from immunostaining or intensity differences between TOP-3 populations. The assay did not clarify whether TOP-3 forms more foci per nucleus than RMH-1 and vice versa. Thus, the understanding of cooperation between RMH-1 and TOP-3 requires additional analysis. It is also important to investigate, how TOP-3 localizes in the *rmh-1* mutant and *vice versa*, to get more insight on the interdependency of the two proteins in forming various recombination complexes.

7.2 The TOP-3 zinc finger motif is required for wild type loading/activity of the BTR complex, but is dispensable for many activities that contribute to recombination in the germline

The removal of the ZnF from the TOP-3 protein does not have a big impact on the viability of the worms, where I found only very subtle changes: worms lacking the ZnF were almost as viable as the

wild type. The larval arrest and incidence of males were only slightly increased. Nevertheless, the removal of the ZnF motif had quite a pronounced effect on the number and distribution of TOP-3 foci in the gonad throughout the pachytene zones. The most prominent difference was observed in early pachynema, where TOP-3 lacking the ZnF localized with a 4-fold reduction of bright population and 2-fold reduction of faint population compared to TOP-3 wild type. Interestingly, mid pachytene faint foci and late pachytene bright foci were found at the same levels as the wild type TOP-3 suggesting that the removal of the ZnF motif has differing consequences for the various subcomplexes that act on different recombination intermediates. In addition, I observed that also the localization of RMH-1 and HIM-6 was similarly altered in *top-3_ZnF*. All pachytene nuclei displayed reduced amounts of foci containing both complex members, but the population of early foci was reduced to the greatest extent in contrast to the mid/late pachytene populations. In fact, late foci of RMH-1 as well as of TOP-3_ZnF showed slight but similar reduction.

These findings indicate that the ZnF motif is required for wild-type levels of BTR/TR localization being particularly important during early pachynema or that the early functions of the BTR/TR complex rely more on the ZnF motif of TOP-3 to localize into recombination foci. It seems that in TOP-3 the ZnF is not absolutely essential for complex formation, because all analyzed members managed to localize as chromatin-bound foci. Since domains containing zinc fingers are predicted to mediate DNA-protein interactions as well as protein-protein interactions (Berg and Shi 1996), and zinc fingers of Top3α in *D. melanogaster* have been shown to bind DNA and Blm(Hartman Chen 2012), it is possible that its absence disables loading of the TOP-3/BTR complex to a subset of recombination intermediates. Since the complex manages to localize in foci, it is possible, that its loading is only partially disabled in some types of intermediates as shown for the ZnF T1 of TOP3α in *A. thaliana* which targets the topoisomerase to Holliday junctions (Dorn et al. 2018). The most prominent reduction during early pachynema suggests, that the removal of the ZnF interferes with the loading particularly to early intermediates. Alternative or additional to the loading, the absence of the ZnF motif might disrupt the processing activity of the complex. In consequence of this, resolution of intermediates can be delayed and/or altered giving rise to structures whose turnover/maturation doesn't occur in a wild-type manner. This could generate fewer recombination intermediates that would go through meiosis and this could manifest itself as the lower counts of TOP-3 or RMH-1 foci in the mutant. The hypothesis, that the ZnF motif has a more prominent role during early pachynema, is further supported by the co-localization studies between TOP-3 and RMH-1. We found that in absence of the TOP-3 ZnF motif, only 25% of TOP-3 early foci co-localized with RMH-1 in contrast to 60% in wild type. In addition, co-localization in later pachytene stages was only slightly reduced.

The fact that TOP-3_ZnF localizes in foci during all analyzed stages of meiotic prophase I contradicts the hypothesis that the only function of zinc fingers is to mediate the DNA interaction and also raises

the question about the presence of a factor that mediates the TOP-3 recruitment to DNA. It may be an unknown factor with important function in meiosis or, and more likely, DNA recruitment/binding might be executed via another complex member of the BTR complex. It is also possible that TOP-3 requires this factor only when the ZnF is dysfunctional.

7.3 The TOP-3 zinc finger motif is important for processing and maturation of early intermediates

The importance of the TOP-3 ZnF motif in meiosis is already revealed by the aberrant profile of the recombination marker RAD-51 in the *top-3_ZnF* mutant. By quantifying its localization, I looked at ssDNA (formed after the resection) coated by RAD-51 before and after the strand-exchange since the protein is a crucial mediator of the homolog strand invasion (Alpi et al. 2003). The invasion process generates nascent D-loops inducing RAD-51 removal that is followed by strand extension engaging the extended D-loop in further steps of recombination (Hunter and Kleckner 2001; Alpi et al. 2003). Since *top-3_ZnF* accumulated aberrant numbers of RAD-51 foci from the beginning of the transition zone to the end of mid pachynema, it is possible that the absence of ZnF motif alters the kinetics of RAD-51 loading on ssDNA as well as its removal from the invaded strand. Increased accumulation of RAD-51 containing recombination foci might reflect several problems like the following: 1) the increased numbers might reflect ectopic invasions, normally not seen in the wild type. 2) The invasion might be stuck due to the absence of the ZnF motif which alters the loading/activity of the BTR complex required for proper resolution of the ectopic invasion. This can lead to increased accumulation of RAD-51 since the protein can't be removed from stuck ssDNA. But, it is also possible that the cell notices this problem of reduced strand engagements and reacts by forming more DSBs to make sure crossover recombination get successfully established, leading to more ssDNA that are coated by RAD-51 increasing the number of foci. Nevertheless, we observed that RAD-51 was removed in a manner identical to wild type in *top-3_ZnF*, suggesting the successful resolution of intermediates even despite the aberrant kinetics of foci dynamics. Moreover, the double mutant *spo-11; top-3_ZnF* which lacks the formation of DSBs, didn't show any RAD-51 foci throughout entire meiotic prophase I, indicating that recombination intermediates which have problems to be processed due to the absence of ZnF motif are specifically meiotic. The RAD-51 phenotype in *top-3_ZnF* did not result from compromised topoisomerase activity necessary for the decatenation of the joint molecules, since diakinesis of *top-3_ZnF* didn't display fusions that have been found to occur in *top-3 delta* oocytes. The *top-3 delta* worms accumulate tremendous amounts of DNA lesions already in the gonad mitotic compartment, a feature not seen in the *top-3_ZnF* mutant also corroborating the view that for executing the topoisomerase activity TOP-3 does not always need the ZnF and that the ZnF mediated DNA association might only be needed for certain activities of the BTR complex. Interestingly, the

mutants of *rmh-1, him-6* and *rmif-2* (the RMI2 ortholog, unpublished) show a distinct crossover defect indicated by the presence of univalents. The *top-3_ZnF* mutant however did not show any univalents at all, which lets me conclude that not all activities of the BTR need the TOP-3 ZnF or that this activity does not rely on the TOP-3 protein at all.

As stated before, the altered kinetics of RAD-51 foci could indicate the presence of ectopic invasions, which slow down the RAD-51 turnover. In order to look specifically at such intermediates, we measured their occurrence by analyzing the frequency of heterologous recombination. In wild type, heterologous recombination is an extremely rare event occurring particularly due to the strand-exchange between non-homologous sequences (Ortiz et al. 2018). We showed that the *top-3_ZnF* increased this illegitimate recombination more than 4-times over the wild type, implying that ZnF motif might be important for eliminating aberrant D-loops. However, the amount of heterologous recombination was considerably higher in the *him-6* mutants (Ortiz et al. 2018), *him-6* 6,6% versus *top-3_Zn* 0,27%. I therefore might need to consider that the removal of ectopic invasions might most likely not be the only function of ZnF motif. It might be also possible that it is a shared function between the ZnF domain and the topoisomerase domain meaning that if I could repeat the same assay in the *top-3 delta* allele, I would be able to see an increase in the percentage of heterologous recombination. It is also possible that heterologous recombination can be removed through decatenation in the sense of strand cutting and strand passage activities mediated by topoisomerase and the rest of the BTR complex and this activity does not rely on the TOP-3 ZnF and DNA recruitment is mediated through another mechanism.

Mapping of the crossover frequency allowed me to uncover how important the ZnF motif is for maturation of early/mid intermediates, knowing that the crossovers seen in late pachynema could be established much earlier. Indeed, I measured an increased rate of total recombination with the concomitant occurrence of double and rarely triple crossovers, indicating the existence of additional exchange in *top-3_ZnF*. However, these extra crossovers were not labeled by crossover promoting factors MSH-5 and COSA-1 known to locate to the final crossover sites (Zalevsky et al. 1993; Yokoo et al. 2012), suggesting that these additional exchanges are distinct from *C. elegans* canonical crossovers. Interestingly, I noticed that *top-3_ZnF* expressed reduced numbers of MSH-5 in early and mid pachytene nuclei (where it probably marks the recombination intermediates with both crossover and noncrossover outcomes). This and the early reduction of BTR complex localization into recombination foci implies that the absence of the ZnF motif disrupts/delays the maturation of early/mid intermediates in a way that it could impair crossover designation/establishment. This can happen due to altered processivity and/or loading of the TR/BTR complex to early intermediates in absence of the ZnF. However, extra crossovers may also indicate the function that has been uncovered in *A. thaliana*, where the ZnF motif of TOP3α collaborates with RMI1 to eliminate the additional

crossovers (Séguéla-Arnaud et al. 2016). These extra crossovers may be class II which result from intermediates who are dependent on Mus81 for their resolution (de los Santos et al. 2003; Kohl and Sekelsky 2013). I could further speculate that the ZnF motif is involved in crossover interference believed to block additional crossovers along the whole length of a *C. elegans* chromosome once one already has matured to a certain stage, but the quantification of MSH-5 and COSA-1 would rather argue that additional crossovers made in the *top-3_ZnF* mutant do not belong to the class of interfering crossovers. However, further analysis is needed to understand the nature of these extra crossovers. But regardless of additional exchange and delayed maturation of intermediates, late pachytene nuclei of *top-3_ZnF* manage to display the same number of COSA-1 and MSH-5 labeled intermediates as the wild type. Thus, the *top-3_ZnF* mutant forms at least one obligate crossover of class I per every homologous pair known to be the canonical CO-pathway in *C. elegans* (Hiller and Villeneuve 2003).

As already stated, the absence of the ZnF motif increased the frequency of crossovers on chromosome arms as well as the centers. The increase at chromosome centers could mean that the absence of the ZnF in TOP-3 disrupts the process of crossover distribution. The ZnF motif might cooperate here with RMH-1 known to discourage the crossovers in the center of the chromosomes (Jagut et al. 2016). Since *C. elegans* chromosomes lack centromeres, the crossover position determines bivalent organization in short and long domains that are needed for orientation and subsequent separation of homologous chromosomes (Albertson et al. 1997; de Carvahlo et al. 2008). I noticed that about 31% of *top-3_ZnF* mutant oocytes demonstrated aberrant round shaped bivalents (with a tiny hole in the middle) with aberrant arms' length. However, all analyzed diakinesis of *top-3_ZnF* localized the axial proteins HTP-3 and HTP-1 in a wild-type manner, meaning that bivalents are still formed as in the wild type and that the round shapes probably do not result from increased crossovers at the center of chromosomes. This is supported by Altendorfer et al. which showed that only those crossovers that are positioned at the very center of chromosomes distribute axial proteins symmetrically and affect the generation of bivalent subdomains leading eventually to missegregation (Altendorfer et al. 2020). Therefore, round shaped bivalent in *top-3_ZnF* mutant could be the result of overall increase of crossover frequency and that additional analysis is necessary to understand the nature of processes that lead to the generation of round shaped bivalents in the *top-3_ZnF* mutant.

7.4 The TOP-3 zinc finger motif is involved in a parallel activity to MUS-81 LEM-3 by processing of early intermediates

The nucleases MUS-81 and LEM-3 have been recently proposed to cooperate to resolve joint molecules (Hong et al. 2018). My analysis of the *mus-81; top-3_ZnF* phenotype supplement these findings by providing strong evidence that the ZnF motif is important for TOP-3 activity predicted to

be parallel to MUS-81 as already postulated for *A. thaliana*: TOP3 missing the ZnF T1 accumulates recombination intermediates that require the function of the nuclease MUS81 (Dorn et al. 2018). The majority of the aberrantly accumulated RAD-51 foci was not disengaged from chromatin in the double mutant *mus-81; top-3_ZnF* indicating the presence of unrepaired and unresolved intermediates. In addition, *mus-81* has been shown to delay processing of early intermediates by aberrant localization of RMH-1 (Hong et al. 2018). This coincides with *top-3_ZnF* which reduces/delays the localization of RMH-1 as well as MSH-5 in early/mid pachynema concluding that parallel activities of the TOP-3 ZnF and MUS-81, which are particularly important for early intermediates. In addition, I observed unusual aggregates in diakinesis of the double mutant, which seemed to be generated by fusions of fragments/univalents and bivalents, suggesting that the absence of ZnF motif enhances defects coming from MUS-81 inactivity. This is also supported by the elevated occurrence of dissociated bivalents which are univalents connected via chromosomal linkages considered to result from intermediates that engage recombination but are not resolved (Jagut et al. 2016; Hong et al. 2018). However, the wild-type presence of the axial elements HTP-3 and HTP-1 didn't reveal any defects in synapsis or bivalent organization. Nevertheless, I conclude that the ZnF motif contributes to processing of early recombination intermediates in parallel to MUS-81-LEM-3 activity, since worms lacking both nucleases and Znf motif displayed enhanced defects in diakinesis morphology and strand-invasion kinetics. Moreover, the absence of the early activity of the TOP-3 ZnF motif MUS-81 becomes important to produce bivalents that can be properly segregated.

7.5 RMH-2 cooperates with the TOP-3 zinc finger motif by loading TOP-3/BTR onto the early recombination intermediates

Even though the loss of RMH-2 did not exhibit any major meiotic phenotype (Jagut et al. 2016), co-immunoprecipitation studies in the lab have shown a possible direct or indirect interaction between TOP-3 and RMH-2 suggesting the option of a common role in recombination. Since absence of RMH-2 reduced the numbers of TOP-3 foci and even mislocalized the mutated TOP-3_ZnF deleted protein to the cytoplasm, I propose that RMH-2 cooperates with the ZnF in TOP-3 for the loading of the TOP-3/BTR complex to the recombination intermediates. This is consistent with the hypothesis that a certain factor brings the TOP-3 protein to DNA, when the ZnF is absent.

Early localization of TOP-3 as well as TOP-3_ZnF seemed to be more affected than mid/late pachynema indicating that their cooperation might be particularly important during processing of early intermediates. By analyzing the *rmh-2; top-3_ZnF* double mutants I observed aberrant profiles of RAD-51 reflecting defects in processing of recombination intermediates starting already in the mitotic zone. This could already be causing a lot of the diakinesis defects, where I detected fragments together

with DNA masses and bivalents in such extent that I counted to 11 DAPI stained bodies. However, RAD-51 marked intermediates are resolved by late pachynema implying that the repair of DSBs and processing of early intermediates is happening even if it is delayed. Nevertheless, in the *rmh-2* single mutant the crossover promoting factors, such as MSH-5 and COSA-1 were localized in the same way as in the *top-3_ZnF:* Early/mid pachynema displayed reduced numbers of MSH-5, suggesting that early maturation of intermediates requires the cooperation of RMH-2 and the ZnF. In addition, wild-type localization of MSH-5 and COSA-1 in late pachynema indicated that *rmh-2* as well as *top-3_ZnF* formed wild-type numbers of the class I crossovers marked by MSH-5 and COSA-1.

Looking at all these previously described similarities between TOP-3_ZnF and RMH-2 I thought that *rmh-2* could display the same CO frequency/distribution defects that occurred in the absence of the ZnF. For my surprise this was not the case, since the *rmh-2* recombination rate was more similar to the wild type than to the ZnF mutant, meaning that the activity contributed by the ZnF motif revealed by the recombination assay doesn't involve the cooperation with RMH-2, or that the *rmh-2* mutant starts to become essential only upon removal of the ZnF. However, it is necessary to increase the total number for the recombination assay of *rmh-2* worms because I analyzed slightly smaller numbers in contrast to the *top-3_ZnF* mutant. It would also be interesting to know if RMH-2 displays more heterologous recombination compared to the ZnF mutant and/or the double mutant *rmh-2; top-3_ZnF* reaches the *him-6* levels of heterologous recombination, to get more insight into the possible early recombination function of the ZnF motif and into the cooperation between RMH-2 and the ZnF. In addition, it is inevitable to analyze the localization of RMH-2 in *top-3_ZnF* to see if the proteins are interdependent for the localization and the distribution pattern of RMH-1 and HIM-6 in *rmh-2* to understand the RMH-2-ZnF cooperation better. Moreover, it remains to be elucidated if this cooperation is RMH-2 specific or if we see similar synthetic effect also with RMH-1, especially considering that the double mutant *rmh-1; rmh-2* is lethal.

Remarkably, the double mutant *rmh-2; top-3_ZnF* already shows DNA lesions that are imported into meiosis from the mitotic compartment, nevertheless the *top-3 delta* mutant still displays a much more severe phenotype. This suggests that TOP-3 has activities that do not even rely on the combined activities of RMH-2 and the TOP-3 ZnF motif to recruit the protein to DNA.

8. References

Agostinho, A., Meier, B., Sonneville, R., Jagut, M., Woglar, A., Blow, J., Jantsch, V., and Gartner, A. (2013): Combinatorial regulation of meiotic Holliday junction resolution in C. elegans by HIM-6 (BLM) helicase, SLX-4,and the SLX-1, MUS-81 and XPF-1 nucleases. PLoS Genet. 9, e1003591.

Alberts B, Johnson A, Lewis J, et al. Molecular Biology of the Cell. 4th edition. New York: Garland Science; 2002

Albertson, D.G., Rose, A.M., and Villeneuve, A.M. (1997): Chromosome organization, mitosis, and meiosis. In C.Elegans II, D.L. Riddle, T. Blumenthal, B.J. Meyer, and J. Preiss, eds. (Cold Spring Harbor, NY: Cold SpringHarbor Laboratory Press), pp. 47-78.

Alpi, Arno; Pasierbek, Pawel; Gartner, Anton; Loidl, Josef (2003): Genetic and cytological characterization of the recombination protein RAD-51 in Caenorhabditis elegans. In: Chromosoma 112 (1), S. 6–16. DOI: 10.1007/s00412-003-0237-5.

Altendorfer E., Láscarez-Lagunas L., Nadarajan S., Mathieson I., Colaiácovo M. (2020): Crossover position drives chromosome remodeling for accurate meiotic chromosome segregation. Cell Press Volume 30, Issue 7. DOI:10.1016/j.cub.2020.01.079.

Arribere J. A., Bell R. T., Fu B. X., Artiles K. L., Hartman P. S. (2014): Efficient marker-free recovery of custom genetic modifications with CRISPR/Cas9 in Caenorhabditis elegans. Genetics 198: 837–846.

Barber, Louise J.; Youds, Jillian L.; Ward, Jordan D.; McIlwraith, Michael J.; O'Neil, Nigel J.; Petalcorin, Mark I R et al. (2008): RTEL1 maintains genomic stability by suppressing homologous recombination. In: Cell 135 (2), S. 261–271. DOI: 10.1016/j.cell.2008.08.016

Baudrimont, A., Penkner, A., Woglar, A., Machacek, T., Wegrostek, C., Gloggnitzer, J., Fridkin, A., Klein, F., Gruenbaum, Y., Pasierbek, P., et al. (2010): Leptotene/zygotene chromosome movement via the SUN/KASH protein bridge in Caenorhabditis elegans. PLoS Genet. 6, e1001219.

Bellendir, Stephanie P.; Sekelsky, Jeff (2013): An elegans Solution for Crossover Formation. In: PLoS Genet. 9 (7), S. e1003658. DOI: 10.1371/journal.pgen.1003658.

Berg J.M., Shi Y. (1996): The Galvanization of Biology: A Growing Appreciation for the Roles of Zinc. Science Vol.271, Issue 5252, pp. 1081-1085 doi: 10.1126/science.271.5252.1081

Bhalla, N., Wynne, D.J., Jantsch, V., and Dernburg, A.F. (2008): ZHP-3 acts at crossovers to couple meiotic recombination with synaptonemal complex disassembly and bivalent formation in C. elegans. PLoS Genet. 4, e1000235.

Bizard AH, Hickson ID. (2014): The dissolution of double Holliday junctions. Cold Spring Harb Perspect Biol 6: a016477.

Bourlat, S. J., C. Nielsen, A. D. Economou, and M. J. Telford, (2008): Testing the new animal phylogeny: a phylum level molecular analysis of the animal kingdom. Mol. Phylogenet. Evol. 49: 23-31.

Bocquet N., Bizard A.H., Abdulrahman W., Larsen N.B., Faty M., Cavadini S., Bunker R.D., Kowalczykowski S.C., Cejka P., Hickson I.D., (2014): Structural and mechanistic insight into Holliday-junction dissolution by topoisomerase IIIα and RMI1. Nat. Struct. Mol. Biol. 21:261–268. doi: 10.1038/nsmb.2775.

Brenner, S., (1974): The genetics of Caenorhabditis elegans. Genetics 77: 71-94

Brenner, S., (1988): Foreword. The Nematode Caenorhabditis elegans, edited by W. B. Wood, Cold Spring Harbor Laboratory Press, Cold Spring Harbor, NY.

Bussen W, Raynard S, Busygina V, Singh AK, Sung P. (2007): Holliday junction processing activity of the BLM-TopoIIIa-BLAP75 complex. J Biol Chem 282: 31484–31492

Cejka, P., Cannavo, E., Polaczek, P., Masuda-Sasa, T., Pokharel, S., Campbell, J.L., and Kowalczykowski, S.C. (2010): DNA end resection by Dna2-Sgs1-RPA and its stimulation by Top3-Rmi1 and Mre11-Rad50-Xrs2. Nature 467, 112–116.

Cejka P, Kowalczykowski SC. (2010): The full-length Saccharomyces cerevisiae Sgs1 protein is a vigorousDNA helicase that preferentially unwinds Holliday junctions. J Biol Chem 285: 8290–8301.

Cejka P, Plank JL, Bachrati CZ, Hickson ID, Kowalczykowski SC. (2010): Rmi1 stimulates decatenation of double Holliday junctions during dissolution by Sgs1-Top3. Nat Struct Mol Biol 17: 1377–1382.

Cejka, P., Plank, J.L., Dombrowski, C.C., and Kowalczykowski, S.C. (2012): Decatenation of DNA by the S. cerevisiae Sgs1-Top3-Rmi1 and RPA complex: a mechanism for disentangling chromosomes. Mol. Cell 47, 886–896

Champoux JJ. (2001): DNA topoisomerases: Structure, function, and mechanism. Annu Rev Biochem 70: 369–413.

Chen CF, Brill SJ. (2007): Binding and activation of DNA topoisomerase III by the Rmi1 subunit. J Biol Chem 282: 28971–28979.

Corsi A.K., Wightman B., and Chalfie M. A (20015): Transparent window into biology: A primer on Caenorhabditis elegans (June 18, 2015), *WormBook*, ed. The *C. elegans* Research Community, WormBook, doi/10.1895/wormbook.1.177.1

Crittenden, Sarah L.; Eckmann, Christian R.; Wang, Liaoteng; Bernstein, David S.; Wickens,Marvin; Kimble, Judith (2003): Regulation of the mitosis/meiosis decision in the Caenorhabditis elegans germline. In: Philos. Trans. R. Soc. Lond., B, Biol. Sci. 358 (1436), S. 1359–1362. DOI:10.1098/rstb.2003.1333.

Cromie, Gareth A.; Hyppa, Randy W.; Smith, Gerald R. (2008): The fission yeast BLM homolog Rqh1 promotes meiotic recombination. In: Genetics 179 (3), S. 1157–1167.Doi:10.1534/genetIcs .108.088955

Colaiácovo, M.P., MacQueen, A.J., Martinez-Perez, E., McDonald, K., Adamo, A., La Volpe, A., and Villeneuve,A.M. (2003): Synaptonemal complex assembly in C. elegans is dispensable for loading strand-exchange proteins but critical for proper completion of recombination. Dev. Cell 5, 463–447.

Couteau, F., and Zetka, M. (2005): HTP-1 coordinates synaptonemal complex assembly with homolog alignment during meiosis in C. elegans. Genes Dev. 19, 2744–2756

de Carvalho CE, Zaaijer S, Smolikov S, Gu Y, Schumacher JM, Colaiácovo MP. (2008): LAB-1 antagonizes the Aurora B kinase in C. elegans. Genes Dev. 22: 2869–2885. doi: 10.1101/gad.1691208 PMID: 18923084

de los Santos T, Hunter N, Lee C, Larkin B et al. (2003): The Mus81/Mms4 endonuclease acts independently of double Holliday junction resolution to promote distinct subset of crossovers during meiosis in budding yeast. Genetics 164;81-94

Dernburg, A. F.; McDonald, K.; Moulder, G.; Barstead, R.; Dresser, M.; Villeneuve, A. M. (1998): Meiotic recombination in C. elegans initiates by a conserved mechanism and is dispensable for homologous chromosome synapsis. In: Cell 94 (3), S. 387–398.

Deshong, A.J., Ye, A.L., Lamelza, P., and Bhalla, N. (2014): A quality control mechanism coordinates meiotic prophase events to promote crossover assurance. PLoS Genet. 10, e1004291

Dorn A., Röhrig S., Papp K., Schröpfer S., Hartung F., Knoll A., Puchta H. (2018): The topoisomerase 3α zinc-finger domain T1 of Arabidopsis thaliana is required for targeting the enzyme activity to Holliday junction-like DNA repair intermediates. PLoS Genet.14:e1007674. doi: 10.1371/journal.pgen.1007674

Edgley, M. L. et al. (2006): Genetic balancers (April 6, 2006), *WormBook*, ed. The *C. elegans* Research Community, WormBook, doi/10.1895/wormbook.1.89.1.

Ellis, N. A.; Groden, J.; Ye, T. Z.; Straughen, J.; Lennon, D. J.; Ciocci, S. et al. (1995): The Bloom's syndrome gene product is homologous to RecQ helicases. In: Cell 83 (4), S. 655–666.

Fasching, C.L., Cejka, P., Kowalczykowski, S.C., and Heyer, W.-D. (2015): Top3-Rmi1 dissolve Rad51-mediated D loops by a topoisomerase-based mechanism. Mol. Cell 57, this issue, 595–606.

Gaur V, Wyatt HD, Komorowska W, Szczepanowski RH, de Sanctis D, Gorecka KM, West SC, Nowotny M. (2015): Structural and mechanistic analysis of the Slx1–Slx4 endonuclease. Cell Rep doi: 10.1016/j.celrep.2015.02.019.

German J. (1993): Bloom syndrome: A Mendelian prototype of somatic mutational disease. Medicine 72: 393–406.

Geoffrey M Cooper. (2000): The Cell, 2nd edition A molecular Approach. Sunderland (MA) Sinauer Associates. ISBN-10: 0-87893-106-6

Girard C., Roelens B., Zawadzki K.A., Villeneuve A.M. (2018): Interdependent and separable functions of *Caenorhabditis elegans* MRN-C complex members couple formation and repair of meiotic DSBs. Proc. Natl. Acad. Sci. USA. 115:E4443–E4452. doi: 10.1073/pnas.1719029115

Griffiths AJF, Miller JH, Suzuki DT (2000): An Introduction to Genetic Analysis. 7th edition. New York: W. H. Freeman

Goodwin A, Wang SW, Toda T, Norbury C, Hickson ID. (1999): Topoisomerase III is essential for accurate nuclear division in Schizosaccharomyces pombe. Nucleic Acids Res 27: 4050–4058.

Guiraldelli MF, Eyster C, Pezza RJ. (2013): Genome instability and embryonic developmental defects in RMI1 deficient mice. DNA Repair 12: 835–843.

Hall, D. H., Winfrey, V. P., Blaeuer, G., Hoffman, L. H., Furuta, T., Rose, K. L., Hobert, O., Greenstein, D. (1999): Ultrastructural features of the adult hermaphrodite gonad of *Caenorhabditis elegans:* relations between the germ line and soma. Dev Biol. 212: 101-123

Haber J.E. (2013): Genome Stability DNA Repair and Recombination by (Garland Science)

Haber J.E. (2015): TOPing of meiosis. Molecular Cell 57, 577-581. doi.org/10.1016/j.molcel.2015.03.008

Hartman Chen S., Wu C.H., Plank J.L., Hsieh T.S. (2012): Essential Functions of C Terminus of *Drosophila* Topoisomerase IIIα in Double Holliday Junction Dissolution. J. Biol. Chem. 2012, 287:19346-19353. doi: 10.1074/jbc.M112.363044

Hassold, T., Hunt, P. (2001): To err (meiotically) is human: the genesis of human aneuploidy. *Nat Rev Genet* 2, 280–291. https://doi.org/10.1038/35066065

Hartung F, Suer S, Knoll A, Wurz-Wildersinn R, Puchta H. (2008): Topoisomerase 3a and RMI1 suppress somatic crossovers and are essential for resolution of meiotic recombination intermediates in Arabidopsis thaliana. PLoS Genet 4: e1000285

Hatkevich T., and Sekelsky J., (2017): Bloom syndrome helicase in meiosis: Pro-crossover functions of an anti-crossover protein. BioEssays 39: 1700073 10.1002/bies.201700073

Hillers, Kenneth J.; Villeneuve, Anne M. (2003): Chromosome-wide control of meiotic crossing over in C. elegans. In: Curr. Biol. 13 (18), S. 1641–1647

Hillers KJ, Jantsch V, Martinez-Perez E, Yanowitz JL. (2017): Meiosis. WormBook. 2017;2017: 1–43. 10.1895/wormbook.1.178.1

Hodgkin, J. A., and S. Brenner, (1977): Mutations causing transformation of sexual phenotype in the nematode Caenorhabditis elegans. Genetics 86: 275-287

Holliday R., (1964): A mechanism for gene conversion in fungi. Genet. Res. 78: 282–304.

Hong Y., Sonneville R., Wang B., Scheidt V., Meier B., Woglar A., Demetriou S., Labib K., Jantsch V., Gartner A. (2018): LEM-3 is a midbody-tethered DNA nuclease that resolves chromatin bridges during late mitosis. Nat. Commun.9:728. doi: 10.1038/s41467-018-03135-w.

Hong Y., Velkova M., Silva N., Jagut M., Scheidt V., Labib K., Jantsch V., Gartner A. (2018): The conserved LEM-3/Ankle1 nuclease is involved in the combinatorial regulation of meiotic recombination repair and chromosome segregation in *Caenorhabditis elegans*. PLoS Genet.14:e1007453. doi: 10.1371/journal.pgen.1007453.

Hu, P.J., (2007): Dauer (August 08, 2007), WormBook, ed. The C. elegans Research Community, WormBook, doi/10.1895/wormbook.1.144.1

Hubbard, E.J. and Greenstein D. (2000): The *Caenorhabditis elegans* gonad: a test tube for cell and developmental biology. Dev. Dyn. 218: 2-22

Hunter, N. (2006): Meiotic recombination. In Molecular Genetics of Recombination, A. Aguilera and R. Rothstein, eds. (Springer-Verlag), pp. 381–442.

Hunter N, Kleckner N. (2001): The single-end invasion: An asymmetric intermediate at the double-strand break to double-Holliday junction transition of meiotic recombination. Cell 106: 59–70.

Ira G, Malkova A, Liberi G, Foiani M, Haber JE. (2003): Srs2 and Sgs1-Top3 suppress crossovers during double-strand break repair in yeast. Cell 115: 401–411

Jantsch, Verena; Pasierbek, Pawel; Mueller, Michael M.; Schweizer, Dieter; Jantsch, Michael; Loidl, Josef (2004): Targeted gene knockout reveals a role in meiotic recombination for ZHP-3, a Zip3-related protein in Caenorhabditis elegans. In: Mol. Cell. Biol. 24 (18), S. 7998–8006. DOI: 10.1128/MCB.24.18.7998-8006.2004.

Jagut M, Hamminger P, Woglar A, Millonigg S, Paulin L, Mikl M, (2016): Separable Roles for a Caenorhabditis elegans RMI1 Homolog in Promoting and Antagonizing Meiotic Crossovers Ensure Faithful Chromosome Inheritance. PLoS Biol. 14: e1002412 10.1371/journal.pbio.1002412

Karow JK, Constantinou A, Li JL, West SC, Hickson ID. (2000): The Bloom's syndrome gene product promotes branch migration of Holliday junctions. Proc Natl Acad Sci 97: 6504–6508.

Kaur,H., De Muyt,A. and Lichten,M. (2015): Top3-Rmi1 DNAsingle-strand decatenase is integral to the formation and resolution ofmeiotic recombination intermediates.Mol. Cell,57, 583–594.

Keeney, S. (2001): Mechanism and control of meiotic recombination initiation. In: Curr. Top. Dev. Biol. 52, S. 1–53.

Kim YC., Lee J., Koo HS (2000): Functional characterization of Caenorhhabditis elegans DNA topoisomerase IIIα. *Nucleic Acids Research*, Volume 28, Issue 9, 1 May 2000, Pages 2012–2017, https://doi.org/10.1093/nar/28.9.2012

Kim, Y., Rosenberg, S.C., Kugel, C.L., Kostow, N., Rog, O., Davydov, V., Su, T.Y., Dernburg, A.F., and Corbett,K.D. (2014): The chromosome axis controls meiotic events through a hierarchical assembly of HORMA domain proteins. Dev. Cell 31, 487–502

Kimble, J. and D. Hirsh, (1979): The post-embryonic cell lineages of the hermaphrodite and male gonads in Caenorhabditis elegans. Dev. Biol. 70: 396-417.

Kleckner Nancy (1996): Meiosis: How could it work? Proc. Natl. Acad. Sci. USA Vol. 93, pp. 8167-8174.

Knoll A., Schröpfer S., Puchta H. (2014): The RTR complex as caretaker of genome stability and its unique meiotic function in plants. *Front. Plant Sci.* 5:33. 10.3389/fpls.2014.00033

Kohl, K.P., and Sekelsky, J. (2013): Meiotic and mitotic recombination in meiosis. Genetics 194, 327–334.

Krejci L, Altmannova V, Spirek M, Zhao X. (2012): Homologous recombination and its regulation. Nucleic Acids Res 40: 5795–5818.

Kusano K, Berres ME, Engels WR. (1999): Evolution of the RECQ family of helicases: A Drosophila homolog, Dmblm, is similar to the human Bloom syndrome gene.Genetics 151: 1027–1039.

Li W,Wang JC. (1998): Mammalian DNA topoisomerase IIIa is essential in early embryogenesis. Proc Natl Acad Sci 95: 1010–1013.

Libuda, D.E., Uzawa, S., Meyer, B.J., and Villeneuve, A.M. (2013): Meiotic chromosome structures constrain and respond to designation of crossover sites. Nature 502, 703–706.

Lints, R. and Hall, D.H. (2009): Reproductive system, germ line. In *WormAtlas*. doi:10.3908/wormatlas.1.23

Lints, R. and Hall, D.H. (2009): Reproductive system, overview. In WormAtlas. doi:10.3908/wormatlas.1.21

León-Ortiz AM, Panier S, Sarek G, Vannier JB, Patel H, Campbell PJ, Boulton SJ. (2018): A distinct class of genome rearrangements driven by heterologous recombination. Molecular Cell;69:292–305. doi: 10.1016/j.molcel.2017.12.014.

Lu, J.; Mullen, J. R.; Brill, S. J.; Kleff, S.; Romeo, A. M.; Sternglanz, R. (1996): Human homologues of yeast helicase. In: Nature 383 (6602), S. 678–679. DOI: 10.1038/383678a0.

Lui, Doris Y.; Colaiácovo, Monica P. (2013): Meiotic development in Caenorhabditis elegans. In: Adv. Exp. Med. Biol. 757, S. 133–170. DOI: 10.1007/978-1-4614-4015-4_6.

MacQueen, Amy J.; Colaiácovo, Mónica P.; McDonald, Kent; Villeneuve, Anne M. (2002): Synapsis-dependent and -independent mechanisms stabilize homolog pairing during meiotic prophase in C. elegans. In: Genes Dev. 16 (18), S. 2428–2442. DOI: 10.1101/gad.1011602.

Martin, J.S., Winkelmann, N., Petalcorin, M.I.R., McIlwraith, M.J., and Boulton, S.J. (2005): RAD-51-dependent and -independent roles of a Caenorhabditis elegans BRCA2-related protein during DNA double-strand break repair. Mol. Cell. Biol. 25, 3127–3139.

Martinez-Perez, E., and Villeneuve, A.M. (2005). HTP-1-dependent constraints coordinate homolog pairing and synapsis and promote chiasma formation during C. elegans meiosis. Genes Dev. 19, 2727–2743.

Martinez-Perez, E., Schvarzstein, M., Barroso, C., Lightfoot, J., Dernburg, A.F., and Villeneuve, A.M. (2008): Crossovers trigger a remodeling of meiotic chromosome axis composition that is linked to two-step loss of sister chromatid cohesion. Genes Dev. 22, 2886–2901

McKim, K.S., Howell, A.M., and Rose, A.M. (1988): The effects of translocations on recombination frequency in Caenorhabditis elegans. Genetics 120, 987–1001.

McVey, Mitch; Andersen, Sabrina L.; Broze, Yuri; Sekelsky, Jeff (2007): Multiple functions of Drosophila BLM helicase in maintenance of genome stability. In: Genetics 176 (4), S. 1979–1993. doi:10.1534/genetics.106.070052.

Minn, I.L., Rolls, M.M., Hanna-Rose, W., and Malone, C.J. (2009): SUN-1 and ZYG-12, mediators of centrosome-nucleus attachment, are a functional SUN/KASH pair in Caenorhabditis elegans. Mol. Biol. Cell 20,4586–4595.

Mullen JR, Nallaseth FS, Lan YQ, Slagle CE, Brill SJ. (2005): Yeast Rmi1/Nce4 controls genome stability as a subunit of the Sgs1-Top3 complex. Mol Cell Biol 25: 4476–4487.

Nabeshima, K., Villeneuve, A.M., and Colaiácovo, M.P. (2005): Crossing over is coupled to late meiotic prophase bivalent differentiation through asymmetric disassembly of the SC. J. Cell Biol. 168, 683–689.

Nagaoka SI, Hassold TJ, Hunt PA. (2012): Human aneuploidy: Mechanisms and new insights into an age-old problem.Nat Rev Genet 13: 493–504.

Nakayama H. (2005): Escherichia coli RecQ helicase: A player in thymineless death. Mutat Res 577: 228–236.

Nguyen H, Labella S, Silva N, Jantsch V, and Zetka M (2018): C. elegans ZHP-4 is required at multiple distinct steps in the formation of crossovers and their transition to segregation competent chiasmata. PLoS genetics 14, e1007776.

Ohkura Hiroyuki (2015): Meiosis: An Overview of Key Differences from Mitosis. *Cold Spring Harb Perspect Biol* 2015;7:a015859

O' Neil, Nigel J.; Martin, Julie S.; Youds, Jillian L.; Ward, Jordan D.; Petalcorin, Mark I R; Rose, Anne M.; Boulton, Simon J. (2013): Joint molecule resolution requires the redundant activities of MUS-81 and XPF-1 during Caenorhabditis elegans meiosis. In: PLoS Genet. 9 (7), S. e1003582. DOI: 10.1371/journal.pgen.1003582.

Paix A, Folkmann A, Rasoloson D, Seydoux G. (2015): High efficiency, Homology-Directed genome editing in *Caenorhabditis elegans* Using CRISPR-Cas9 Ribonucleoprotein Complexes Genetics. 201:47–54. doi: 10.1534/genetics.115.179382.

Penkner, A.M., Fridkin, A., Gloggnitzer, J., Baudrimont, A., Machacek, T., Woglar, A., Csaszar, E., Pasierbek, P., Ammerer, G., Gruenbaum, Y., and Jantsch, V.l. (2009): Meiotic chromosome homology search involves modifications of the nuclear envelope protein Matefin/SUN-1. Cell 139, 920–933

Phillips, C.M., and Dernburg, A.F. (2006): A family of zinc-finger proteins is required for chromosome-specific pairing and synapsis during meiosis in C. elegans. Dev. Cell 11, 817–829.

Plank JL, Chu SH, Pohlhaus JR, Wilson-Sali T, Hsieh TS. (2005): Drosophila melanogaster topoisomerase IIIa preferentially relaxes a positively or negatively supercoiled bubble substrate and is essential during development. J Biol Chem 280: 3564–3573.

Raynard S, BussenW, Sung P. (2006): A double Holliday junction dissolvasome comprising BLM, topoisomerase IIIa, and BLAP75. J Biol Chem 281: 13861–13864

Rosu, Simona; Libuda, Diana E.; Villeneuve, Anne M. (2011): Robust crossover assurance and regulated interhomolog access maintain meiotic crossover number. In: Science 334 (6060), S. 1286–1289. DOI: 10.1126/science.1212424.

Sanford, C., and Perry, M.D. (2001): Asymmetrically distributed oligonucleotide repeats in the Caenorhabditis elegans genome sequence that map to regions important for meiotic chromosome segregation. Nucleic Acids Res.29, 2920–2926.

Sato, A., Isaac, B., Phillips, C.M., Rillo, R., Carlton, P.M., Wynne, D.J., Kasad, R.A., and Dernburg. A.F. (2009): Cytoskeletal forces span the nuclear envelope to coordinate meiotic chromosome pairing and synapsis. Cell 139, 907–919.

Saito, Takamune T.; Youds, Jillian L.; Boulton, Simon J.; Colaiácovo, Monica P. (2009): Caenorhabditis elegans HIM-18/SLX-4 interacts with SLX-1 and XPF-1 and maintains genomic integrity in the germline by processing recombination intermediates. In: PLoS Genet. 5 (11), S. e1000735. DOI: 10.1371/journal.pgen.1000735.

Saito, Takamune T.; Lui, Doris Y.; Kim, Hyun-Min; Meyer, Katherine; Colaiácovo, Monica P. (2013): Interplay between structure-specific endonucleases for crossover control during Caenorhabditis elegans meiosis. In: PLoS Genet. 9 (7), S. e1003586. DOI: 10.1371/journal.pgen.1003586.

Schvarzstein, M., Pattabiraman, D., Libuda, D.E., Ramadugu, A., Tam, A., Martinez-Perez, E., Roelens, B., Zawadzki, K.A., Yokoo, R., Rosu, S., et al. (2014): DNA helicase HIM-6/BLM both promotes MutSg-dependent crossovers and antagonizes MutSg-independent interhomolog associations during Caenorhabditis elegans meiosis. Genetics 198, 193–207

Schwacha A, Kleckner N. (1995): Identification of double Holliday junctions as intermediates in meiotic recombination. Cell 83: 783–791.

Séguéla-Arnaud M., Choinard S., Larchevêque C., Girard C., Froger N., Crismani W., Mercier R. (2016): RMI1 and TOP3α limit meiotic CO formation through their C-terminal domains. Nucleic Acids Res. 45:1860–1871. doi: 10.1093/nar/gkw1210.

Smolikov, S., Schild-Prüfert, K., and Colaiácovo, M.P. (2009): A yeast two-hybrid screen for SYP-3 interactors identifies SYP-4, a component required for synaptonemal complex assembly and chiasma formation in Caenorhabditis elegans meiosis. PLoS Genet. 5, e1000669

Sulston, J. E. and H.R. Horvitz, (1977): Post-embryonic cell lineages of the nematode, Caenorhabditis elegans. Dev. Biol. 56: 110-156.

Sun H, Treco D, Schultes NP, Szostak JW. (1989): Double strand breaks at an initiation site for meiotic gene conversion.Nature 338: 87–90.

Sun H, TrecoD, Szostak JW. (1991): Extensive 30-overhanging, single-stranded DNA associated with the meiosis-specific double-strand breaks at the ARG4 recombination initiation site. Cell 64: 1155–1161

Tang,S., Wu,M.K.Y., Zhang,R. and Hunter,N. (2015): Pervasive andessential roles of the Top3-Rmi1 decatenase orchestraterecombination and facilitate chromosome segregation in meiosis.Mol. Cell,57, 607–621.

Villeneuve, A.M. (1994): A cis-acting locus that promotes crossing over between X chromosomes in Caenorhabditis elegans. Genetics 136, 887–902.

Wallis JW, Chrebet G, Brodsky G, Rolfe M, Rothstein R. (1989): A hyper-recombination mutation in S. cerevisiae identifies a novel eukaryotic topoisomerase. Cell 58: 409–419.

Wicky, C., A. Alpi, M. Passannante, A. Rose, A. Gartner et al., (2004): Multiple genetic pathways involving the Caenorhabditis elegans Bloom's syndrome genes him-6, rad-51, and top-3 are needed to maintain genome stability in the germ line. Mol. Cell. Biol. 24: 5016–5027.

Winand, N.J., Panzer, J.A., and Kolodner, R.D. (1998). Cloning and characterization of the human and Caenorhabditis elegans homologs of the Saccharomyces cerevisiae MSH5 gene. Genomics 53, 69–80.

Wood, Andrew J.; Severson, Aaron F.; Meyer, Barbara J. (2010): Condensin and cohesion complexity: the expanding repertoire of functions. In: Nat. Rev. Genet. 11 (6), S. 391–404. doi:10.1038/nrg2794

Woglar A, Villeneuve AM. (2018): Dynamic architecture of DNA repair complexes and the synaptonemal complex at sites of meiotic recombination. Cell 173:1678–1691. doi: 10.1016/j.cell.2018.03.066

Wu L, Hickson ID. (2002): The Bloom's syndrome helicase stimulates the activity of human topoisomerase IIIa. Nucleic Acids Res 30: 4823–4829
Wu L, Hickson ID. (2003): The Bloom's syndrome helicase suppresses crossing over during homologous recombination. Nature 426: 870–874

Wynne, D.J., Rog, O., Carlton, P.M., and Dernburg, A.F. (2012): Dynein-dependent processive chromosome motions promote homologous pairing in C. elegans meiosis. J. Cell Biol. 196, 47–64

Yin, Y., and Smolikove, S. (2013): Impaired resection of meiotic double-strand breaks channels repair to nonhomologous end joining in Caenorhabditis elegans. Mol. Cell. Biol. 33, 2732–2747

Yokoo R, Zawadzki KA, Nabeshima K, Drake M, Arur S, Villeneuve AM. (2012): COSA-1 reveals robust homeostasis and separable licensing and reinforcement steps governing meiotic crossovers. Cell 149: 75–87.

Youds JL,Mets DG,McIlwraith MJ,Martin JS,Ward JD, NJ ON, Rose AM, West SC, Meyer BJ, Boulton SJ. (2010): RTEL-1 enforces meiotic crossover interference and homeostasis. Science 327: 1254–1258

Zalevsky, J.; MacQueen, A. J.; Duffy, J. B.; Kemphues, K. J.; Villeneuve, A. M. (1999): Crossing over during Caenorhabditis elegans meiosis requires a conserved MutS-based pathway that is partially dispensable in budding yeast. In: Genetics 153 (3), S. 1271–1283.

Zakharyevich, K., Tang, S., Ma, Y., and Hunter, N. (2012). Delineation of joint molecule resolution pathways in meiosis identifies a crossover-specific resolvase. Cell 149, 334–347

Zetka, M. C.; Kawasaki, I.; Strome, S.; Müller, F. (1999): Synapsis and chiasma formation in Caenorhabditis elegans require HIM-3, a meiotic chromosome core component that functions in chromosome segregation. In: Genes Dev. 13 (17), S. 2258–2270.